CANADIAN THESES

THÈSES CANADIENNES

NOTICE

The quality of this microfiche is heavily dependent upon the quality of the original thesis submitted for microfilming. Every effort has been made to ensure the highest quality of reproduction possible.

If pages are missing, contact the university which granted the degree.

Some pages may have indistinct print especially if the original pages were typed with a poor typewriter ribbon or if the university sent us an inferior photocopy.

Previously copyrighted materials (journal articles, published tests, etc.) are not filmed.

Reproduction in full or in part of this film is governed by the Canadian Copyright Act, R.S.C. 1970, c. C-30.

AVIS

La qualité de cette microfiche dépend grandement de la qualité de la thèse soumise au microfilmage. Nous avons tout fait pour assurer une qualité supérieure de reproduction.

S'il manque des pages, veuillez communiquer avec l'université qui a conféré le grade.

La qualité d'impression de certaines pages peut laisser à désirer, surtout si les pages originales ont été dactylographiées à l'aide d'un ruban usé ou si l'université nous a fait parvenir une photocopie de qualité inférieure.

Les documents qui font déjà l'objet d'un droit d'auteur (articles de revue, examens publiés, etc.) ne sont pas microfilmés.

La reproduction, même partielle, de ce microfilm est soumise à la Loi canadienne sur le droit d'auteur, SRC 1970, c. C-30.

THIS DISSERTATION HAS BEEN MICROFILMED EXACTLY AS RECEIVED

LA THÈSE A ÉTÉ MICROFILMÉE TELLE QUE NOUS L'AVONS REÇUE

THE UNIVERSITY OF ALBERTA

WAVE PHENOMENA IN FLUID-FILLED DISTENSIBLE TUBES: DISPERSION, DISSIPATION AND REFLECTION

BY

© RONALD PETER SAWATZKY

A THESIS

SUBMITTED TO THE FACULTY OF GRADUATE STUDIES AND RESEARCH

IN PARTIAL FULFILMENT OF THE REQUIREMENTS FOR THE DEGREE

OF DOCTOR OF PHILOSOPHY

IN

APPLIED MATHEMATICS

DEPARTMENT OF MATHEMATICS

EDMONTON, ALBERTA

SPRING 1987

ISBN 0-315-37669-4

THE UNIVERSITY OF ALBERTA

RELEASE FORM

NAME OF AUTHOR: RONALD PETER SAWATZKY

TITLE OF THESIS: WAVE PHENOMENA IN FLUID-FILLED DISTENSIBLE TUBES: DISPERSION, DISSIPATION AND REFLECTION

DEGREE: DOCTOR OF PHILOSOPHY

YEAR THIS DEGREE GRANTED: 1987

Ron Sawatzky

Apt. 301, 15107 45 Ave.

Edmonton, Alberta T6H 5K8

DATE: November 19, 1986

THE UNIVERSITY OF ALBERTA

THE FACULTY OF GRADUATE STUDIES AND RESEARCH

The undersigned certify that they have read, and recommend to the Faculty of Graduate Studies and Research for acceptance, a thesis entitled WAVE PHENOMENA IN FLUID-FILLED DISTENSIBLE TUBES: DISPERSION, DISSIPATION AND REFLECTION submitted by RONALD PETER SAWATZKY in partial fulfilment of the requirements for the degree of DOCTOR OF PHILOSOPHY in APPLIED MATHEMATICS.

Supervisor

External Examiner

DATE: November 19, 1986

ABSTRACT

The propagation of transient pressure perturbations through a viscoelastic tube containing a viscous fluid is considered. The dispersion equation appropriate for a viscoelastic shell theory model is derived and analysed in the low to intermediate frequency regime. An asymptotic formula is developed for the wave number k in terms of the circular frequency ω. This approximation is uniformly valid throughout the range of interest in ω and the coefficient of fluid viscosity μ, except at the point $\omega = 0$, $\mu = 0$ where the dependence of k upon ω and μ is nonuniform. The approximate solution of the dispersion equation derived here is used to examine the transient response of the fluid-filled tube model in two situations: a semi-infinite tube subjected to a disturbance at its end and two dissimilar tubes connected at a junction that are subjected to a disturbance at one end. These boundary-value problems are posed respectively to describe the propagation of an impulse along a tube in the absence of reflections and to describe the reflection and transmission of an impulse at a junction between two tubes. The solutions to both problems are constructed by means of Fourier integrals. The propagation of the pulses is depicted graphically for various values of the parameters that characterize the tube and the fluid. The role of fluid viscosity is compared with that of wall viscoelasticity in both the propagation and reflection of these pulses. Particular emphasis is placed on parameter values pertinent to impulse experiments studying wave propagation in large arteries and water-filled latex tubes.

ACKNOWLEDGEMENT

This dissertation owes its existence to three people who gave generously of their time and knowledge throughout its preparation: my supervisor, Professor T.B. Moodie, whose enthusiasm for research was infectious and whose guidance remained patient and constant; Professor R.J. Tait, who offered his critical insight through thoughtful discussions; and Patricia Myers, who applied her fine editorial talents to a thesis badly in need of them. I am grateful for financial support from Professors Moodie and Tait, as well as from The University of Alberta, The Province of Alberta, the Killam Scholarship Committee, and the Alberta Heritage Scholarship Fund.

TABLE OF CONTENTS

LIST OF FIGURES

CHAPTER I

Introduction

Dass die wichtigsten Dinge durch Rohren in der Welt ausgerichtet werden.

G.C. Lichtenberg

In his lecture to the Royal Society of London on the function of the heart and arteries, the physician and physicist Thomas Young explicitly acknowledged the importance of mechanics in investigating the relationship between the circulation of the blood and 'the muscular and elastic powers of the heart and arteries' (Young, 1809). Young sought to understand the physical events that take place under normal conditions in the mammalian cardiovascular system, and thereby make a contribution to physiology. The large body of literature discussing the mechanics of the circulation that has accumulated since Young's pioneering work has kept its focus on this central problem. A secondary feature of this literature has been its contribution to medicine through the analysis of particular abnormal or diseased states in the hope of improving their diagnosis or treatment. Any approach to the analysis of circulatory variables for diagnostic or therapeutic purposes, then, requires an accurate model of the mechanics of both a healthy and a diseased cardiovascular system.

It is with one aspect of the mechanics of the circulation, that of wave propagation in large arteries, that this thesis is concerned. The most common wave encountered in the circulation is the arterial

pressure pulse. This wave is excited by the pressure disturbance created as blood is ejected from the heart into the entrance to the aorta. The following description of the transmission of the pulse is taken from Caro et al. (1978). As blood is pumped into the entrance to the aorta, the pressure there rises and the vessel wall is stretched. When the rate of cardiac ejection begins to decline, the pressure falls and the distended wall returns to its equilibrium state. The inertia of the fluid keeps it moving forward after the pressure difference driving the flow disappears. This causes the first section of artery wall to overshoot its equilibrium position and an oscillatory motion is set up. At the same time the next section of wall becomes distended. As this recoils, the fluid driven out distends a further section of the wall which also recoils. Thus the disturbance is propagated along the arterial system in the form of a pressure wave. The wall motions associated with the pressure wave are primarily radial. Similar waves can be excited artificially by generating a pressure disturbance at any location in the circulation.

Pressure waves in the large arteries, and for that matter in any fluid-filled distensible tube, owe their existence to a balance between a restoring force and inertia. The restoring force is supplied by the elasticity of the artery wall while the inertia is supplied principally by the blood and, to a lesser degree, by the vessel wall. The pressure wave in an artery can propagate in either direction. The natural pulse wave originates at the heart and travels distally, although it is modified by components reflected from the periphery. The presence of viscous forces will cause the wave motion to be damped. In the

cardiovascular system, mechanisms for dissipation exist in the blood through its viscosity, and in the vessel wall through its viscoelastic properties. Thus the mechanical properties of large arteries are directly responsible for the characteristics exhibited by the pressure waves that pass along them.

Mathematical theories can contribute to understanding the physical events that take place in the cardiovascular system when they are 'firmly linked to experiment, using, explaining and predicting experimental results' (Pedley, 1980). Young was the first to successfully exploit the symbiotic relationship between theory and experiment within the context of the circulatory system. He derived a formula for the velocity of propagation of a pressure pulse through an incompressible fluid contained in an elastic tube (Young, 1808), and discussed the application of his formula to blood flow (Young, 1809). Since then, a small army of researchers has pursued his ideas, establishing mathematical models as indispensable tools in obtaining an accurate description of the propagation process. Concurrently, many experimentalists have been examining the passage of pressure waves through the arterial system. Detailed expositions of these research developments are found in McDonald (1974) and Caro et al. (1978).

Interestingly enough, the first mathematical paper on blood flow was not by Thomas Young. That distinction belongs to the famous Swiss mathematician Leonhard Euler. In 1775, he developed equations governing the flow of blood in the arteries. This work was not published, however, until 1862 (Euler, 1862). In Euler's formulation of the problem, the fluid and vessel wall were treated as deformable

media whose motions are governed by the equations of continuum mechanics. The equations he produced described the one-dimensional flow of an inviscid, incompressible fluid in an elastic tube. His governing equations are a reasonably complete representation of blood flow in arteries. Euler, however, was unable to develop any solutions to his equations.

As is noted above, Young was the first to derive the velocity of propagation of the pulse wave in blood flow. He derived his formula by drawing an analogy with the propagation of sound in a compressible fluid. He pointed out that the pressure change generated in a compressed gas is equivalent to the pressure change generated in an inflated tube. Thus he was able to obtain the formula

$$c_0 = [\Delta P/\rho(\Delta V/V)]^{1/2} \qquad (1.1)$$

for the velocity of the pulse wave in blood flow by adapting Newton's formula for the velocity of sound in air. In eqn. 1.1, ρ is the fluid density, ΔP is the change in fluid pressure, and $\Delta V/V$ is the corresponding relative change in the volume occupied by the tube. Young studied other aspects of the mechanics of blood flow as well, including the pressure drop along arterial segments due to viscous losses. The latter research was continued in more detail by Poiseuille.

During the nineteenth century Young's formula for pulse wave velocity was rederived in various ways by a number of investigators,

including the Weber brothers, Moens, Korteweg and Lamb. A summary of their work is set down by Skalak (1966). To Korteweg is attributed the following version of the formula for c_0 :

$$c_0 = [Eh/2\rho R]^{1/2} , \qquad (1.2)$$

where h and E are the thickness and Young's modulus of the tube wall, and R is the tube radius. Equation 1.2 is known as the Korteweg-Moens equation for the wave speed.

The analysis of pressure and flow in the circulation advanced significantly at the turn of the century with Otto Frank's lumped system model. Frank and his colleagues were able to derive fair approximations of the pressure and flow waves observed in large arteries, although they concluded that for accurate description and timing of waveforms, considerations of wave propagation must be taken into account. Their model is incapable of accounting for spatial variation, so it is unable to represent a wave propagation process.

The modern era of analysis of wave propagation in blood flow began with the work of McDonald and Womersley in the 1950's. They initiated the development of comprehensive theories of wave propagation regarding the circulatory system as a system of elastic tubes. An excellent review of the history of the mechanics of the circulation has been written by McDonald (1974), while a brief summary of the subject is presented in Skalak et al, (1981).

During the past twenty-five years, the theory of the propagation

of the arterial pressure pulse has been quite thoroughly worked out (McDonald, 1974; Caro et al., 1978; Pedley, 1980). The principal features of the theory are outlined concisely by Pedley (1984). The resistance of the artery to circumferential stretch is primarily responsible for providing the restoring force needed for wave propagation. This force is balanced mostly by the axial inertia of the blood. If the two factors named above are the only ones modelled in a linear theory, waves of constant form are predicted, with the waveform of average velocity the same shape as that of pressure. That neither of these predictions are observed is evident from, for example, Fig. 12.26 of Caro et al. (1978). If blood viscosity is included in the model, the shape of the velocity waveform can be accurately predicted from the pressure measured at the same site (McDonald, 1974; Pedley, 1980). However, blood viscosity does not have a great influence on the shape of the pressure waveform, except to attenuate high frequency components. A slight steepening of the pressure and velocity waves is predicted when sources of nonlinearity are represented in the model, but this is not thought to be of importance in normal subjects. It is believed that the change of shape of the pressure pulse can be attributed for the most part to the fact that arteries are not infinite uniform tubes. Their cross-sectional area and elastic properties can vary with distance, and there are many bifurcations, each of which acts as a site of wave reflection. A clear summary of the linear theory of wave reflection and transmission in a network of branched tubes is contained in Lighthill (1978).

Thus, it is evident from the discussion above that a reasonable

understanding of the normal pulse wave has been obtained from a linear theory that incorporates the effects of the circumferential stiffness of the artery wall, the axial inertia and viscosity of the blood, and the presence of arterial junctions. One facet of the propagation process that is not explained by any of these factors, however, is the attenuation observed in the pressure and velocity waveforms. This attenuation is considerably larger than can be predicted solely by blood viscosity (Pedley, 1980). Therefore, other sources of energy loss must be found. Dissipation in the arterial wall is suspected to be a major contributor to the loss of energy in the pulse wave. Experiments indicate that viscous dissipation in arteries is not negligible. This dissipation can be included in the model of wave propagation considered here by representing the mechanical response of arteries as viscoelastic. In this event, significant attenuation of the pulse is predicted (Caro et al., 1978). The damping expected is of the same order of magnitude as that observed in experiments (McDonald, 1974). For this reason any attenuation of the pressure and velocity waveforms that cannot be explained by blood viscosity is usually attributed to the viscoelasticity of the artery wall.

However, uncertainty about the magnitude of the attenuation produced by wall viscoelasticity has resulted from experiments more recent than those cited in McDonald (1974). In one set of experiments, the decay with distance measured in pressure and velocity was much greater than that predicted from knowledge of blood viscosity and wall viscoelasticity (Milnor and Bertram, 1978). In another experimental study, the opposite occurred (Greenwald and Newman, 1982). There the

pressure pulses were attenuated far less than would be expected from conventional estimates of wall viscoelasticity. The defects in the present understanding of pulse wave attenuation stem from an 'inadequate specification of the mechanical properties of artery walls' (Pedley, 1984).

Part of the problem may lie with the viscoelastic models chosen to represent the arterial wall, and with the values of the parameters used in these models to predict wave attenuation. Viscoelastic measurements are difficult under any circumstances, and the variability of the circulatory system introduces further complications. Thus, great care must be taken not only to obtain accurate measurements of the viscoelastic response of arteries, but to model this response accurately as well.

Another aspect of the theory described here that needs to be considered more deeply is the use of a 'tube law' to represent the mechanical properties of an artery. One of the drawbacks of a tube law is that it can account for the resistance of the tube to circumferential stretch only. While circumferential stretch may be the most important factor involved in the tube's mechanics, it is not necessarily true that other features are then insignificant. In fact, it is well known that the tube law approach is valid only for waves that are very long: that is, for waves whose length is much greater than the tube radius (Lighthill, 1978).

The natural arterial pulse satisfies the long wavelength condition. For example, the fundamental wave in the human aorta is about 4 m long, as its frequency is roughly 1 Hz. This is enormous

compared to the radius of the aorta which is less than 2 cm. Even the shortest waves present are longer than 40 cm, as the natural pulse in humans does not contain frequencies much above 10 Hz (Caro et al., 1978). However, some disturbances generated artificially by researchers studying wave propagation in the arterial system may contain waves of the same order of magnitude as the radius of the artery through which they are travelling. For example, Anliker et al. (1968) and Greenwald and Newman (1982) have produced disturbances containing frequencies of up to 150 Hz. The shortest waves in these experiments are just three to four times greater than the radius of the corresponding arteries. Under these circumstances, the use of a tube law to represent the mechanical properties of the arteries cannot be justified with any confidence. Consequently, it is necessary to consider secondary factors noted previously in any attempt at constructing a theory of pulse wave propagation to accurately model experiments such as the ones cited above.

One theory containing a description of tube mechanics more complicated than that of a tube law has been studied by Moodie et al. (1982). These authors use a simple bending theory model of a viscoelastic shell to represent the mechanical properties of an artery. In this model they incorporate the radial inertia, rotatory inertia and flexural rigidity of the tube wall, as well as its circumferential stiffness. Hence, this model is still valid even when a disturbance contains waves whose length is of the same order of magnitude as the radius of the tube. The theory was tested against experiments on

water-filled latex tubes by comparing the predicted transmission characteristics with those observed in a pressure impulse generated at the entrance of a very long tube (Moodie et al., 1984; Moodie et al., 1986). The broadening and attenuation of the pulse measured in the experiments agreed well with the theoretical predictions.

In the series of papers by Moodie and his colleagues, the viscosity of the fluid contained in the tube was neglected. They argued that, compared with wall viscoelasticity, fluid viscosity has little influence on the shape of a pressure pulse. This view is consistent with conclusions drawn from theories of wave propagation based on a tube law, and with observations of the normal arterial pulse (Caro et al., 1978). Nevertheless, the following question remains: what is the role of fluid viscosity in pressure pulses of the sort generated by Greenwald and Newman (1982), where frequencies range between 0 and 150 Hz, and how does this role compare with that of wall viscoelasticity? This dissertation explores the answers to that question.

CHAPTER II

Background: Wave Propagation in Large Arteries

A striking characteristic of the mammalian cardiovascular system is its geometric and mechanical complexity. Blood flows through a system of asymmetrically branched tubes that bend and vary in bore. The tubes' geometry can change with body position and activity. The walls of arteries are both inhomogeneous and anisotropic, as they are composed of several layers of connective tissue, smooth muscle cells, and other components. Their elastic properties are time-dependent and markedly nonlinear. Blood is not a Newtonian fluid but a suspension of particles with an apparent viscosity that depends on shear rate. Despite this complexity, most of the progress in understanding the mechanics of the circulatory system has been based on investigations of simple models. As an example, considerable insight into the mechanics of wave propagation has been gained from theoretical and experimental models using systems of straight, uniform, latex rubber tubes filled with water. The success of these and other theories in explaining a variety of mechanical phenomena that occur in the cardiovascular system indicates that the mechanics of this system are well approximated by simple models under many circumstances.

This chapter provides a description of the mechanics of wave propagation in the large arteries of the circulatory system as background for the study being undertaken in this dissertation. The chapter is divided into three parts. In the first two parts, the geometric and mechanical properties of the system are discussed, as

well as the conditions of blood pressure and flow associated with the propagation of the normal arterial pulse therein. In the third part, a survey of mathematical models concerning the propagation of pressure disturbances in fluid-filled distensible tubes is presented. The survey focuses on the relevance of these models to problems of wave propagation in the circulation.

Many books and reviews have been published on the mechanics of the circulation. Among the most important are the monographs by McDonald (1974), Caro et al. (1978) and Pedley (1980). The books by McDonald and Caro et al. contain considerable detail on the structure and properties of the whole cardiovascular system, together with much discussion of the physics of the normal arterial pulse. These works form the basis for the material in the first two parts of this chapter. The book by Pedley concentrates on the mathematical analysis of cardiovascular mechanics, and is the principal source for the material in the third part of the chapter.

Geometric and Mechanical Properties

In this section, we briefly describe the anatomy and structure of the large arteries, and their geometric and mechanical properties. The anatomy of the canine aorta and its major branches is illustrated in Fig. 2.10 of McDonald (1974), and many of the relevant dimensions are listed in Table I of Caro et al. (1978). The initial part of the aorta, the descending aorta, is relatively straight. The aorta then curves though 180° in a complicated three-dimensional way, giving off branches to the heart, head, and upper limbs. It pursues a fairly

straight course down through the diaphragm to the abdomen, where it distributes branches to the abdominal organs. Low in the abdomen it terminates, forming two iliac arteries and the sacral artery (absent in man). Similarly, all other large arteries are curved and branched in a complicated way. There are relatively few straight stretches of artery without branches. The human arterial tree is similar in all these respects.

The aorta, like most arteries, tapers along its length. The rate of taper appears to vary from individual to individual and probably from species to species. Despite the fact that individual arteries taper, the total cross-sectional area of the arterial tree increases with distance from the heart. At most branches the ratio of the sum of the areas of the daughter vessels to that of the parent is greater than one. The branches in the chest have ratios close to one, while those in the upper abdomen have slightly greater values. However, at the termination of the abdominal aorta there may be a marked contraction, with ratios as low as 0.75. This is more likely to occur in humans than in dogs. Beyond the early branches, the cross-sectional area of the arterial tree expands dramatically.

It is evident from Table I of Caro et al. (1978) that the thickness of the artery wall varies considerably throughout the circulation. As one moves peripherally, the walls become thinner. However, the internal radius in the large central arteries decreases at the same rate as the wall thickness, so the ratio of h to R remains virtually constant at approximately 0.1. This ratio is independent of species as well as site.

The dimensions of the larger arteries depend not only on body size and position in the circulation, but also on age. Two well-known changes accompany aging of the cardiovascular system: dilation and thickening. For example, the thoracic aorta dilates and its wall becomes thicker. The wall thickness increases slightly more than the radius. The smaller arteries branching from the aorta do not change appreciably in radius, but their walls thicken considerably. Thus, old vessels dilate and thicken differently at different sites. The big vessels tend to dilate and thicken, while the smaller ones show only wall thickening.

The walls of all arteries have a similar structure and are composed of similar materials, although their proportions vary in different parts of the circulation. The wall is divided into three zones: the tunicas intima, media, and adventitia. The innermost layer, the intima, consists of the endothelium, a single layer of cells that extends as a continuous lining to all blood vessels, and a subendothelial layer containing collagen fibres. The endothelial cells do not play a significant role in the mechanical properties of blood vessels. The subendothelial layer is anchored to the inner boundary of the media. The media is the thickest part of the wall and dominates its mechanical behaviour. Its structure in the large central arteries differs from that in the arteries farther from the heart. For this reason, arteries are generally classified as either elastic or muscular vessels. The transition is not abrupt as one proceeds peripherally, although there may be a sudden transition where a small muscular artery arises from an elastic one (Stehbens, 1979). In elastic arteries the

media consists of multiple concentric layers of elastic tissue (elastin) separated by thin layers of connective tissue, collagen fibres, and sparse smooth muscle cells. In muscular arteries the media is almost entirely composed of spirally wound smooth muscle cells arranged in layers with small amounts of connective tissue, collagen, and elastic tissue between them. The outermost layer of the arterial wall, the adventitia, is often as thick as the media but is less important mechanically. It consists of collagen bundles sparsely interrupted by elastin fibres that merge with the surrounding connective tissue. This region contains the vasa vasorum, small vessels that supply the walls of large arteries with blood.

The mechanical properties of blood vessels are determined by the relative amounts of the various wall constituents, their individual physical properties, and the way in which they are architecturally coupled. About 70% of the weight of the arterial wall is water. This has a negligible effect on the mechanical properties of the wall apart from making it incompressible. Elastin, collagen, and smooth muscle fibres constitute most of the rest of the wall material. The smooth muscle content in large distributing arteries is approximately 25-35%. Its proportion increases in smaller arteries. Although the total content of elastin and collagen remains very nearly constant along the aorta and its major branches, the arteries in the proximal part of the arterial tree, especially those in the thorax, possess more elastin than collagen. As one proceeds peripherally, there is a decrease in elastin and an increase in collagen (Cox, 1979).

Both elastin and collagen are long chains of protein molecules.

Elastin fibres are relatively extensible and are easily stretched by small forces. Collagen is much stiffer. The difference in stiffness between elastin and collagen has been used to explain the fact that arteries are observed to increase in stiffness with stretch. It has been suggested that at low strains the collagen fibres are slack and the stress is born by elastin. As the strain increases the collagen fibres straighten and support the stress. While this explanation is plausible, the nonlinear properties of elastin are likely also of some importance (Cox, 1979). As well as increasing in stiffness with stretch, arteries become stiffer with distance from the heart. An explanation for this phenomenon is also based on the difference in mechanical properties between elastin and collagen. As is noted in the preceding paragraph, the ratio of the elastin to collagen content changes with distance from the heart. The correlation between mechanical properties and elastin-collagen ratio is reasonable for the larger arteries, but it does not hold in general for peripheral arteries (Cox, 1979).

Other factors must contribute as well to the determination of the mechanical properties of blood vessels. One candidate is the architectural arrangement of elastin and collagen fibres within the arterial wall. Unfortunately, little is known at the present time about the contribution of architecture to the mechanical properties of the arterial wall.

While there is a fairly clear relationship between the physical properties of elastin and collagen and the elastic behaviour of the whole artery wall, the influence of smooth muscle on the properties of

larger arteries is a matter of some controversy. A summary of smooth muscle activity is presented in Caro et al. (1978), McDonald (1974), and Cox (1979). Smooth muscle is approximately as stiff as elastin, but its level of stiffness depends on the degree of physiological activity. Smooth muscle contributes little to the axial tension in the wall. Rather, it produces active tension independent of stress. The viscous properties exhibited by arteries, such as stress relaxation, creep, and hysteresis, are attributed primarily to the presence of smooth muscle, although collagen demonstrates viscoelastic behaviour too.

As the arrangement of the various fibres in the arterial wall is very complicated and not homogeneous, it is impossible to deduce the elastic properties of the wall as a whole from those of its constituents. Yet it is necessary to describe the response of the wall to different applied stresses. This is done in the following way. The arterial wall is treated as though it were a homogeneous material, and modelled by a stress-strain law for a homogeneous elastic tube. Then experiments are carried out, either in vitro or in vivo, on intact arterial segments to measure the deformation of the wall as a whole as it responds to known applied stresses. From these measurements, the values of the elastic parameters appearing in the theoretical stress-strain relations can be calculated. Thus, the response of the artery wall to mechanical stress is represented by effective elastic parameters, whose values are the ones that would occur if arteries were indeed homogeneous. In this way, the different constituent parts of the wall are lumped together, insofar as their

mechanical properties are concerned. Most commonly, the theoretical stress-strain relations used to model arteries are linear equations for an isotropic, incompressible, circular cylinder. In this case only a single elastic parameter appears, an effective Young's modulus. Other stress-strain relations have been considered as well. They are discussed in detail by Patel and Vaishnav (1980).

Various techniques that have been developed to study the elastic properties of the whole arterial wall are examined at length in Cox (1979). A very popular method for studying vascular elasticity is to directly measure changes in blood vessel dimension, such as external radius or segment length, that occur with changes in transmural pressure. It is always a distending pressure that is employed in these experiments, since the pressure in arteries in vivo is always greater than the external pressure. The strains that develop in the artery wall as the result of a distending pressure can be determined immediately from the measurements of dimension, while the corresponding stresses can be calculated by means of appropriate equations from the theory of elasticity. Once the stresses and strains in the artery wall are known, it is a straightforward matter to compute the effective elastic parameters used to describe the mechanical response of the wall concisely. For example, in a thin-walled tube where the ratio of wall thickness to tube radius is small, as in arteries, the circumferential stress is approximated by the formula

$$\sigma_\theta = PR/h \,, \qquad (2.1)$$

where P is the distending pressure. The circumferential strain under any circumstances is just the relative change in vessel radius (or diameter), $\Delta R/R_0$, where R_0 is the unstretched radius. Thus, if the wall behaviour is assumed to be linear, isotropic, and incompressible, the only elastic parameter, the effective Young's modulus, is given by

$$E = \frac{PR}{h(\Delta R/R_0)} \quad . \qquad (2.2)$$

It is seen from eqn. 2.1 that the relationship between the circumferential stress and the distending pressure is very simple in a thin-walled tube. Consequently, many researchers who use the technique of inflating segments of blood vessels to study vascular elasticity report the results of their experiments as graphs of distending pressure versus vessel diameter, rather than as graphs of circumferential stress versus circumferential strain. The two sets of graphs will have the same shape except where the circumferential strain is large, since the difference between σ_θ and P arising from the scaling factor R/h is much greater where the strain is large than where the strain is small.

One of the difficulties encountered in the experiments discussed in the preceding paragraph is that their results depend greatly on the presence and nature of constraints to inflation, particularly axial constraints. For example, graphs of pressure versus diameter measured in segments free to lengthen are significantly different from the

graphs obtained when vessels are held at a fixed stretched length, or maintained under a constant axial force (Cox, 1979). Therefore, the nature of the axial constraint on a blood vessel in vivo is an important experimental consideration.

It is well known that arteries are tethered to surrounding tissue and are subjected to considerable longitudinal stretch. When a segment of artery is excised , its length decreases by 30-40%. The tethering greatly inhibits longitudinal wall movement. For this reason, it is common practice in in vitro studies of vascular elasticity to maintain the intact arterial segment at its in vivo length. However, small changes in the length of segments of arteries in vivo have been shown to occur (Cox, 1979). Consequently, some researchers have chosen an alternative approach to conducting in vitro experiments. Rather than keeping its length fixed, they maintain a constant axial force on the vessel. It turns out that the differences in the results obtained from the two methods are not great, particularly with regard to the pressure-diameter relationship (Cox, 1979).

An important arterial property discovered by experiments on vascular elasticity is that the stress-strain law in the vessel wall is not linear. For example, the graphs of circumferential stress versus circumferential strain constructed from the results for inflation experiments are not straight lines. In a typical graph, the slope of the curve remains constant until the strain reaches a critical value. Subsequently, the slope increases with strain. This indicates that arteries respond to stretching by increasing their resistance to further stretch. A similar result occurs in experiments in which the

vessel is kept at a constant radius and stretched longitudinally. The graphs of longitudinal stress versus longitudinal strain constructed from such experiments share the same qualities as the stress-strain curves of the inflation experiments (Caro et al., 1978).

Since the stress-strain law in arteries is not linear, it is not proper to define linear elastic constants, such as a Young's modulus, for the wall material. However, this difficulty can be overcome if only small deformations about some equilibrium state, not necessarily an unstretched one, are being considered. Then the stress-strain relations can be linearized about the equilibrium state, and linear elastic parameters can be defined. They are called **incremental moduli** because in general they will differ from one equilibrium state to another.

As has been mentioned previously, all arteries in vivo are in a state of radial distension, as well as being stretched longitudinally. The physiological range of transmural pressure is 50 to 150 mm Hg, with an approximate mean of 100 mm Hg (1.3×10^4 N/m^2). In this range of pressure, the relationship between circumferential stress and circumferential strain in the artery wall is nonlinear (Caro et al., 1978). However, as we shall see later in this chapter, the wall deformations produced by normal variations in blood flow do not depart much from the distended equilibrium state in vivo. Hence, these deformations may be analysed by linearizing the stress-strain relations for the blood vessel wall about the equilibrium state, and defining incremental elasic moduli to represent the mechanical response of the wall. The only stipulation is that the values used for the incremental

elastic parameters should be those for the appropriate equilibrium state.

Experiments investigating vascular elasticity indicate that not only is the response of the arterial wall to applied stress nonlinear, it is also not isotropic, uniform, or truly elastic. For example, the incremental elastic modulus defined as the ratio of longitudinal stress to longitudinal strain is usually not the same in an artery as the incremental elastic modulus calculated from the ratio of circumferential stress to circumferential strain. This implies that the mechanical properties of blood vessels vary with direction: that is, they are anisotropic. Further evidence to support this claim comes from observations that intact segments of arteries lengthen upon inflation. However, these segments do not change volume during this manoeuvre, so they must be incompressible (Cox, 1979). The two observations would be incompatible in a cylinder composed of an isotropic material as it should shorten under these circumstances. They are consistent only if the mechanical properties of blood vessels are anisotropic.

The anisotropic behaviour of the artery wall is due in part to the wall's nonlinear response. If the vessel is subjected to unequal values of initial strain in different directions, it will appear to be anisotropic even if it is composed of an isotropic material. To see this, suppose that an isotropic cylinder is deformed so that the axial strain is not identical to the tangential strain. Then at this equilibrium state, the incremental axial modulus would be calculated from a different position on the stress-strain curve than would the

incremental tangential modulus. If the stress-strain curve is nonlinear, the values of the two moduli will not be equal, in general. However, even at equal values of wall strain, it has been demonstrated that blood vessels do not behave in an isotropic manner (Cox, 1979).

The mechanical response of arteries, however, is not completely asymmetric. When only normal stresses are applied to a vessel segment, it is observed that negligible shearing strains develop (Patel and Vaishnav, 1980). This suggests that artery walls possess axes of symmetry in the radial, tangential, and longitudinal directions, and that therefore they may be modelled as orthotropic materials. This approach has been explored in detail by Patel and Vaishnav (1980). The incremental elastic moduli for an orthotropic cylinder can be calculated solely from stresses applied circumferentially (by a distending pressure) and longitudinally (by a longitudinal stretch). Under physiological conditions, these are the two directions in which the stresses in a blood vessel are the largest. The radial stress in arteries is much smaller than either the circumferential or the longitudinal stress since artery walls are thin. Despite the fact that arteries ought to be treated as orthotropic materials, the assumption of isotropy remains attractive because of the simplifications that accrue from it.

There is evidence to support the use of isotropy to model the response of the arterial wall under conditions that exist during normal blood flow (Caro et al., 1978; Cox, 1979). At the <u>in vivo</u> state of radial distension and longitudinal stretch, the longitudinal and circumferential moduli are approximately equal. As well, it is the

circumferential elastic modulus that is more important than the longitudinal under normal physiological conditions. The axial constraints exerted on blood vessels *in vivo* inhibit longitudinal wall motions much more than radial ones, so the latter turn out to be dominant. The tangential elastic modulus is relatively independent of axial wall strain, and its values determined from isotropic and anisotropic approaches are reasonably similar in the physiological pressure range. This suggests that an isotropic, incompressible model is a reasonable approximation to the true state of vascular elasticity.

In general, the response of blood vessels to an applied stress is not strictly elastic. Rather, it is viscoelastic, as the response depends upon the rate at which the stress is applied. Arteries display typical properties of viscoelastic materials, namely stress relaxation, creep, and hysteresis. Viscoelastic properties of arteries have been studied in two ways, either as transient responses to abrupt changes in length or force, or as steady-state sinusoidal responses to sinusoidal variations in these quantities. Studies using the latter approach are simpler to perform and therefore more common. The variation in strain induced in an artery wall by a cyclical applied stress lags slightly behind that stress, and is smaller in amplitude than it would be in a purely elastic material. In addition, both the phase and the amplitude ratio between stress and strain depend on the frequency at which the stress is applied. The behaviour of the wall can still be represented by incremental mechanical parameters. However, they must be considered complex-valued and frequency-dependent, rather than real-valued and independent of frequency. For example, in an incompressible, isotropic

model of the viscoelastic response of arteries, there is a complex-valued viscoelastic modulus instead of a real-valued elastic one. The real part of this parameter is the dynamic elastic modulus for the artery, while the imaginary part is the viscous modulus. As is noted above, the phase lag between stress and strain is slight in arteries making the viscous modulus very small compared with the elastic modulus.

Another way to represent the viscoelastic response of arteries is to use phenomenological models. General models of this kind have been developed through the linear theory of viscoelasticity to approximate the stress-strain relation in any viscoelastic material (Pipkin, 1972; Christensen, 1982). The simplest of the phenomenological models utilize mechanical analogues involving springs and dashpots to represent the viscoelastic properties of a continuum. It is often the case that a model containing but a few constants is adequate to cover the response of a given viscoelastic material. This is in sharp contrast to the two empirical functions of frequency that are required to represent the viscoelasticity of the artery wall when the approach described in the preceding paragraph is used. Thus, as long as the viscoelastic response of blood vessels can be represented by a phenomenological model containing only a few parameters, it is preferable to use such a model rather than the one based on frequency-dependent mechanical parameters, even though both methods are equivalent.

A number of researchers have attempted to describe the viscoelastic response of the arterial wall using spring and dashpot

models. Most commonly, the two models considered have been the Kelvin-Voigt and the standard linear solid. They are the least complicated of the phenomenological models, containing just two and three constants respectively. The Kelvin-Voigt model is able to represent the viscoelastic properties of arteries over small ranges of frequency (Caro et al., 1978). The standard linear solid provides a better approximation over a wider frequency range (Chow and Apter, 1968; Cox, 1972). Nevertheless, there has been some criticism of the ability of these two models to adequately predict the viscoelastic response of blood vessels (Cox, 1979). Other models possessing a greater number of parameters have been suggested as more appropriate representatives of arterial viscoelasticity (Westerhof and Noordergraaf, 1970; Cox, 1972; Goodman and Imaeda, 1977).

No consensus has been reached, however, regarding the best phenomenological model for arteries. It is likely that a model containing a distribution of constants is required to fully represent the viscoelastic response of blood vessels (Cox, 1979). However, obtaining such a distribution from measurements of viscoelastic response is extremely difficult. It requires a level of accuracy that has not yet been achieved in experimental studies. For this reason, the two simplest phenomenological models, the Kelvin-Voigt and the standard linear solid, remain the most popular models used to approximate the viscoelastic properties of arteries.

An interesting and important characteristic of the mechanical properties of arteries is their regional variation. For example, the elastic modulus of arteries increases with distance from the heart as a

rule. As one moves from the ascending aorta distally to its bifurcation at the iliac junction there is a continuous rise in the value of the elastic modulus. In addition, there may be a sharp increase in stiffness at those junctions where a muscular artery arises from an elastic one. As is noted earlier in this chapter, this variation in stiffness may be partly related to the fact that the relative proportion of elastin to collagen varies with position in the circulation. The principal effect of the increase in elastic modulus with distance from the heart lies in its contribution to the amplification of the arterial pulse as it propagates away from the heart.

The mechanical properties of the larger arteries vary not only with position in the circulation, but also with age. In the thoracic aorta at the mean physiological pressure (100 mm Hg), the incremental Young's modulus increases steadily with age. More peripherally, however, there is either no change or a fall (Caro et al., 1978). Learoyd and Taylor (1966) have argued that these observations are consistent with the hypothesis that the arterial wall grows weaker with age. The thoracic aorta becomes dilated as it grows older, as is noted previously. The apparent increase in stiffness, then, is a reflection of the nonlinearity in the stress-strain relation for this vessel, as the equilibrium state for the old artery has shifted to the right along its stress-strain curve where the elastic modulus is greater. However, if the elastic moduli for the thoracic aorta are compared at different ages for a fixed value of the vessel radius, there is a significant decrease with age. Thus, the weakening of this artery as it grows

older is masked by the effects of its dilation. In the peripheral arteries this dilation does not occur, so the decrease in elastic modulus is apparent immediately.

We conclude this section on the geometric and mechanical properties of the large arteries with a very brief description of the mechanical properties of blood. Much more detail can be found in Caro et al. (1978) and McDonald (1974). Blood is a suspension of formed elements in plasma. These formed elements, namely red cells, white cells, and platelets, occupy about 45% of the volume of blood. In vessels whose diameters exceed 0.01 cm, blood can be regarded as effectively homogeneous, because the scale of the microstructure is so much smaller than that of the flow (Pedley, 1980). The remaining question to be answered is whether or not blood in large vessels behaves as a Newtonian fluid: that is, is the ratio of shear stress to shear rate independent of shear rate? It is found that the measured viscosity is independent of shear rate, provided the shear rate is sufficiently large, about 100/s (Pedley, 1980). Under the flow conditions that exist in large arteries, the shear rate usually exceeds this critical value, although exceptions occur near the centre of a straight vessel, and during that short part of the cardiac cycle when the flow is very near zero. The importance of temporary non-Newtonian effects in blood on unsteady arterial fluid dynamics has not been investigated. Therefore, blood is generally assumed to act as a Newtonian fluid (Pedley, 1980).

The density of blood does not vary appreciably under normal conditions in the cardiovascular system. Changes in pressure lead to

wall deformation rather than to fluid compression. This observation is explained by the enormous difference in magnitude between the resistance of blood to compression and the resistance of the arterial wall to distension. The resistance of blood to compression, as characterized by its bulk modulus, is very nearly that of water, or about 10^9 N/m^2. On the other hand, the resistance of the arterial wall to distension is approximately Eh/2R, or about 10^5 N/m^2 (McDonald, 1974). Therefore, the changes in the density of blood that occur with variations in pressure in the circulatory system are insignificant compared with the corresponding changes in strain in the artery wall. Consequently, blood can be treated as an incompressible fluid.

In summary, we reiterate that there is a great deal of variability in the properties of the cardiovascular system. The dimensions and mechanical response of arteries vary greatly with age and body size, as well as with the site in the circulation at which they are measured. This variability must be treated with caution when quantitative analyses are undertaken. The problem of measuring as simple a parameter as the wall thickness of an artery illustrates the difficulties encountered in obtaining quantitative information about the cardiovascular system. The principal source of inconsistency in measuring this paramater is the imprecision with which the limits of the outer wall can be defined in relation to the surrounding tissues. This is compounded by the variation the wall thickness shows with species, body size, age, site, blood pressure, and smooth muscle activity. If we wish to calculate a derived parameter such as the Korteweg-Moens wave speed defined in eqn. 1.2, other measurements are

required as well. To calculate c_0, we also need the radius and incremental Young's modulus of the artery wall, and the blood density. These measurements will be subject to a number of biological influences too, and will therefore exhibit scatter. Consequently, a parameter like c_0 may range widely even when it is calculated from accurate and compatible measurements. If it is calculated from poorly chosen data, the result is nonsense.

Blood Pressure and Flow

It is the pressure generated by the heart, sometimes referred to as excess pressure (Caro et al., 1978) and more commonly called 'blood pressure', that is alone responsible for the motion of the blood. The pressure rises rapidly in the left ventricle at the beginning of systole and soon exceeds the pressure in the aorta, causing the valve to open. Blood is ejected, and aortic pressure rises. About half way through ejection, aortic pressure climbs above the pressure in the left ventricle, so that an adverse pressure gradient is established across the aortic valve. This causes deceleration of the outflow, and this is maintained as both pressures fall. A kink in the aortic pressure curve, the dicrotic notch, marks the closure of the aortic valve. Thereafter, the ventricular pressure falls very rapidly as the heart muscle relaxes, while aortic pressure falls more slowly as blood flows out peripherally. The sequence of events is illustrated by the pressure records in Fig. 12.13 of Caro et al. (1978).

Measurements of pressure made instantaneously at a number of sites along the aorta are shown in Fig. 12.14 of Caro et al. (1978). The

pulse is seen to be delayed with distance down the vessel, indicating that it is propagated along the aorta as a wave. The shape of the pressure pulse changes dramatically as it propagates. The amplitude increases, the front becomes steeper, and the dicrotic notch is lost. The mean pressure, that is, the pressure averaged over a cardiac cycle, falls very gradually. These changes continue as the pulse wave passes into the other large arteries.

Measurements of the radial expansion and contraction of the arterial wall accompanying the passage of the pressure wave have been recorded simultaneously with measurements of the pressure within the vessel. It is observed that the motion of the wall is virtually in phase with the pressure. There is little evidence of the hysteresis that might be expected on account of the wall's viscoelastic properties. The change in radius is small. The relative change in radius, that is, the circumferential strain, is about 7% (Caro et al., 1978). This observation justifies the use of a linear theory to describe the mechanical behaviour of the wall. The radial wall motions associated with the pressure wave also cause some longitudinal motions of the vessel wall as it is stretched or compressed, but these are secondary and have negligible influence on the propagation of the wave (Caro et al., 1978).

In order to complete this description of the normal physiological conditions existing in large arteries, it is necessary to consider the blood flow along the aorta and its branches. In Fig. 12.16 of Caro et al. (1978), the pressure and flow-rate are shown in the ascending aorta close to the aortic valve. Forward motion of blood in the ascending

aorta begins when the aortic valve opens and blood is ejected from the ventricle. Acceleration at the beginning of ejection is abrupt and short-lived. An analogy has been drawn of a column of blood being struck by a hammer. It is not entirely inappropriate (Caro et al., 1978). The velocity rises rapidly to a peak and promptly, but more slowly, falls again. There is a brief period of backward flow as the aortic valve closes, and then the blood comes almost to rest for the remainder of the cardiac cycle.

At any location in the cardiovascular system, the motion of blood is driven by the local pressure gradient, which in turn is determined by the propagation of the pressure pulse. In Fig. 12.19 of Caro et al. (1978), records of the pressure and average velocity, that is, the velocity averaged over the tube's cross-section, are displayed at points progressively farther from the heart. The amplitude of the velocity waveform decreases continuously, in contrast to the peaking and steepening of the pressure pulse. Initially, the pressure and flow-rate rise in phase with each other, but thereafter they diverge considerably. The peak of the flow wave precedes that of the pressure wave. Moreover, the velocity drops more rapidly than the pressure. The brief period of backflow remains throughout the length of the aorta. It is thought that the arrival of reflected components of the pressure wave have a part in these differences. As well, the gradual stiffening and tapering of the aorta probably has an effect (Caro et al., 1978).

It is interesting to compare the velocity of blood flow with that of the pulse wave. Table I of Caro et al. (1978) gives measured values

of the wave speed c and the peak averaged blood velocity $\bar{v}_{max}$ at various sites in the canine cardiovascular system. In the ascending aorta the ratio $\bar{v}_{max}/c$ is as large as 0.25. Farther away from the heart, two factors combine to make this ratio decrease to less than 0.1. The wave speed increases since vessels become stiffer toward the periphery. Concurrently, the blood velocity falls. There are pathological conditions under which the values of $\bar{v}_{max}/c$ can be very close to 1. Either the arterial wall is very floppy, so that c is low, or the stroke volume is greatly increased. Under these pathological conditions, the front of the pulse wave becomes very steep and blood velocities well in excess of the usual are recorded.

The importance of the ratio of average blood velocity to pulse wave velocity, $\bar{v}/c$, arises from the question of whether the motion of blood can be approximated by linear equations. Of all the terms in the equations of motion for an incompressible Newtonian fluid, the only nonlinear ones are the convective acceleration terms. Their magnitude, relative to that of the local acceleration terms, is $\bar{v}/c$. Hence, it is reasonable to neglect the convective acceleration terms when $\bar{v}/c$ is very small. Thus, the assumption of linearity in analysing pulse wave propagation under normal conditions is appropriate, except possibly in the ascending aorta.

It is noted above that the word 'average', when used as an adjective to describe 'blood velocity', refers to the cross-sectional average. The flow-rate is just the average velocity multiplied by the artery's cross-sectional area. It is much easier to measure the

flow-rate than the axial velocity at a particular point in the cross-section of a blood vessel. As a result, considerably more data is available on the average velocity at various stations in the large arteries than on the local velocity. Nevertheless, recent technological advances have enabled experimentalists to obtain accurate measurements of the local blood velocity more easily.

The most popular place to measure local velocity has been the centre of an artery. A sequence of velocity waveforms, measured on the centre-lines of the arteries in question, is displayed together with the corresponding pressure waveforms in Fig. 12.26 of Caro et al. (1978). Their general features are similar to those seen in Fig. 12.19 of Caro et al. (1978), except that they show more fluctuations. This indicates that some of the high frequency components in the waveforms have been averaged in time by the flow meters recording the average velocities.

The average velocity over the artery's cross-section and the local velocity at the centre of the vessel will be approximately the same if, and only if, the velocity profile is virtually flat over most of the vessel cross-section with very thin boundary layers at the wall. In the largest arteries this is the case. A fairly flat profile, presumably surrounded by a thin boundary layer, is observed throughout the cardiac cycle in the ascending aorta. Marked skews in the velocity profile develop in the aortic arch. It is thought that they are produced as a consequence of the curvature of the arch and the branches issuing from it. Profiles in the descending aorta remain flat during systole. Apparently, the large branches upstream exert little

influence in this regard. The profile tends to be rounder with distance from the heart. In the abdominal aorta, the velocity profiles reflect the complexity of the local geometry with marked skews and asymmetries. Just downstream, the mesenteric, coeliac, and renal arteries branch off the aorta. Closer to the termination of the aorta, the velocity profile during systole is M-shaped. The profile is rounded and approximately symmetric in the iliac artery.

Thus, the presence of relatively flat velocity profiles in most large arteries means that measurements made by a probe only roughly positioned in the centre of the vessel are representative of the centre-line velocity and, that the centre-line velocity is close to the average velocity. In regions of complicated geometry, of course, such a correspondence does not exist.

This concludes the first two parts of the chapter: a description of the geometric and mechanical properties of large arteries, and a description of the blood pressure and flow associated with the propagation of the normal arterial pulse. It is evident that the cardiovascular system is very complicated, both in its mechanical properties and in its geometry. Nevertheless, it shares fundamental features with less complicated systems of tubes. Although the arterial wall is not homogeneous, and its response to applied stresses is, in general, not linear, isotropic, or perfectly elastic, its response to the stresses imposed under normal physiological conditions is very nearly the linear one of a homogeneous, isotropic, elastic tube. A more accurate model of the mechanical response of arteries can be obtained merely by making adjustments to this idealized version.

Similarly, blood is not homogeneous and its response to mechanical stress is not that of a Newtonian fluid. However, it is reasonable to approximate blood as a homogeneous Newtonian fluid under normal conditions of flow in the large arteries. Finally, the geometry of the circulatory system is certainly not that of a straight circular cylinder. Many of the features present in the tortuous course of the arteries, however, including the bends, bifurcations, taperings, and stenoses, can be viewed as short geometric transitions between straight segments.

In modelling physical phenomena, it is, almost without exception, fruitful to consider simple models before introducing the many modifying features present in reality. In the last part of this chapter, we describe a very simple model of wave propagation in large arteries. Then, we introduce various modifications that have been incorporated into the basic theory to account for the observed characteristics of the arterial pulse not predicted by the simple theory. Finally, we stake a claim to the direction undertaken in this dissertation, and outline the features of pulse propagation to be examined in depth.

Mathematical Models of Wave Propagation

The simplest model of pressure wave propagation in large arteries is a linear long wavelength (LLW) theory. A detailed description of this theory is found in Pedley (1980). This theory is appropriate to pressure wave propagation in straight, uniform, elastic tubes containing a homogeneous, inviscid fluid. As is noted in the previous

section, the velocity profiles in large arteries are approximately flat, suggesting that the effect of viscosity is confined to thin boundary layers on the walls. Thus, the neglect of viscosity in the simple model is reasonable. Consequently, only longitudinal variations in the excess pressure

$$p_e = p - p_0 \tag{2.3}$$

are considered. Here, p is the fluid pressure and p_0 its undisturbed value.

When the pressure pulse is sufficiently small, both the wall and the fluid mechanics are approximately linear. If, as well, the wavelengths of all disturbances are large compared with the tube radius, it can be shown that p_e satisfies the classical wave equation

$$\frac{\partial^2 p_e}{\partial x^2} = c_0^{-2} \frac{\partial^2 p_e}{\partial t^2}, \tag{2.4}$$

where the wave speed c_0 is defined by

$$c_0^{-2} = A_0^{-1} \left[\frac{d(\rho A)}{dp_e}\right]_{p_e=0} \tag{2.5}$$

(Pedley, 1980). Here, ρ is the fluid density as stated earlier, x the axial coordinate, t the time and A the tube's cross-sectional

area. The subscript '0' refers to quantities evaluated at $p_e = 0$.

Equation 2.5 can be rewritten as

$$c_0^{-2} = \rho_0\left[\frac{1}{\rho}\frac{d\rho}{dp_e} + \frac{1}{A}\frac{dA}{dp_e}\right]_{p_e=0} = \rho_0(K+D) \quad , \tag{2.6}$$

where K is the compressibility of the fluid and D the distensibility of the tube. The quantity K is the reciprocal of the resistance of the fluid to compression and the quantity D is the reciprocal of the resistance of the tube wall to distension. It is argued in the first part of this chapter that blood can be treated as an incompressible fluid, as $K/D \approx 10^{-4}$: that is, $K + D \approx D$. Then

$$c_0 = [\rho D]^{-1/2} \quad , \tag{2.7}$$

where we have put $\rho_0 = \rho$ = constant. Equation 2.7 is the result derived by Thomas Young. According to this theory, the speed at which pressure waves propagate along blood vessels is governed by a balance between the restoring force generated from the resistance of the arterial wall to circumferential stretch and the axial inertia of blood. If the artery is modelled as a thin-walled isotropic tube, as is usual, $D^{-1} = Eh/2R$. In this case, the wave speed is

$$c_0 = [Eh/2\rho R]^{1/2} \quad , \tag{2.8}$$

the Korteweg-Moens wave speed. If it is assumed that the tube is

prevented from moving longitudinally by external constraints, that is, 'tethered', E must be replaced in eqn. 2.8 by $E/(1-\nu_E^2)$, where ν_E is Poisson's ratio. Further, if the tube is incompressible, $\nu_E = \frac{1}{2}$ and $E = 3G$, where G is the shear modulus. Then, eqn. 2.8 is replaced by

$$c_0 = [2Gh/\rho R]^{1/2} . \qquad (2.9)$$

The general solution of eqn. 2.4 representing waves travelling in the positive x direction is $p_e = f(t-x/c_0)$, where f is a function to be determined by boundary or initial conditions. Thus, pressure waves propagate through a single uniform tube without distortion at the constant velocity c_0. The values of c_0 predicted from eqn. 2.8 are given in Table I of Caro et al. (1978) for comparison with values of c measured in the canine cardiovascular system. In the large arteries the measured value of c differs from c_0 by no more than 15%, well within normal experimental error and physiological variability. This suggests that the simplifications introduced into the theory are not sources of great inaccuracy in the calculation of wave speed.

According to the LLW theory, not only does the pressure pulse remain undistorted as it is transmitted, but the velocity pulse is identical to the pressure pulse with the exception that its amplitude is scaled by the factor $1/\rho c_0$. In fact, it is evident from Figs. 12.14, 12.19, and 12.26 of Caro et al. (1978) that the pressure wave and velocity wave change shape as they propagate through the large

arteries. As well, the shape of the velocity pulse is not the same as that of the pressure pulse and the amplitude of the velocity pulse falls with distance from the heart whereas that of the pressure pulse initially rises.

One factor cited as a source of the distortion in the pressure pulse and the velocity pulse is wave reflection at junctions and other sites of geometric or mechanical transition in the arterial tree. Reflections in a system of uniform tubes containing sites of abrupt geometric or mechanical change can be accounted for in the LLW theory by applying appropriate conditions across these discontinuities. Thus, the LLW theory predicts that waves are reflected at any location where there is a change in the local (characteristic) impedance

$$Z = \rho c_0 / A \ . \tag{2.10}$$

If two tubes of impedance $Z^{(1)}$ and $Z^{(2)}$ are connected, the ratio of the reflected to the incident pressure wave is

$$R_c = [1 - Z^{(1)}/Z^{(2)}]/[1 + Z^{(1)}/Z^{(2)}] \tag{2.11}$$

while the ratio of the transmitted to the incident pressure wave is[4]

$$T_c = 2/[1 + Z^{(1)}/Z^{(2)}] \ . \tag{2.12}$$

The ratio of the impedances $Z^{(1)}/Z^{(2)}$ is called the discontinuity

coefficient λ_c .

The rate of energy transfer in the reflected wave relative to that in the incident wave is R_c^2 . Similarly, the rate of energy transfer in the transmitted wave relative to that in the incident wave is $\lambda_c T_c^2$. Thus, R_c^2 is called the reflection coefficient and $\lambda_c T_c^2$ the transmission coefficient. It follows from eqns. 2.10 and 2.11 that

$$R_c^2 + \lambda_c T_c^2 = 1 \ . \qquad (2.13)$$

This demonstrates that no energy is lost at a discontinuity using this theory.

It is predicted by the LLW theory that a major site of reflection encountered by the pulse wave as it travels down the human aorta is the aortic bifurcation. The reflection coefficient is largest at this junction. The total cross-sectional area of the two iliac arteries is less than that of the abdominal aorta by as much as 20%. As well, the iliac arteries are stiffer than the abdominal aorta. The wave speed in the former is at least 10% greater than in the latter. Thus, the value of R_c at the aortic bifurcation is greater than zero, approximately 0.16. Hence, a positive reflection occurs: that is, the reflected pressure wave takes the same sign as the incident pressure wave. Meanwhile, the reflected velocity wave is opposite in sign to the incident velocity wave. A positive reflection at the aortic bifurcation is consistent with the observed increase in amplitude of the pressure pulse as it moves away from the heart, and with the corresponding drop in the flow-rate pulse. Moreover, it is argued by

Mills et al. (1970) that a step seen in the descending part of the velocity wave (see Fig. 12.26 of Caro et al., 1978) is the mark of a wave reflected from the iliac bifurcation. On the other hand, the pressure waveforms measured by Mills and his colleagues contain so many fluctuations that it is difficult to interpret any one as a reflection from the termination of the aorta.

It is evident, then, that the LLW theory has some merit as a model of arterial pulse propagation. Its estimate for the velocity of the pulse is very good. Moreover, the changes in amplitude demonstrated by the pressure and flow pulses are consistent with the explanation that these pulses are reflected at various sites in the circulation, such as the aortic bifurcation. Nevertheless, wave reflection alone is unable to predict accurately the following features observed in the pulses as they travel through the large arteries: amplification and steepening of the pressure pulse, attenuation of the velocity pulse, phase difference between the peaks of the pressure and velocity pulses, spreading of the pulse waves, and progressive smoothing of fluctuations in the pulses. Thus, other factors must be involved that modify the predictions of this simple theory. We discuss four of them below.

1. In the simple theory, it is assumed that the properties of the fluid and the tube wall are uniform. Arteries are not uniform along their length. In particular, the aorta becomes narrower and stiffer as one moves away from the heart. This tapering is at least partly responsible for the peaking of the pressure pulse (Caro et al., 1978).

2. The simple model does not account for the dissipation of energy as a result of viscous losses in the fluid and the tube wall.

Dissipative mechanisms in blood and in the arterial wall are capable of making significant contributions to the attenuation observed in the velocity pulse.

3. In the simple theory, the only mechanical property of the tube wall considered is its resistance to circumferential stretch. The inertia of the vessel wall and other elastic features, such as the wall's resistance to bending, are not included. When these properties are incorporated into the simple model, a dispersive theory of wave propagation is obtained. In a dispersive theory, the shape of a pulse is modified as it evolves (Whitham, 1974).

4. Finally, nonlinearities have not been accounted for in the LLW theory. As is discussed in the first two parts of this chapter, there are two sources of nonlinear behaviour in the circulation. The first is the convective acceleration of blood along the axis of the vessel. The second comes from the wall mechanics. Since the arterial wall becomes stiffer with stretch, its distensibility depends on the state of strain and hence, on the blood pressure. Nonlinearities are not expected to be of great influence in the normal pulse, but they could produce some of the changes in the pulse's shape, such as the steepening.

The nonlinear theories concentrate mainly on the mechanics of the fluid and neglect, for example, the viscoelastic, bending, and inertial effects of the wall. The principal method for incorporating nonlinear features is to reduce the governing equations for the fluid to one-dimensional equations. Thus, as is also the case in the LLW theory, the velocity and pressure are represented by their averages

over the tube's cross-section. The fluid equations are augmented by an equation relating the cross-sectional area of the tube to the transmural pressure. This equation captures the nonlinear resistance to circumferential stretch demonstrated by arteries, but it neglects all other mechanical properties of the arterial wall. This formulation is precisely the one proposed by Euler. This model can be solved by the method of characteristics, unknown in Euler's time, as the set of governing equations form a hyperbolic system. Lambert (1958) was the first to solve this model of blood flow using the method of characteristics. Unfortunately, his choice of numerical parameters was unrealistic and consequently his results were also (Skalak et al., 1981).

The principal prediction arising from this theory is that nonlinearities cause the front of the wave to steepen. Such steepening is commonly observed in the aorta and other large arteries, but it is not thought to be of great importance in normal subjects (Caro et al., 1978). In patients whose arteries are abnormally distensible or in whom the amplitude of the pulse is very large, the steepening can be quite important. In the model, the steepening ultimately generates a shock. However, the nondissipative equations from which the existence of this discontinuity is predicted break down before the shock actually occurs, as the neglected dissipative terms become important.

The model described above can be modified to incorporate dissipation by inserting an empirical friction term into the equation of motion for the fluid (Streeter et al., 1963; Olsen and Shapiro, 1967). The friction term usually used is either the one for

quasi-steady laminar flow or the one for quasi-steady turbulent flow. These choices may lead to inaccuracies as blood flow is unsteady. Another source of dissipation is wall viscoelasticity. Internal friction in the wall has proven to be more difficult to incorporate into nonlinear models than fluid friction. For one thing, the use of even the simplest linear model of viscoelasticity complicates the set of characteristic equations associated with the governing equations to such an extent that they can no longer be integrated directly (Pedley, 1980). More importantly, it is very difficult to develop nonlinear constitutive relations for viscoelastic materials. Holenstein et al. (1980) have attempted to surmount these difficulties by introducing a semi-empirical creep funttion to represent the viscoelastic properties of the arterial wall. However, their model is not truly nonlinear as they assumed linearity in the viscoelastic response of arteries. Although they claim better agreement with observation for their model than had been obtained previously with elastic models, the success of their approach in predicting pulse attenuation accurately remains open to debate (Pedley, 1984).

The nonlinear one-dimensional model of Euler can be refined to include not only dissipative effects, but also the nonuniformity and repeated branching of the arterial tree. The latter two properties of the circulatory system are modelled by treating the arteries as tapered porous tubes. This idea was introduced by Streeter et al. (1963) and developed further by Skalak and Stathis (1966). It was extended by Anliker et al. (1971) in a thorough investigation of the canine

systemic circulation. The same approach has been employed by Stettler et al. (1981) in a model of the human arterial pathway extending from the heart to the foot. The results of computer simulations of models of this sort always show a broad qualitative agreement with experiment (Pedley, 1980). They clearly show peaking and steepening of the pressure pulse, and development of considerable reverse flow in the abdominal aorta. A decline in peak velocity with distance from the heart, however, is not seen except in the viscoelastic model of Holenstein et al. (1980).

The shortcomings in the predictions of these nonlinear models reflect inadequate treatment of not only the fluid viscosity, but more importantly, the mechanical properties of the arterial wall. On the other hand, it is precisely the wall mechanics that are of greatest importance in linear theories of arterial pulse propagation. These linear theories are capable of describing elastic phenomena other than just the wall's resistance to circumferential stretch. Furthermore, viscoelasticity can be consistently incorporated into the stress-strain relations for the wall with the use of linear phenomenological models. Even fluid viscosity can be handled in the linear theory without resorting to empirical methods. This is accomplished by including the radial motions of the fluid, as well as the axial, in the governing equations.

The linear models follow the approach of Young, as is illustrated in the earlier discussion of the LLW theory. Hence, it is assumed in these models that the tube wall deforms very slightly from some equilibrium position. Moreover, the convective acceleration of the

fluid is ignored. Thus, linear equations describing the fluid motion are combined with linear elastic or viscoelastic equations governing the deformation of the wall.

In general, the linear theories are two-dimensional as they model axisymmetric fluid motion in a circular cylindrical tube. The only component of fluid velocity considered to be insignificant is the one in the tangential direction. In some models, however, the velocity and pressure are represented by their averages over the tube's cross-section, as they are in the nonlinear theories. These models, then, are only one-dimensional.

An example of a one-dimensional linear model is the simple one of the LLW theory, in which the tube is treated as a uniform, thin-walled, isotropic, elastic membrane and the fluid as inviscid. Only the radial motion of the tube wall and the longitudinal motion of the fluid are represented in this model. The LLW theory can be extended to two dimensions by including the longitudinal motion of the tube wall and the radial motion of the fluid in the governing equations. The two-dimensional model is analysed most easily by seeking travelling wave solutions to its set of governing equations. These travelling wave solutions are assumed to be proportional to $\exp[i(kx-\omega t)]$, where k is the wave number and ω is the circular frequency of the given wave. In order for such travelling wave solutions to exist, k and ω must be related. The relation between k and ω is called the **dispersion equation** (Whitham, 1974) or, in the older literature, the 'frequency equation'. With each solution of the dispersion equation there is associated a mode of vibration of the fluid-filled tube.

The principal result of this two-dimensional extension of the LLW theory is that two modes of vibration are predicted. The two modes are distinguished by the direction of the principal movement of the tube wall. In one mode, the wall vibrates primarily in the radial direction whereas the wall motion is mainly longitudinal in the other model. When the waves are very long, the mode that is primarily radial propagates with the velocity c_0 derived by Young. For this reason, it is usually called Young's mode. The other mode travels at a greater velocity. In honour of the person who first demonstrated the existence of longitudinal waves in a fluid-filled tube (Lamb, 1898), this mode is called Lamb's mode. This mode is not observed in arteries in situ, however, on account of the longitudinal tethering of the surrounding tissue mass (Caro et al., 1978). Hence, Lamb's mode is usually omitted from linear theories applied to arterial wave propagation.

The LLW theory can be modified in another way by including dissipative mechanisms in the model of wave propagation. Linear theories that incorporated wall viscoelasticity and/or fluid viscosity into the equations of motion were introduced by a number of authors during the first half of the twentieth century. Brief reviews of this collection of work are given in McDonald (1974) and Cox (1969). Some models were one-dimensional and others were two-dimensional. Those models that accounted for fluid viscosity were two-dimensional as they required the radial motion of the fluid, as well as the axial, to be present in the governing equations. The most general linear theories to include dissipative effects in their models of wave propagation were produced independently by Morgan and Kiely (1954) and Womersley (1955).

As the latter article considered the details of fluid motion as well as those of wave propagation and described its results within the context of the dimensions of the arterial tree, the conclusions of this paper rather than those of the former provide the basis for the discussion of wave propagation in large arteries presented below.

In Womersley's paper, as well as in Morgan and Kiely's, it is the contribution of fluid viscosity to wave propagation in fluid-filled distensible tubes, not that of wall viscoelasticity, that receives primary consideration. In fact, Womersley did not even represent wall viscoelasticity in his model of wave propagation while Morgan and Kiely mention it only in passing. Womersley found that the principal effects of fluid viscosity are to reduce the speed of propagation of a given wave and to attenuate it. Further, fluid viscosity causes a phase difference between the peak of the pressure wave and the peak of the flow-rate wave. The flow-rate wave leads. If the flow-rate is calculated from the observed pressure gradient at a given site in the circulation, it is found to match the observed flow-rate very well, even when the wall is treated as a rigid tube (McDonald, 1974). The shape of the pressure waveform, of course, is a consequence of wall elasticity.

The predictions of Womersley's theory stem from the dispersion equation for his model. The presence of fluid viscosity is noticed immediately in the dispersion equation. This relation, strictly real in the absence of dissipation, becomes complex when fluid viscosity appears. Therefore its solution, yielding, for example, k as a function of ω, is complex. Hence, a single wave of frequency ω is

modulated by the factor $\exp[-(\text{Im } k(\omega))x]$ as it propagates along the tube. As the imaginary part of k remains positive for all ω, the wave is always attenuated. The attenuation is evidently frequency-dependent, as is the phase velocity $c = \omega/\text{Re } k$.

Womersley identified the parameter

$$\alpha = R(\omega/\nu)^{1/2} , \qquad (2.14)$$

where ν is the kinematic viscosity of the fluid, as the single parameter controlling the behaviour of the phase velocity and the attenuation. For $\alpha > 3$, the phase velocity is approximately equal to the Korteweg-Moens wave speed c_0, as is seen in Fig. 11.3 of McDonald (1974). For $\alpha < 3$, however, the curve representing c as a function of α falls steeply. Thus, the higher frequency components in a disturbance will travel with greater speed than the lower frequency components. This phenomenon is called dispersion. In large arteries, however, the condition $\alpha > 3$ holds for all of the components of the arterial pulse (Caro et al., 1978). Hence, the shape of the pulse is not changed significantly as a result of the dispersion caused by fluid viscosity.

The impact of fluid viscosity on wave attenuation is of much greater importance than its impact on the velocity of wave propagation. The attenuation introduced by fluid viscosity is predicted to be measurable even in the largest arteries. As is evident from the discussion above, waves decay by the factor $\exp[-(\text{Im } k)\lambda]$ as they travel a distance equal to their wavelength λ. This decay

decreases with increasing α, that is, with increasing frequency. The attenuation per unit distance, however, increases as frequency is increased. For example, a wave of frequency 2 Hz is predicted to be attenuated by only 5% through the length of a dog's aorta. On the other hand, for waves in the frequency range 40-100 Hz the attenuation is predicted to be 24-33% through the same length (Caro et al., 1978). The decrease in wavelength with increasing frequency is responsible for this apparent paradox.

It is interesting to compare the attenuation predicted by Womersley's theory with the attenuation observed in arteries. A number of experiments have been conducted to measure attenuation characteristics in arteries (McDonald, 1974). Most of these experiments are performed over the range of frequencies that exist in the natural pulse wave. In the dog, this means a frequency range of 2-20 Hz. A few experiments have been performed at much higher frequencies, that is, over the range 40-150 Hz. The results of the studies conducted over these widely separated frequency bands are compatible. They demonstrate that a far greater degree of damping exists in the circulation than is predicted by Womersley's theory. Attenuation derived from the effects of fluid viscosity can account for only 1/4 to 1/3 of the damping observed (McDonald, 1974). The additional attenuation is believed to be associated with dissipative mechanisms in the vessel wall.

The introduction of viscoelastic, as opposed to purely elastic, tube wall properties can be accomplished in a straightforward manner in linear theories by exploiting the connection between the viscoelastic

material parameters and their elastic counterparts. When this connection is used to introduce viscoelasticity into Womersley's model, it is only the Young's modulus E that is changed. This modulus is no longer a real-valued constant. Rather, it becomes the frequency-dependent complex-valued quantity $E_R + i\omega E_I$, where E_R and E_I can be functions of frequency. Consequently, the result of wall viscoelasticity is to increase the phase velocity slightly, by the factor $1 + \frac{1}{2}\omega^2 E_I^2/E_R^2$, and to increase the imaginary part of k by the amount $\pi\omega E_I/E_R$. In measurements of arterial viscoelasticity performed over the frequency range of the natural pulse, $\omega E_I/E_R$ lies between 0.1 and 0.2. This is the same order of magnitude that is predicted for $\omega E_I/E_R$ from the experiments measuring attenuation characteristics discussed in the preceding paragraph. For this reason, wall viscoelasticity has been adopted as the most important source of attenuation in the cardiovascular system, with fluid viscosity playing a secondary role.

The description of Womersley's theory given above has concentrated on predictions of the characteristics of wave propagation in a single uniform tube. To be valuable as a model of wave propagation for the arterial system, however, Womersley's theory must be able to handle wave reflection from sites of geometric and mechanical discontinuity. It turns out that this theory can be adapted to deal with wave reflection at sites of abrupt geometric and mechanical change in the same way that the LLW theory has been adapted (Womersley, 1957b). The application and interpretation of Womersley's linear theory to the arterial system has been thoroughly developed. The details are

discussed in the books by McDonald (1974) and Caro et al. (1978). Comparisons of predictions based on Womersley's theory with observations from experiments have been very good. This supplies strong support for the hypothesis that the relationship between pressure and flow-rate in the circulation is a linear one.

M.G. Taylor has used Womersley's theory as a foundation for employing transmission line equations to model wave propagation in the arterial system, and has discussed wave reflections from this point of view. As the transmission line equations are one-dimensional, this approach is not unlike that of the nonlinear theories mentioned earlier. In particular, it is possible to incorporate the aorta's tapering and increase in stiffness along its length into the governing equations by using techniques analogous to those employed for treating nonuniform transmission lines. For further details concerning the work of Taylor, the interested reader may consult McDonald (1974).

During the 1960's, many extensions of Womersley's original model were proposed. These linear theories were produced in an attempt to account for the transmission characteristics of the normal arterial pulse more precisely. Efforts were concentrated on developing more general models for the response of the arterial wall, as it was understood that the mechanical properties of the wall dominate the behaviour of the pulse. Womersley's model for the wall was the same as that of the LLW theory: a thin-walled isotropic elastic membrane. It is evident from the discussion in the first part of this chapter that while such a model is a reasonable first approximation for the response of arteries to mechanical stress, blood vessels really behave in a more

complicated fashion. For this reason, Womersley's theory of wave propagation in arteries was modified by a number of authors to include the effects of a thick wall, initial stresses, anisotropic wall properties, and viscoelasticity.

A comprehensive review of the literature appearing in the 1960's is given in the article by Cox (1969). Most authors characterized the propagation characteristics of their model by means of two quantities, the phase velocity c and the transmission coefficient per wavelength $\exp[-(\text{Im } k)\lambda]$. These quantities were usually plotted as functions of frequency to illustrate the results of the analyses. Cox compared the various theories and found that they all shared the qualitative behaviour of Womersley's model.

The results of Cox's study provide additional support for the use of the thin-walled, isotropic, elastic membrane model of the artery wall in the description of the normal arterial pulse. Of course, wall viscoelasticity must be included in order to model wave attenuation accurately, as is discussed above. The influence of wall thickness, however, is insignificant at the values of the ratio h/R pertinent to large arteries. Furthermore, the effects of initial stresses and wall anisotropy on the propagation properties of the normal pulse are also negligible (Atabek, 1968), with the following exception: the Korteweg-Moens wave speed c_0 is dependent on the state of initial stress in the artery. This dependence can be dealt with very easily, however, by choosing a value for the incremental Young's modulus based on the initial state of stress, as is discussed in the first section of this chapter. We conclude, therefore, that the arterial pulse is

adequately modelled by representing the blood vessel wall as a thin-walled, isotropic, viscoelastic membrane.

It is evident, then, that the understanding of the normal arterial pulse wave is fairly complete. Consequently, it would seem that there is little left to be done regarding the matter of wave propagation in large arteries. It is at this point that the following question rears its ugly head: what about arterial wave propagation at frequencies outside the band represented in the normal pulse wave? The question is not merely an academic one. As is noted in Chapter I, the natural pulse has a very short frequency range. It can be described very accurately by 10 harmonic terms (Caro et al., 1978). This means that, in humans, the frequency range of the arterial pulse is approximately 1-10 Hz while in the dog it is roughly 2-20 Hz. On the other hand, it is pointed out in Chapter I that researchers studying wave propagation in the arterial system have artificially generated disturbances containing frequencies of up to 150 Hz. Moreover, some of the energy in the artificial pulse used in the experiments of Greenwald and Newman (1982) is concentrated near $\omega = 0$, that is, at frequencies lower than those existing in the normal pulse wave. Thus, it is also of considerable practical interest to study arterial wave propagation at frequencies below and above those encountered in the natural pulse.

Unfortunately, the analyses of arterial wave propagation discussed so far in this chapter are not able to resolve the question raised in the preceding paragraph. It is not the models themselves that are unsatisfactory: rather, their validity is limited to the frequency range of the normal pulse as a result of the simplifying assumptions

introduced in the course of obtaining solutions to the governing equations of the models.

The problems with typical analyses of arterial wave propagation stem from the approximations made in solving the dispersion equation of the particular model being examined. For one thing, when a viscous fluid is involved, the dispersion equation is often simplified by assuming that α^2 is much greater than $|kR|^2$, where α is the Womersley parameter defined in eqn. 2.14. This is a reasonable assumption as long as ω is not too small. However, when ω is very near to zero the assumption may not be warranted. Consequently, the solution to the dispersion equation may not be valid under these circumstances.

Another assumption always made in analyses of arterial wave propagation is that the nondimensional quantity $\omega R/c_0$ is very small. This assumption is equivalent to the long wavelength condition mentioned in Chapter I. As a typical value of the ratio R/c_0 in large arteries is 5×10^{-4} s, it is evident that the long wavelength condition is always satisfied in the normal pulse wave. However, at a frequency of 50 Hz, $\omega R/c_0 \approx 0.15$. This is a bit large to justify confidently the use of the long wavelength condition. At frequencies greater than 50 Hz, confidence in the suitability of this condition is undermined even further. The violation of the long wavelength condition produces an error in the typical solution of the dispersion equation in the following way. The dispersion equation is usually solved by determining k as a function of ω in terms of powers of

$\omega R/c_0$. Terms of up to order $O((\omega R/c_0)^2)$ are retained and higher order terms dropped. The phase velocity, then, consists of a term of order $O(1)$ and a term of order $O(\omega R/c_0)$. If the quantity $\omega R/c_0$ is not very small, however, the higher order terms are not insignificant. Some of them may have to be included in the solution for k in order to obtain results that are sufficiently accurate.

It is evident, then, that conventional analyses of arterial pulse propagation have produced solutions that are inadequate outside the frequency band contained in the normal pulse. These solutions are not justified at either very small frequencies or very large ones. This problem has been addressed in a pair of recent papers by Rubinow and Keller (1971, 1978). Their description of linear wave propagation in fluid-filled distensible tubes is the most complete in the literature. Their model is based on the linearized equations of motion for a compressible, viscous fluid augmented by the linear viscoelastic equations for an isotropic vessel wall of arbitrary thickness, suitably specialized to an axially symmetric geometry. It is presumed that an arbitrary constraint is exerted on the outer surface of the tube wall. Under the assumption that the tube is thin-walled, and for appropriate choice of the external constraint, the equations governing the motion of the wall reduce to those of a tethered, isotropic, viscoelastic membrane. The general theory of Rubinow and Keller is valid, however, at all frequencies.

Rubinow and Keller demonstrated that an infinite number of modes of wave propagation can exist in their fluid-filled distensible tube

model. Only two of these are tube modes. The rest are acoustical. The acoustical modes depend on the compressibility of the fluid for their existence while the tube modes depend on the distensibility of the tube wall. At very long wavelengths, the pair of tube modes turn into Young's mode and Lamb's mode respectively. When the speed of sound in the fluid is large, that is, when the fluid's bulk modulus is large, the acoustical modes have little influence on the tube modes and, in fact, exist at very high frequencies only. This confirms that the usual assumption of fluid incompressibility is a good one for blood or water.

The thrust of the two papers by Rubinow and Keller was aimed toward establishing the nature of the dependence of the roots of the dispersion equation on the physical properties of the arterial system. They were particularly interested in the following pair of parameters: the circular frequency ω and the kinematic fluid viscosity ν. Part of their analysis was directed toward analysing the dispersion relation in the limiting case $\omega \to 0$, $\nu \to 0$. They discovered that the dependence of k_0 on ω and ν is not uniform at $\omega = 0$, $\nu = 0$. This result had not been acknowledged before in the literature. It follows from their analysis that the solution of the dispersion equation obtained under the assumption of an inviscid fluid is not correct at $\omega = 0$, as every fluid possesses some viscosity: that is, in the limiting case $\omega \to 0$, $\nu \to 0$, the proper root of the dispersion equation is obtained by taking the limit as $\omega \to 0$ first, then the limit as $\nu \to 0$. If the order of the limits is inverted, the corresponding root is incorrect. Nevertheless, Rubinow and Keller

demonstrated that Young's velocity c_0 gives an accurate prediction of the speed of the natural pulse, as the phase velocity in a viscous fluid is not much different from c_0 at the frequencies contained in this pulse. Their conclusion confirms that of Womersley discussed earlier in this section. Although Rubinow and Keller accounted for the viscoelastic properties of the vessel walls in their model, they did not investigate the influence of viscoelasticity on wave propagation in any detail.

One of the strengths of Rubinow and Keller's work is that they not only analysed the roots of the dispersion equation for various limiting cases of the parameters involved, but they also computed the roots of this equation numerically over a broad range of frequency. Thus, their results are valid well beyond the frequency range of the normal pulse wave, both above and below this limited frequency band. In particular, their analysis is valid for the frequencies present in the disturbances cited above that are generated artificially.

Rubinow and Keller limited their analysis of wave propagation in fluid-filled distensible tubes to considerations of steady-state oscillations at a fixed frequency. They characterized their results by means of two quantities, the phase velocity $c = \omega/\mathrm{Re}\, k$ and $\mathrm{Im}\, k$. The latter variable controls wave attenuation. The variation of c and $\mathrm{Im}\, k$ with ω, and the dependence of the two quantities on other parameters important in the arterial system, was illustrated with a variety of graphs. In this respect, Rubinow and Keller did not advance beyond the approach employed by most authors writing in the 1960's.

It is true, of course, that general solutions can be constructed from the steady-state ones given by Rubinow and Keller through the technique of Fourier superposition. However, this is more easily said than done. The behaviour of the Fourier integral solutions of wave transmission in their fluid-filled distensible tube model is not obvious, as the integrands are very complicated. Consequently, if these general solutions are to be studied in detail, one must resort to numerical integration.

Rubinow and Keller's model is so all-encompassing, however, that it contains several parameters that have not been evaluated experimentally. These parameters are involved with the nature of the constraint exerted on the external wall of the vessel. As the cost of conducting a numerical study to determine the influence these parameters have on wave propagaton is prohibitive, it seems wiser to consider a special case of Rubinow and Keller's model. A good choice would be to model the vessel wall as a tethered, isotropic, viscoelastic membrane. It has been suggested previously in this section that this model gives a reasonable approximation to the response of the arterial wall, at least for the frequencies present in the normal pulse. It is still not straightforward, however, to use Rubinow and Keller's analysis to compute general solutions of wave propagation in such a fluid-filled tube model.

The major stumbling block lies in their technique for solving the dispersion equation. The dispersion equation must be solved at each value of ω required in the numerical integration of the Fourier integrals mentioned above. As a very large number of points will be

needed in this numerical integration, the solution of the dispersion equation must be obtained as efficiently as possible. The optimal approach is to solve the dispersion equation analytically. However, Rubinow and Keller calculate analytical solutions only over very short frequency ranges. The bulk of their solutions are obtained numerically. As the dispersion relation is a complex-valued transcendental equation, the calculation of its solution numerically is not a simple procedure. Consequently, the cost of evaluating the Fourier integrals that require this solution would be astronomical.

For this reason, we seek to develop analytical solutions of the dispersion equation describing wave propagation through an incompressible, viscous fluid contained in a tethered, incompressible, isotropic, viscoelastic tube over a fairly wide range of frequencies in this dissertation. To be specific, the range of frequencies of interest are those involved in the experiments of Greenwald and Newman (1982) cited in Chapter I. In fact, so as to err on the side of caution, it will be assumed that the nondimensional parameter $\omega R/c_0$ lies in the interval

$$0 \leq \omega R/c_0 \leq 1.5 \ . \qquad (2.15)$$

For the typical tube mentioned previously in which $R/c_0 \approx 5\times10^{-4}$ s, this means that the frequency range is 0-500 Hz.

The approach taken here to modelling wave propagation in fluid-filled distensible tubes will not parallel the one displayed in

Rubinow and Keller's papers (Rubinow and Keller, 1971; Rubinow and Keller, 1978), in which the dispersion equation plays the dominant role. Rather, this thesis follows the path travelled in a series of papers by Moodie and his colleagues, as illustrated clearly in Moodie et al. (1982): that is, it is the transient response of the fluid-filled tube that is emphasized.

In the paper cited above, Moodie and his colleagues presented an investigation of the transient response of a simple bending theory model of a viscoelastic tube containing an inviscid fluid. Thus, they considered not only membrane effects, but also the influence of higher order terms involving rotatory inertia and flexural rigidity in the mechanical response of the tube wall. In a related paper (Moodie et al., 1985), it was demonstrated that immediately after the onset of a disturbance, those higher order terms have a negligible impact on the subsequent propagation of the pressure pulse when the frequencies contained in the pulse satisfy the condition expressed in eqn. 2.15. This conclusion establishes support for the claim that a tethered, isotropic, viscoelastic membrane is a reasonable model for the arterial wall not only over the frequency range of the normal pulse, but also over the much broader range represented by eqn. 2.15.

The practical importance of investigating the transient response of arteries to disturbances containing frequencies in the range 0-250 Hz is derived from impulse techniques that have been employed in experimental studies of wave propagation in the cardiovascular system. Impulse methods were utilized by several researchers in the 1950's (McDonald, 1974), but thereafter fell into disuse. It is only very

recently that these techniques have been reintroduced to investigate arterial wave propagation. A summary of some typical experiments is given below.

In a series of recent papers (Greenwald and Newman, 1982; Newman et al., 1983; Greenwald et al., 1985), propagation and reflection phenomena in water-filled latex tubes were analysed by means of impulse techniques. The impulse generated is of very short duration, roughly 5 ms. As arterial propagation velocities typically lie between 4 and 10 m/s, the incident pulse and any reflected components may be adequately resolved even when the pressure measurement site is only a few centimetres from the reflection site (Greenwald and Newman, 1982). The evolution of a typical pulse is shown in Fig. 1 of Newman et al. (1983). The pulse undergoes a pronounced change in shape with transmission. It broadens, is attenuated, and its oscillatory tail is damped as the wave travels down the tube. The same general pattern for this pulse wave has been observed in canine aortas (Newman et al., 1981). These observations give strong evidence that wave propagation is a dispersive and dissipative phenomenon.

Nevertheless, Fourier analysis of these pressure pulses did not confirm the dispersive character of impulse propagation (Newman et al., 1983; Greenwald et al., 1985). For example, the phase velocity in the latex tubes of Newman et al. (1983) was apparently independent of frequency over the frequency range 5-100 Hz. Moreover, the ratio of the amplitudes of the reflected and incident waves varied little with frequency in the reflection experiments described in the same paper. They increased by only 10% over the frequency range analysed there.

These results sound a warning that the propagation properties of pulses cannot be ascertained adequately from graphs of phase velocities and transmission coefficients plotted as functions of frequency. Sometimes a small change in the frequency dependence of these quantities results in a substantial change of character in the pulse as a whole, as is demonstrated in Moodie et al. (1985). Under other circumstances, larger changes in the frequency dependence have little qualitative effect on the pulse.

The tests carried out by Moodie and his colleagues (Moodie et al., 1984; Moodie et al., 1986) demonstrate the success of their theory in predicting the transmission characteristics observed in a pressure impulse generated at the entrance of a very long water-filled latex tube. However, fluid viscosity is not accounted for in their theory. This thesis explores the role of fluid viscosity in the propagation of pressure pulses of the sort generated in the experiments of Greenwald and Newman (1982), and contrasts that role with the one of wall viscoelasticity. To accomplish this, the influence of viscosity and viscoelasticity is investigated not only with regard to the evolution of a pressure pulse as it travels down a tube, but also with regard to the reflection and transmission of the pulse at discontinuities in the tube. Then, the results of these analyses are compared with experimental observations of propagation and reflection phenomena. Finally, further experiments are suggested to test the theory developed here more deeply.

CHAPTER III

Mathematical Formulation of the Problem

The aim of this dissertation is put forward and discussed in detail in the preceding two chapters. Here, we reiterate our fundamental query: what is the role of fluid viscosity in the propagation of pressure pulses through fluid-filled distensible tubes? In order to answer this question, an appropriate model of the transient response of a fluid-filled distensible tube is required. The mathematical formulation of such a model forms the content of this chapter.

The present analysis has its roots in the work of Moodie and his colleagues (Moodie et al., 1982; Moodie et al., 1985) wherein the motion of a viscoelastic tube containing an inviscid fluid is investigated. The model of a fluid-filled distensible tube employed in this thesis is the same one developed by Moodie and his colleagues, except that their model is extended here to include a viscous fluid. Consequently, the papers of Moodie et al. have been relied on heavily in the preparation of the following derivation of this model.

Basic Assumptions

We start the derivation by delineating the basic physical assumptions underlying the model. The vessel containing the fluid is assumed to be a tethered circular cylinder. The wall of this vessel is assumed to be composed of a material that is incompressible, isotropic, homogeneous, and viscoelastic. This cylindrical wall is assumed to be thin, in that the ratio of the wall thickness to the internal diameter

of the cylinder is small. The fluid contained within the tube is assumed to behave as an incompressible Newtonian fluid. It is evident from the discussion in Chapter II that not only are these assumptions appropriate for the latex rubber tubes used by Greenwald and Newman (1982) and many other researchers, they are also reasonable in the case of arteries.

The viscoelastic response of the tube is modelled as that of a Kelvin-Voigt solid. This is the simplest model where the response to a change in stress after a sufficiently long period of time has elapsed is elastic rather than viscous (Pipkin, 1972). Under conditions of very rapid change in stress or strain, the Kelvin-Voigt solid is not an appropriate viscoelastic model as its response to an instantaneous change in stress is not elastic (Pipkin, 1972). However, such conditions are not of interest in this dissertation. Here, we are interested in studying disturbances whose frequency spectra are contained in the low to medium frequency range defined by eqn. 2.15. The Kelvin-Voigt solid is adequate to model viscoelasticity in a material subjected to disturbances in this frequency range. In fact, as is demonstrated subsequently, at low frequencies any linear viscoelastic solid tends to behave as a Kelvin-Voigt material. We emphasize, however, that our analysis is not restricted to a particular viscoelastic model in that more elaborate ones can be handled with minor alterations.

The model of the transient response of a fluid-filled distensible tube formulated in this chapter is a linear one. Thus, it is restricted in its validity to small amplitude perturbations about an

equilibrium state. Furthermore, all perturbations are axisymmetric and their frequency content is assumed to be in the low to medium frequency range mentioned in the preceding paragraph. These assumptions about the disturbances to be investigated here are applicable to most experiments studying the mechanics of wave propagation in the cardiovascular system, whether the experiments are carried out in latex tube models or in the arteries themselves. In particular, the conditions outlined above are satisfied by the pressure impulses used in the experiments of Greenwald and Newman (1982).

Before deriving the governing equations for our model of a fluid-filled distensible tube, it is necessary to describe this tube and the motions therein more precisely. Consider a uniform thin-walled circular cylindrical tube containing a fluid, as illustrated in Fig. 3.1. The axis of the tube is taken to be horizontal and in the x-direction. The radius of the middle surface of the vessel wall is denoted by R. The density and wall thickness of the tube are γ and h respectively. The wall material is assumed to behave as an incompressible Kelvin-Voigt linear viscoelastic solid. The mechanical model representing this Kelvin-Voigt solid is depicted in Fig. 3.2. Thus, the viscoelastic properties of the wall are characterized by a retardation time τ and an equilibrium shear modulus G_e. The fluid is assumed to be incompressible and viscous with dynamic viscosity μ and density ρ.

The initial state of the fluid-filled tube is one in which the fluid is at rest and the tube is undeformed. This state is chosen as the equilibrium state about which the small-amplitude perturbations

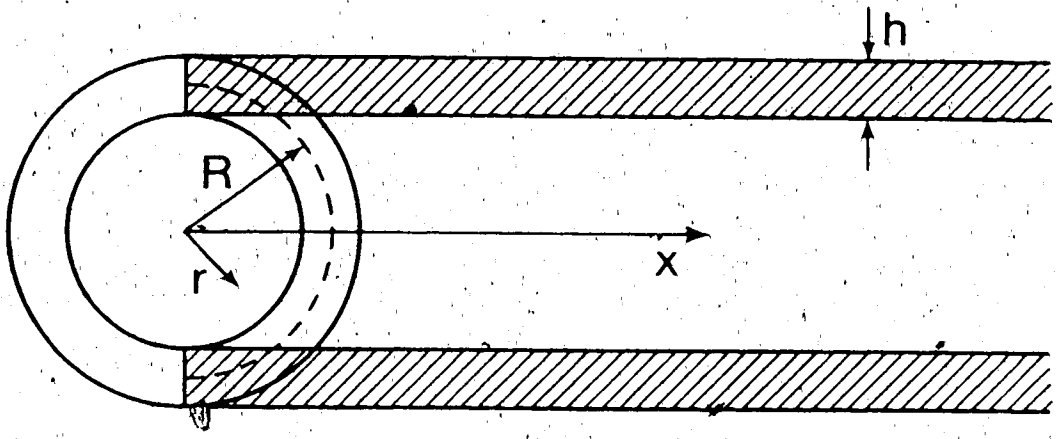

Fig. 3.1. Geometry of the undeformed vessel.

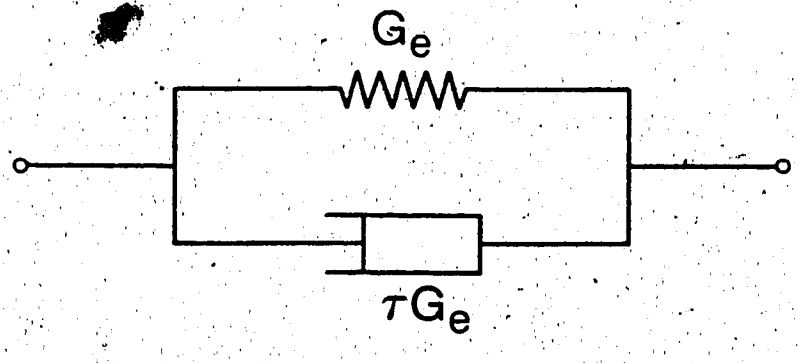

Fig. 3.2. Mechanical model for a Kelvin-Voigt solid.

occur. The analysis can be readily adapted, however, for a different choice of equilibrium state. In Chapter II it is pointed out that, for the most part, the effects of an equilibrium state involving initial stresses can be accounted for by suitably altering the Korteweg-Moens wave speed c_0.

An axisymmetric perturbation of the initial state in which the fluid is at rest and the tube undeformed results in a pressure perturbation $p(r,x,t)$ from the unperturbed uniform pressure in the tube. Here r is the radial coordinate measured from the axis of the tube and t is the time. Let $v_x(r,x,t)$ and $v_r(r,x,t)$ respectively be the axial and radial components of the corresponding perturbation in fluid velocity. The radial displacement of the tube wall from its undeformed position is denoted by $w(x,t)$. As the tube is assumed to be 'tethered', axial motion of the wall is ignored.

A typical disturbance in the fluid-filled tube is depicted schematically in Fig. 3.3. The motion involves four dependent variables: p, v_x, v_r, and w. These variables satisfy equations of motion describing the response of the tube to an axially symmetric perturbation from the undeformed state. The equations of motion consist of a set of equations governing the dynamics of the vessel wall and a set of equations governing the dynamics of the fluid. The two sets of equations are linked by conditions that apply at the interface between the fluid and the solid.

The formulation of a model representing the transient response of a fluid-filled distensible tube is not complete without prescribing initial and boundary conditions to supplement the equations of motion.

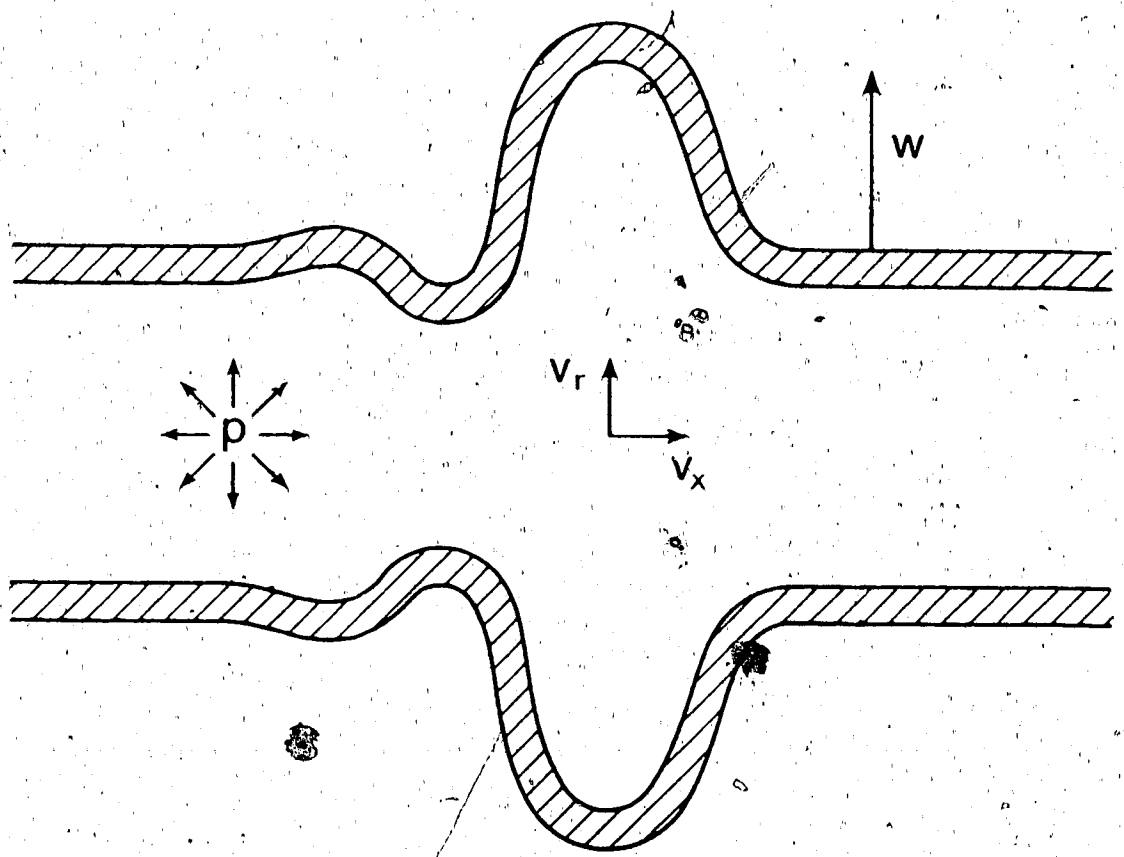

Fig. 3.3. Schematic view of motion in the tube.

These conditions describe the specific disturbance that generates motion in the tube as well as the effect that the ends of the tube have on this disturbance.

Thus, the problem to be solved in this dissertation is posed mathematically by the equations of motion for the fluid-filled tube together with the initial and boundary conditions. The remaining sections in this chapter are spent deriving these equations and conditions.

Wall Equations

The first set of equations we derive are those governing the dynamics of the vessel wall. As a consequence of the connection between the respective constitutive equations for a viscoelastic material and an elastic one, a formal similarity exists between the equations of motion for a linear viscoelastic solid and those for a linear elastic solid. The material constants appearing in the elastic case are simply replaced by linear operators in the viscoelastic one (Christensen, 1982). Therefore, we first consider the governing equations for an elastic wall and then make use of the aforementioned formal similarity to obtain the governing equations for a viscoelastic wall.

The full set of equations governing the motion of the wall of an elastic tube is three-dimensional. As the vessel wall is assumed to be thin, this set of equations can be reduced to two dimensions by making use of shell theory. In shell problems, it is advantageous to employ a coordinate system formed by two axes in the middle surface of the shell

and a third axis normal to the middle surface. When the shell is thin, it is reasonable to integrate the three-dimensional equations along the third axis over the width of the shell to obtain an averaged set of equations that is two-dimensional.

Many shell theories have been developed, corresponding to a variety of approximations of the integrals involved. Here, we have chosen to use the shell equations derived by Moodie et al. (1982) for a tethered tube. Their derivation follows the approach introduced by Herrmann and Mirsky (1956). As the motion of the shell is assumed to be axially symmetic, these equations are one-dimensional.

In the article by Moodie and his colleagues, two sets of shell equations were produced. One set retains the effect of the shear deformation of the wall while the other set omits this effect. In order to study the influence of shear deformation on wave propagation, Moodie et al. (1982) solved a sample initial-value problem. They found very little difference in the radial displacement of the tube wall, whether or not shear was taken into account. They gave the following explanation for this result. When shear deformation is included in the shell equations, two modes of wave propagation exist. In the solution of the initial-value problem, the amplitude of one mode is considerably greater than the amplitude of the other. Over the range of frequencies encountered in the problem, the phase velocity of the dominant mode is nearly the same as that of the single mode arising when shear deformation is neglected. Consequently, shear has little influence on the waves propagating through the tube. Therefore, Moodie and his colleagues concluded that the neglect of shear deformation was

justified for disturbances contained in the frequency band present in their initial-value problem. As the frequency band considered here covers but a small portion of the former band, it follows that we, too, may neglect shear deformation in our problem.

Therefore, we introduce the following elastic shell equation, as given by Moodie et al. (1982), to describe the motion of the tethered incompressible vessel wall:

$$4G\left[\frac{h}{R^2}w + \frac{h^3}{12}\frac{\partial^4 w}{\partial x^4}\right] = P - \gamma h\frac{\partial^2 w}{\partial t^2} + \frac{\gamma h^3}{12}\frac{\partial^4 w}{\partial x^2 \partial t^2} . \qquad (3.1)$$

In eqn. 3.1, G is the elastic shear modulus while P, strictly speaking, refers to the net radial stress across the tube wall, directed outwardly. If the fluid contained within the tube is assumed to be inviscid, however, P is just the transmural pressure as is noted in Chapter II.

Equation 3.1 represents a balance of the radial forces acting on the shell wall. Starting from the left and omitting P, the terms depict in turn the contributions of the wall's flexural rigidity, circumferential stiffness, radial inertia, and rotatory inertia to this balance. The effects of certain of these terms on wave propagation are not significant over the frequency range considered here. Greater detail regarding this point will be provided later in this section.

The viscoelastic shell equation for the vessel wall is now obtained from the elastic one by using the formal similarity that exists between the viscoelastic and elastic equations to replace the

elastic constant G in eqn. 3.1 with the appropriate viscoelastic linear operator $\hat{G}$. To determine the viscoelastic operator $\hat{G}$ associated with the elastic constant G, we compare the linear stress-strain relation for the elastic solid with that of the viscoelastic solid. For an incompressible, isotropic, elastic solid, the linear stress-strain law is

$$\sigma_{ij} = 2G\epsilon_{ij} , \tag{3.2}$$

where σ_{ij} are the deviatoric stress components and ϵ_{ij} the deviatoric strain components. The most general formulation of the corresponding constitutive relation for a viscoelastic solid is

$$\sigma_{ij} = 2 \int_{-\infty}^{t} G(t-t') \frac{d\epsilon_{ij}(t')}{dt'} dt' , \tag{3.3}$$

where $G(t)$ is the relaxation function for the viscoelastic material (Christensen, 1982). For convenience, we have omitted explicit reference to spatial dependence in eqn. 3.3. A comparison of eqns. 3.2 and 3.3 reveals that $\hat{G}$ is the integral operator defined by

$$\hat{G}y = \int_{-\infty}^{t} G(t-t') \frac{dy(t')}{dt'} dt' . \tag{3.4}$$

Equation 3.4, then, is the most general representation of $\hat{G}$.

In order to make use of the general form for $\hat{G}$, $G(t)$ must be

specified. Unfortunately, it is not an easy matter to determine the relaxation function for a given viscoelastic material. In particular, no general relaxation function has been constructed for the artery wall, as is mentioned in Chapter II. For that matter, relaxation functions for latex rubber tubes of the sort used by Greenwald and Newman (1982) have not been constructed either. Consequently, we are free here to make our own choice for $G(t)$.

Our choice for $G(t)$ is the simplest one possible, namely the relaxation function for a Kelvin-Voigt solid: that is,

$$G(t) = G_e[H(t) + \tau\delta(t)], \tag{3.5}$$

where $H(t)$ represents the Heaviside step function and $\delta(t)$ the Dirac delta function (Pipkin, 1972). The factors that motivated our selection of $G(t)$ are outlined in the introduction to this chapter. Other reasonable choices of $G(t)$ could have been made, however. In particular, the relaxation function for the standard linear solid is popular in studies of wave propagation through viscoelastic tubes (Chow and Apter, 1968; Moodie et al., 1982). As well, we could have chosen relaxation functions for more complicated viscoelastic models that have been put forward as appropriate representatives of arterial viscoelasticity (Westerhof and Noordergraaf, 1970; Cox, 1972; Goedhard and Knoop, 1973; Goodman and Imaeda, 1977).

It is our contention, however, that the influence of any of these viscoelastic models on wave propagation over the frequency band considered here will not be much different from that of the

Kelvin-Voigt solid. This statement is based on a property of the Kelvin-Voigt solid mentioned earlier in this chapter without justification: any linear viscoelastic solid tends to behave as a Kelvin-Voigt solid at low frequencies. We demonstrate that the Kelvin-Voigt solid does indeed possess this feature by means of the arguments marshalled below.

Consider the general constitutive law for a linear viscoelastic solid as given by eqn. 3.3:

$$\sigma = 2 \int_{-\infty}^{t} G(t-t') \frac{d\epsilon(t')}{dt'} dt' , \qquad (3.6)$$

where σ is one of the stress components and ϵ one of the strain components. In preparing to analyse the general behaviour of a viscoelastic solid implied by eqn. 3.6, we list several restrictions imposed on $G(t)$ from considerations of its role as a relaxation function for the viscoelastic solid (Christensen, 1982).

Since the asymptotic behaviour of the viscoelastic solid as $t \to \infty$ is assumed to be that of an elastic solid,

$$\lim_{t \to \infty} G(t) = G_e \neq 0 . \qquad (3.7)$$

As well, it is assumed that the stress depends more strongly on the recent past than on the distant history of the strain. This is called the hypothesis of **fading memory**. This assumption is satisfied if

$$\left| \frac{dG}{dt} \right|_{t=t_1} \leq \left| \frac{dG}{dt} \right|_{t=t_2} , \quad \text{for} \quad t_1 > t_2 > 0 . \tag{3.8}$$

Finally, in the situation considered here, resting conditions are presumed to hold prior to $t = 0$. Hence,

$$G(t) = 0 , \quad \text{for} \quad t < 0 . \tag{3.9}$$

The same physical considerations that led to the restrictions on $G(t)$ contained in eqns. 3.7 - 3.9 require conditions to be imposed on σ, ε, and their derivatives. Firstly, it is assumed that σ, ε, and their derivatives remain finite as $t \to \infty$, since the behaviour of the viscoelastic solid is assumed to be elastic as $t \to \infty$. Secondly, it is assumed that σ, ε, and their derivatives vanish for $t < 0$, as the solid is assumed to be at rest until $t = 0$.

The behaviour of a linear viscoelastic solid having the properties outlined above is most easily analysed by using Fourier transforms, and making appropriate approximations for low frequency. To this end, we define the transform pair $f(t)$ and $\bar{f}(\omega)$ by

$$\bar{f}(\omega) = \int_{-\infty}^{\infty} f(t) e^{i\omega t} \, dt , \tag{3.10}$$

$$f(t) = \frac{1}{2\pi} \int_{-\infty+i\Delta}^{\infty+i\Delta} \bar{f}(\omega) e^{-i\omega t} \, d\omega , \tag{3.11}$$

where $\Delta = \text{Im}\ \omega > 0$ is chosen sufficiently large that the path of integration in the complex ω-plane passes above all of the singularities of $\bar{f}(\omega)$.

If $f(t)$ vanishes for $t < 0$ and remains finite as $t \to \infty$, it can be shown that $\bar{f}(\omega)$ exists for all $\Delta > 0$. However, $\bar{f}(\omega)$ does not exist when $\Delta = 0$ unless $f(t) \to 0$ sufficiently rapidly as $t \to \infty$. Thus, the functions of interest to us, namely G, σ, ε, and their derivatives, do possess Fourier transforms when $\Delta > 0$ but not necessarily when $\Delta = 0$. This technique of using Fourier transforms involving the complex variable ω is equivalent to the more common practice of using Laplace transforms performed in the variable $s = -i\omega$.

We now apply the Fourier transform, defined by eqn. 3.10, to the stress-strain relation for a linear viscoelastic solid given by eqn. 3.6. In doing so, we observe that eqn. 3.6 involves the convolution of G with $\frac{d\varepsilon}{dt}$. Therefore, according to the convolution theorem, the Fourier transform of eqn. 3.6 is

$$\bar{\sigma}(\omega) = 2\bar{G}(\omega)[-i\omega\bar{\varepsilon}(\omega) - \varepsilon(0)] , \qquad (3.12)$$

with the use of the well-known rule for the transform of a derivative. As resting conditions apply prior to $t = 0$, we assume that $\varepsilon(0) = 0$: that is, there is no jump in strain at $t = 0$. In this case, eqn. 3.12 becomes

$$\bar{\sigma}(\omega) = -2i\omega\bar{\varepsilon}(\omega)\bar{G}(\omega) \ . \qquad (3.13)$$

Thus, in the transform domain, the influence of the relaxation function $G(t)$ is made more clear.

If the motion being investigated contains solely low frequency components, it is necessary to know $\bar{G}(\omega)$ as a function of ω only in the neighbourhood of $\omega = 0$. It is possible to approximate $\bar{G}(\omega)$ for small $|\omega|$ by expanding it as a truncated series in powers of ω. We accomplish this by following a procedure described in Pipkin (1972). First, observe that

$$\int_0^\infty G_e \, e^{i\omega t} dt = -\frac{G_e}{i\omega} \ . \qquad (3.14)$$

Consequently,

$$\bar{G}(\omega) = -\frac{G_e}{i\omega} + \int_0^\infty (G(t) - G_e)e^{i\omega t} dt \ , \qquad (3.15)$$

as $G(t)$ vanishes for $t < 0$. Next, take only the zeroth order term in the expansion for $e^{i\omega t}$ in powers of ω: that is, $e^{i\omega t}$ is approximated as

$$e^{i\omega t} = 1 + O(\omega) \ . \qquad (3.16)$$

Then, eqn. 3.15 becomes

$$\bar{G}(\omega) = -\frac{G_e}{i\omega} + \eta_v \,, \tag{3.17}$$

where

$$\eta_v = \int_0^\infty (G(t) - G_e)dt \,. \tag{3.18}$$

It is assumed that $G(t) \to G_e$ sufficiently rapidly as $t \to \infty$ that the integral in eqn. 3.18 converges. The quantity η_v is the coefficient of viscosity for the viscoelastic solid.

In this way, a two-term expansion for $-i\omega\bar{G}(\omega)$ has been obtained, namely

$$-i\omega\bar{G}(\omega) = G_e - i\omega\eta_v = G_e(1 - i\omega\tau) \,, \tag{3.19}$$

where $\tau = \eta_v/G_e$ is the retardation time alluded to previously. Thus, the stress-strain in the transform domain, given by eqn. 3.13, is approximated at low frequencies as

$$\bar{\sigma}(\omega) = 2G_e(1 - i\omega\tau)\bar{\varepsilon}(\omega) \,. \tag{3.20}$$

This is precisely the transformed stress-strain law for a Kelvin-Voigt solid, as is demonstrated below.

The relaxation function for a Kelvin-Voigt solid is given in eqn. 3.5. The coefficients G_e and τ there are the same ones appearing in eqn. 3.19. With the use of eqn. 3.10, the transform of $G(t)$ as described in eqn. 3.5 is

$$\bar{G}(\omega) = -\frac{G_e}{i\omega} + G_e\tau \ . \qquad (3.21)$$

Therefore, with the substitution of eqn. 3.21 into eqn. 3.13, the transformed stress-strain law for a Kelvin-Voigt solid is

$$\bar{\sigma}(\omega) = 2G_e(1 - i\omega\tau)\bar{\varepsilon}(\omega) \ . \qquad (3.22)$$

This result is exactly eqn. 3.20. Thus, we conclude that at low frequencies all linear viscoelastic solids behave as Kelvin-Voigt solids.

We turn now to the problem of determining the viscoelastic operator $\hat{G}$ associated with the Kelvin-Voigt solid. When $G(t)$ from eqn. 3.5 is substituted into the equation providing the general representation for $\hat{G}$, namely eqn. 3.4, the result is

$$\hat{G}y = G_e(y + \tau\frac{dy}{dt}) \ . \qquad (3.23)$$

Thus, in the case of a Kelvin-Voigt solid, $\hat{G}$ is simply the linear differential operator

$$\hat{G} = G_e(1 + \tau\frac{\partial}{\partial t}) \ . \qquad (3.24)$$

It is seen from eqn. 3.24 that the viscoelastic operator $\hat{G}$ reduces to

the elastic constant G in the limiting case $\tau = 0$, as G_e and the elastic shear modulus G are one and the same.

Equation 3.24 establishes the particular viscoelastic operator $\hat{G}$ used in this thesis. Consequently, we are finally ready to return to the problem of obtaining the viscoelastic shell equation for the vessel wall. As is noted earlier, the viscoelastic shell equation is simply the elastic shell equation with G replaced by $\hat{G}$. Hence, according to eqn. 3.1, the viscoelastic shell equation is

$$4G_e\left(1 + \tau \frac{\partial}{\partial t}\right)\left[\frac{h}{R^2} w + \frac{h^3}{12} \frac{\partial^4 w}{\partial x^4}\right] = P - \gamma h \frac{\partial^2 w}{\partial t^2} + \frac{\gamma h^3}{12} \frac{\partial^4 w}{\partial x^2 \partial t^2} . \qquad (3.25)$$

We now take the opportunity to clarify a remark about the shell equation made earlier in this section. It was stated previously that the effects of certain of the terms in the shell equation on wave propagation are not significant over the frequency range considered in this dissertation. The terms alluded to are those representing the wall's flexural rigidity and rotatory inertia: $\frac{h^3}{12} \frac{\partial^4 w}{\partial x^4}$ and $\frac{\gamma h^3}{12} \frac{\partial^4 w}{\partial x^2 \partial t^2}$. Almost immediately after the onset of a disturbance that does not contain high frequencies, these terms cease to contribute in a quantitative sense to the motion of the vessel wall (Moodie et al., 1985). Hence, they are not included in the subsequent analysis.

Therefore, the viscoelastic shell equation considered here is

$$4G_e\left(1 + \tau \frac{\partial}{\partial t}\right)\frac{h}{R^2} w = P - \gamma h \frac{\partial^2 w}{\partial t^2} . \qquad (3.26)$$

The fact that bending moments are ultimately omitted from the shell equation means that, in the end, the vessel wall is treated as a membrane.

Fluid Equations

The equations governing the motion of the incompressible, viscous fluid contained within the tube are the Navier-Stokes equations, together with the continuity equation. Their axisymmetric forms are

$$\frac{\partial v_r}{\partial t} + v_r \frac{\partial v_r}{\partial r} + v_x \frac{\partial v_r}{\partial x} = -\frac{1}{\rho}\frac{\partial p}{\partial r} + \nu\left[\frac{\partial^2 v_r}{\partial r^2} + \frac{1}{r}\frac{\partial v_r}{\partial r} - \frac{v_r}{r^2} + \frac{\partial^2 v_r}{\partial x^2}\right], \qquad (3.27)$$

$$\frac{\partial v_x}{\partial t} + v_r \frac{\partial v_x}{\partial r} + v_x \frac{\partial v_x}{\partial x} = -\frac{1}{\rho}\frac{\partial p}{\partial x} + \nu\left[\frac{\partial^2 v_x}{\partial r^2} + \frac{1}{r}\frac{\partial v_x}{\partial r} + \frac{\partial^2 v_x}{\partial x^2}\right], \qquad (3.28)$$

$$\frac{\partial v_x}{\partial x} + \frac{\partial v_r}{\partial r} + \frac{v_r}{r} = 0 , \qquad (3.29)$$

where $\nu = \mu/\rho$ is the kinematic viscosity of the fluid.

The only nonlinear terms in these equations are the convective acceleration terms: $v_r \frac{\partial v_r}{\partial r} + v_x \frac{\partial v_r}{\partial x}$ in eqn. 3.27 and $v_r \frac{\partial v_x}{\partial r} + v_x \frac{\partial v_x}{\partial x}$ in eqn. 3.28. We can estimate the magnitudes of these convective acceleration terms, relative to those of the corresponding local

acceleration terms $\frac{\partial v_r}{\partial t}$ and $\frac{\partial v_x}{\partial t}$, by adopting the same approach as Womersley (1955). In this method, trial solutions proportional to $\exp[i(kx-\omega t)]$ are assumed for all of the variables appearing in eqns. 3.27 - 3.29. These trial solutions enable us to determine the relative magnitudes of the spatial and temporal derivatives of the variables involved. For example, $\frac{\partial v_x}{\partial x} \sim k\, O(v_x)$ and $\frac{\partial v_x}{\partial t} \sim \omega\, O(v_x)$. Further, we estimate $\frac{\partial v_x}{\partial r}$ to be no larger than $\frac{1}{R} O(v_x)$. Similar estimates apply to the other variables. In addition, $\frac{v_r}{r}$ is assumed to be no larger than the order of $\frac{\partial v_r}{\partial r}$.

When these estimates are applied to the continuity equation, eqn. 3.29, it is clear that $v_r \sim kR\, O(v_x)$. Therefore, $v_r \frac{\partial v_r}{\partial r} \sim kv_x\, O(v_r)$ and $v_x \frac{\partial v_r}{\partial x} \sim kv_x\, O(v_r)$. Consequently, the ratio of the convective acceleration terms to the local acceleration terms in eqn. 3.27 is kv_x/ω. This ratio is of the order of magnitude of v_x/c, since the ratio $\omega/Re\, k$ is just the phase velocity c. The same estimate obtains in eqn. 3.28. Thus, neglecting the nonlinear terms in the governing equations for the fluid is equivalent to assuming that the ratio

$$\frac{v_x}{c} \ll 1 . \qquad (3.30)$$

The restriction imposed earlier in this chapter stating that the

disturbances in the fluid-filled tube must be sufficiently small that a linear theory is valid means, then, that these motions must satisfy the inequality 3.30.

The maximum value of the local axial velocity is always larger than $\bar{v}$, the axial velocity averaged over the tube's cross-section. Consequently, if the phase velocity c is of the same order of magnitude as the Korteweg-Moens wave speed c_0, the condition

$$\frac{\bar{v}}{c_0} \ll 1 \tag{3.31}$$

is approximately equivalent to the condition 3.30. It is condition 3.31 that is usually cited as the criterion for neglecting the convective acceleration terms in the fluid equations. This is reasonable in the case of the normal arterial pulse or the impulses generated by Greenwald and Newman (1982), since c_0 is of the same order of magnitude as the measured phase velocity c in these pulses as is discussed in Chapter II.

An estimate of the magnitude of the viscous terms in the fluid equations can be obtained by using the same approach that yielded an estimate for the magnitude of the convective acceleration terms. Note that the viscous terms are the terms in brackets in eqns. 3.27 and 3.28. It turns out that the ratio of the viscous terms to the local acceleration terms is $\nu/\omega R^2$. Now the kinematic viscosity of whole blood is $\nu = 3.79\times10^{-2}$ cm^2/s (Patel and Vaishnav, 1980), about four times that of water. In a typical latex rubber tube, $R = 0.4$ cm

(Newman et al., 1983). Hence, over the frequency range 0-500 Hz, $\nu/\omega R^2$ varies from very large to very small.

Thus, the viscous terms can be much larger than the local acceleration terms, but over most of the frequency range considered here they are much smaller. In fact, the viscous terms are smaller than the convective acceleration terms except at very low frequencies. For example, in the experiments of Greenwald and Newman (1982), the viscous terms are estimated to be larger than the convective acceleration terms only for frequencies well below 1 Hz. However, the energy contained in impulses of the sort generated by Greenwald and Newman is not insignificant in the neighbourhood of $\omega = 0$. The frequency component containing the most energy in these impulses is the one associated with $\omega = 0$. The contribution of the viscous terms at very low frequencies, then, may have an impact on the propagation of the pulse as a whole.

Therefore, the viscous terms are retained in the fluid equations even though the convective acceleration terms are not. Consequently, the equations governing the motion of the fluid are taken to be

$$\frac{\partial v_r}{\partial t} = -\frac{1}{\rho}\frac{\partial p}{\partial r} + \nu\left[\frac{\partial^2 v_r}{\partial r^2} + \frac{1}{r}\frac{\partial v_r}{\partial r} - \frac{v_r}{r^2} + \frac{\partial^2 v_r}{\partial x^2}\right], \qquad (3.32)$$

$$\frac{\partial v_x}{\partial t} = -\frac{1}{\rho}\frac{\partial p}{\partial x} + \nu\left[\frac{\partial^2 v_x}{\partial r^2} + \frac{1}{r}\frac{\partial v_x}{\partial r} + \frac{\partial^2 v_x}{\partial x^2}\right], \qquad (3.33)$$

$$\frac{\partial v_x}{\partial x} + \frac{\partial v_r}{\partial r} + \frac{v_r}{r} = 0 \quad . \tag{3.34}$$

The neglect of the convective acceleration terms can also be viewed as a first order approximation to the full set of fluid equations (Atabek and Lew, 1966).

Auxiliary Conditions

As is noted earlier in this chapter, the fluid equations and the shell equations are coupled by conditions that apply at the interface between the fluid and the solid. This interface is located at the inner surface of the tube wall. Therefore, its radius is $r = R - h/2$. Hereafter, the distinction between the radius of the inner and middle surface of the vessel wall is dropped. The inner radius of the tube, then, is approximated by R. This modification has a negligible effect on the results when $h/R < 0.1$ (Tait et al., 1981).

The conditions at the interface between the fluid and the solid are based on the following physical principles: the tractions and the velocities must be continuous across the interface. The continuity of the radial and axial components of velocity at the inner surface of the tube wall yields the pair of conditions

$$v_r(R,x,t) = \frac{\partial w(x,t)}{\partial t} \quad , \tag{3.35}$$

$$v_x(R,x,t) = 0 \quad . \tag{3.36}$$

As the tube is tethered, only normal tractions must be matched at the

interface. Hence,

$$P(x,t) + p_e(x,t) = \left(p - 2\mu \frac{\partial v_r}{\partial r}\right)\Big|_{r=R} , \qquad (3.37)$$

where p_e is the external pressure load. In this dissertation we assume that p_e is constant and equal to the undisturbed fluid pressure within the tube: that is, $p_e = 0$.

In order to complete the mathematical formulation of a model representing the transient response of a fluid-filled distensible tube, it is necessary to supply initial and boundary conditions. We begin by considering the conditions appropriate for a boundary-value problem in a semi-infinite tube. The problem of prescribing the conditions at the far end of a tube of finite length, or at the junction between two tubes, is addressed in Chapter VI, where we deal with wave reflection.

Suppose that the fluid and tube wall are set in motion by a disturbance at the end $x = 0$. Quiescent conditions hold initially. It is convenient to prescribe the disturbance in terms of p_m, the fluid pressure averaged over the tube's cross-section, defined mathematically as

$$p_m(x,t) = \frac{1}{A} \iint_A p \, dA . \qquad (3.38)$$

The disturbance created at $x = 0$, then, is represented by the boundary condition

$$p_m(0,t) = \varphi(t) \ , \tag{3.39}$$

where $\varphi(t)$ is a function which rises steadily after $t = 0$ from zero to a maximum value of one and then decreases steadily back to zero. As our investigation is limited to the low to intermediate frequency regime, the Fourier transform of $\varphi(t)$ should be negligible outside this regime. Alternatively, the boundary condition could be prescribed in terms of v_m, the axial component of fluid velocity averaged over the tube's cross-section, defined mathematically in a similar fashion to p_m as

$$v_m = \frac{1}{A} \iint_A v_x \, dA \ . \tag{3.40}$$

The symbol v_m replaces the symbol $\bar{v}$ used earlier in this thesis to denote the average fluid velocity.

Before proceeding further, a remark about the boundary conditions at $x = 0$ is in order. As the shell equation for the vessel wall, eqn. 3.26, contains no spatial derivatives, only one boundary condition is required at $x = 0$. This means that as soon as p_m or v_m are prescribed at $x = 0$, no other conditions can be imposed. Consequently, it is not possible to fix the wall displacement, for example, independently at $x = 0$. This is unsatisfactory, in that the tube is clamped at $x = 0$ in most experiments. In this situation, it is desirable to prescribe the additional boundary condition

$$w(0,t) = 0 \,. \qquad (3.41)$$

Fortunately, it appears that the propagation of the pulses considered here is independent of the wall displacement at $x = 0$, except in the immediate vicinity of this boundary. This is demonstrated in the pair of papers by Moodie and his colleagues (Moodie et al., 1984; Moodie et al., 1986). In the first article, these authors studied the propagation of impulses when the term involving the rotatory inertia of the wall is retained in the shell equation. In this case, a second boundary condition is required at $x = 0$. The condition they prescribed was precisely eqn. 3.41. The pulses predicted under these circumstances, however, are only slightly different from those predicted in the second article, where rotatory inertia is neglected and only a single boundary condition supplied. There are no qualitative differences between the two sets of pulses. Therefore, we are confident that the neglect of rotatory inertia in eqn. 3.26, leading to the inability to restrict the movement of the tube wall at $x = 0$, has very little effect on the propagation of the pulses considered in this dissertation.

The last auxiliary conditions that need to be mentioned here involve the behaviour of the dependent variables at very large times or at very great distances along the tube. In the first place, it is assumed that there are no disturbances emanating from the far end of the infinitely long tube. Therefore p, v_x, v_r, w, and their derivatives vanish as $x \to \infty$, as long as t is finite. Secondly, it

is assumed that the fluid-filled tube stays intact for all time. Consequently, p, v_x, v_r, w, and their derivatives remain finite as $t \to \infty$.

This completes the derivation of the equations of motion and the auxiliary conditions for the model of a fluid-filled distensible tube employed in this thesis. In the last section of this chapter, we express these equations and conditions in dimensionless form.

Nondimensional Governing Equations

The equations of motion for the fluid-filled tube consist of eqns. 3.26 and 3.32 - 3.34, coupled by eqns. 3.35 - 3.37. For the problem of pulse propagation in a semi-infinite tube considered here, the equations above are augmented by the boundary condition 3.39 together with quiescent initial conditions and the conditions at infinity noted in the preceding section.

It is convenient in the sequel to express the problem in nondimensional variables. To this end, we introduce the following dimensionless quantities:

$$\left.\begin{aligned} (\tilde{x},\tilde{r},\tilde{w}) &= (x,r,w)/R, \quad (\tilde{t},\tilde{\tau}) = (t,\tau)c_0/R \ , \\ (\tilde{v}_x,\tilde{v}_r,\tilde{v}_m) &= (v_x,v_r,v_m)/c_0 \ , \\ (\tilde{p},\tilde{p}_m,\tilde{P},\tilde{\varphi}) &= (p,p_m,P,\varphi)/\rho c_0^2 \ , \\ \tilde{k} &= kR \ , \ \tilde{\omega} = \omega R/c_0 \ , \\ \eta &= \frac{1}{8} + \frac{\gamma h}{2\rho R} \ ; \ m = \frac{c_0 R}{\nu} \ . \end{aligned}\right\} \qquad (3.42)$$

Here, c_0 is the Korteweg-Moens wave speed for an incompressible, viscoelastic material: that is,

$$c_0 = [2G_e h/\rho R]^{1/2} . \tag{3.43}$$

As well, k and ω are the same quantities defined in Chapter II, namely the wave number and circular frequency for a wave component. The dimensionless parameters η and m are associated with the combined radial inertia of the fluid and the tube wall, and the viscosity of the fluid respectively. In fact, m is a Reynolds number for this problem. In the absence of a natural velocity scale arising from the flow, the typical velocity used in m is the one associated with the pressure disturbance, namely, c_0.

After substitution of the appropriate nondimensional quantities from eqn. 3.42 into the shell equation 3.26 and the fluid equations 3.32 - 3.34, the following nondimensional equations of motion are obtained:

$$2(1 + \tau \frac{\partial}{\partial t})w = P - 2(\eta - \frac{1}{8})\frac{\partial^2 w}{\partial t^2} , \tag{3.44}$$

$$\frac{\partial v_r}{\partial t} = - \frac{\partial p}{\partial r} + \frac{1}{m} [\frac{\partial^2 v_r}{\partial r^2} + \frac{1}{r}\frac{\partial v_r}{\partial r} - \frac{v_r}{r^2} + \frac{\partial^2 v_r}{\partial x^2}] , \tag{3.45}$$

$$\frac{\partial v_x}{\partial t} = - \frac{\partial p}{\partial x} + \frac{1}{m} [\frac{\partial^2 v_x}{\partial r^2} + \frac{1}{r}\frac{\partial v_x}{\partial r} + \frac{\partial^2 v_x}{\partial x^2}] , \tag{3.46}$$

$$\frac{\partial v_x}{\partial x} + \frac{\partial v_r}{\partial r} + \frac{v_r}{r} = 0 . \tag{3.47}$$

The tildas have been dropped from the nondimensional variables in eqns. 3.44 - 3.47 for convenience, and will be dropped in the succeeding equations as well. The interface conditions 3.35 - 3.37 become

$$v_r(1,x,t) = \frac{\partial w(x,t)}{\partial t} , \tag{3.48}$$

$$v_x(1,x,t) = 0 , \tag{3.49}$$

$$P = \left(p - \frac{2}{m}\frac{\partial v_r}{\partial r}\right)\Big|_{r=1} , \tag{3.50}$$

while the boundary condition 3.39 retains the same appearance, namely

$$p_m(0,t) = \varphi(t) . \tag{3.51}$$

Finally, the averaged pressure p_m and the averaged axial velocity v_m are given by the formulae

$$p_m(x,t) = 2\int_0^1 rp(r,x,t)dr , \quad v_m(x,t) = 2\int_0^1 rv_x(r,x,t)dr . \tag{3.52}$$

Thus, the equations of motion and the auxiliary conditions for the fluid-filled distensible tube are expressed in nondimensional variables via eqns. 3.42 - 3.52. The solution of the mathematical problem posed by these equations forms the content of the following two chapters.

CHAPTER IV

Wave Solutions

The mathematical model of the transient response of a fluid-filled distensible tube formulated in the previous chapter is composed of two parts. The first part consists of the equations governing the dynamics of the vessel wall and the dynamics of the fluid together with the conditions at the solid-fluid interface. These equations and conditions pertain to any pressure wave in the fluid-filled tube. The second part involves the specific initial and boundary conditions needed to augment the equations of motion when a boundary-value problem is posed in a semi-infinite tube. These conditions are appropriate for modelling the propagation of a pulse generated at one end of a vessel sufficiently long that reflections are of no concern during the time interval under consideration.

In this chapter, we construct solutions to the equations forming the first part of the mathematical model: that is, the equations of motion for the fluid-filled tube as represented in a dimensionless form by eqns. 3.44 - 3.50. This is accomplished by means of wave solutions proportional to $\exp[i(kx-\omega t)]$. From these fundamental solutions, general solutions can be constructed via Fourier integrals. The development of particular solutions satisfying the initial and boundary conditions that form the second part of the mathematical model is left for Chapter V.

Fundamental Solutions

As stated in the introduction to this chapter, we utilize trial

solutions proportional to $\exp[i(kx-\omega t)]$ in order to solve the first part of the mathematical problem formulated in Chapter III. Hence, we seek wave solutions of the form

$$\{p, v_x, v_r, w\} = \{\bar{p}, \bar{v}_x, \bar{v}_r, \bar{w}\}\exp[i(kx-\omega t)] \tag{4.1}$$

to eqns. 3.44 - 3.50.

After the substitution of these trial solutions into eqns. 3.44 - 3.50, the following equations involving $\bar{p}(r)$, $\bar{v}_x(r)$, $\bar{v}_r(r)$, and $\bar{w}$ are obtained:

$$2(1-i\omega\tau)\bar{w} = \bar{p}(1) - \frac{2}{m}\frac{\partial \bar{v}_r(1)}{\partial r} + 2\omega^2(\eta - \tfrac{1}{8})\bar{w} , \tag{4.2}$$

$$-i\omega\bar{v}_r = -\frac{\partial \bar{p}}{\partial r} + \frac{1}{m}\left[\frac{\partial^2 \bar{v}_r}{\partial r^2} + \frac{1}{r}\frac{\partial \bar{v}_r}{\partial r} - (k^2 + \frac{1}{r^2})\bar{v}_r\right] , \tag{4.3}$$

$$-i\omega\bar{v}_x = -ik\bar{p} + \frac{1}{m}\left[\frac{\partial^2 \bar{v}_x}{\partial r^2} + \frac{1}{r}\frac{\partial \bar{v}_x}{\partial r} - k^2\bar{v}_x\right] , \tag{4.4}$$

$$ik\bar{v}_x + \frac{\partial \bar{v}_r}{\partial r} + \frac{\bar{v}_r}{r} = 0 , \tag{4.5}$$

$$\bar{v}_r(1) = -i\omega\bar{w} , \tag{4.6}$$

$$\bar{v}_x(1) = 0 . \tag{4.7}$$

We remark that eqn. 4.2 is a consequence of combining eqns. 3.44 and 3.50 prior to the application of the trial solutions.

It is convenient to begin with the solution for $\bar{p}$. This solution is obtained most easily by observing that the fluid pressure p can be decoupled from eqns. 3.45 and 3.46 with the use of eqn. 3.47. Thus, p satisfies Laplace's equation

$$\frac{\partial^2 p}{\partial r^2} + \frac{1}{r}\frac{\partial p}{\partial r} + \frac{\partial^2 p}{\partial x^2} = 0 \ . \tag{4.8}$$

Now, the trial solution for p given in eqn. 4.1 can be inserted into eqn. 4.8 to obtain an equation for $\bar{p}(r)$. The result is the modified Bessel equation of order zero:

$$\frac{\partial^2 \bar{p}}{\partial r^2} + \frac{1}{r}\frac{\partial \bar{p}}{\partial r} - k^2 \bar{p} = 0 \ . \tag{4.9}$$

The solution of eqn. 4.9 regular at $r = 0$ is

$$\bar{p}(r) = a_1 I_0(kr) \ , \tag{4.10}$$

where a_1 is an arbitrary constant and I_0 denotes the modified Bessel function of the first kind of order zero.

The solution for $\bar{p}$ leads in turn to the solutions for $\bar{v}_x$ and $\bar{v}_r$. They are obtained by substituting eqn. 4.10 for $\bar{p}$ into eqns.

4.3 and 4.4. This produces modified Bessel equations of order zero and one respectively for $\bar{v}_x(r)$ and $\bar{v}_r(r)$:

$$\frac{\partial^2 \bar{v}_x}{\partial r^2} + \frac{1}{r}\frac{\partial \bar{v}_x}{\partial r} - \kappa^2 \bar{v}_x = imka_1 I_0(kr) , \qquad (4.11)$$

$$\frac{\partial^2 \bar{v}_r}{\partial r^2} + \frac{1}{r}\frac{\partial \bar{v}_r}{\partial r} - (\kappa^2 + \frac{1}{r^2})\bar{v}_r = mka_1 I_1(kr) , \qquad (4.12)$$

where I_1 denotes the modified Bessel function of the first kind of order one, and κ is given by

$$\kappa = (k^2 - im\omega)^{1/2} . \qquad (4.13)$$

It happens that the dependence of the problem on κ is even, so it is not necessary to specify a branch of κ. The corresponding regular solutions of eqns. 4.11 and 4.12 are

$$\bar{v}_x(r) = a_2 I_0(\kappa r) + \frac{k}{\omega} a_1 I_0(kr) , \qquad (4.14)$$

$$\bar{v}_r(r) = a_3 I_1(\kappa r) - \frac{ik}{\omega} a_1 I_1(kr) . \qquad (4.15)$$

The constants a_2 and a_3 appearing in eqns. 4.14 and 4.15 are not arbitrary. Rather, they are related to each other via eqn. 4.5, and to a_1 by eqn. 4.7. This can be seen by putting eqns. 4.14 and 4.15

into eqns. 4.5 and 4.7 in turn. This yields

$$a_3 = -\frac{ik}{\kappa} a_2 \quad , \quad a_2 = -\frac{k}{\omega} \frac{I_0(k)}{I_0(\kappa)} a_1 \quad . \tag{4.16}$$

Consequently, the solutions for $\bar{v}_x(r)$ and $\bar{v}_r(r)$ can be expressed as

$$\bar{v}_x(r) = \frac{k}{\omega} \left[I_0(kr) - \frac{I_0(k)}{I_0(\kappa)} I_0(\kappa r) \right] a_1 \quad , \tag{4.17}$$

$$\bar{v}_r(r) = -\frac{ik}{\omega} \left[I_1(kr) - \frac{kI_0(k)}{\kappa I_0(\kappa)} I_1(\kappa r) \right] a_1 \quad , \tag{4.18}$$

when eqn. 4.16 is inserted into eqns. 4.14. and 4.15.

Finally, the solution for $\bar{w}$ is immediately determined from that for $\bar{v}_r$ on account of eqn. 4.6. The use of eqn. 4.18 in eqn. 4.6 produces

$$\bar{w} = \frac{k}{\omega^2} \left[I_1(k) - \frac{kI_0(k)}{\kappa I_0(\kappa)} I_1(\kappa) \right] a_1 \quad . \tag{4.19}$$

This completes the solution for $\bar{p}(r)$, $\bar{v}_x(r)$, $\bar{v}_r(r)$, and $\bar{w}$. The corresponding wave solutions, then, can be obtained simply by placing eqns. 4.10, 4.17, 4.18, and 4.19 in turn into eqn. 4.1. Hence,

$$p = I_0(kr)a_1 \exp[i(kx-\omega t)] \ , \tag{4.20}$$

$$v_x = \frac{k}{\omega}\left[I_0(kr) - \frac{I_0(k)}{I_0(\kappa)} I_0(\kappa r)\right]a_1 \exp[i(kx-\omega t)] \ , \tag{4.21}$$

$$v_r = -\frac{ik}{\omega}\left[I_1(kr) - \frac{kI_0(k)}{\kappa I_0(\kappa)} I_1(\kappa r)\right]a_1 \exp[i(kx-\omega t)] \ , \tag{4.22}$$

$$w = \frac{k}{\omega^2}\left[I_1(k) - \frac{kI_0(k)}{\kappa I_0(\kappa)} I_1(\kappa)\right]a_1 \exp[i(kx-\omega t)] \ . \tag{4.23}$$

For future reference, we give the wave solutions here for the averaged pressure p_m and the averaged axial velocity v_m as well. These solutions can be calculated by inserting eqns. 4.20 and 4.21 into the formulae given in eqn. 3.52. After the requisite integrations are performed, the wave solutions for p_m and v_m emerge as

$$p_m = \frac{2I_1(k)}{k} a_1 \exp[i(kx-\omega t)] \ , \tag{4.24}$$

$$v_m = \frac{2}{\omega}\left[I_1(k) - \frac{kI_0(k)}{\kappa I_0(\kappa)} I_1(\kappa)\right]a_1 \exp[i(kx-\omega t)] \ . \tag{4.25}$$

It is evident from eqns. 4.20 - 4.23 that the amplitude of each of the wave solutions has been determined up to the arbitrary constant a_1. The phase relation between the spatial and temporal parts of the wave, however, remains undetermined. The relationship between these

two parts of the wave depends on the connection between the phase parameters k and ω. Our solution has not yet established a link between the two.

It is not surprising that our wave solutions are incomplete, in that one of the equations in the problem remains to be satisfied. This heretofore neglected equation is the shell equation, as represented by eqn. 4.2. The substitution into eqn. 4.2 of eqns. 4.10, 4.18, and 4.19 for $\bar{p}$, $\bar{v}_r$, and $\bar{w}$ respectively reduces the shell equation to

$$2(1-i\omega\tau)\frac{k}{\omega^2}\left[I_1(k) - \frac{kI_0(k)}{\kappa I_0(\kappa)} I_1(\kappa)\right]a_1$$

$$= \left\{I_0(k) - \frac{2ik}{m\omega}\left[I_1(k) - \frac{kI_0(k)}{\kappa I_0(\kappa)} I_1(\kappa)\right]\right\}a_1 \qquad (4.26)$$

$$+ 2(\eta - \tfrac{1}{8})k\left[I_1(k) - \frac{kI_0(k)}{\kappa I_0(\kappa)} I_1(\kappa)\right]a_1 .$$

It is assumed that $a_1 \neq 0$ as otherwise the solutions 4.20 - 4.23 vanish identically. Hence, eqn. 4.26 yields a relation between k and ω: namely, the dispersion equation

$$\frac{k}{\omega^2}(1-i\omega\tau-\omega^2(\eta-\tfrac{1}{8}))\left[I_1(k) - \frac{kI_0(k)}{\kappa I_0(\kappa)} I_1(\kappa)\right]$$

$$= \frac{1}{2} I_0(k) - \frac{ik}{m\omega}\left[I_1(k) - \frac{kI_0(k)}{\kappa I_0(\kappa)} I_1(\kappa)\right] . \qquad (4.27)$$

Equation 4.27 can be viewed either as providing solutions for ω in terms of k, or for k in terms of ω. The presence of the modified Bessel functions I_0 and I_1 makes this dispersion equation a transcendental equation. Consequently, it is not possible to find exact solutions for the roots of eqn. 4.27.

In the problem we are considering in this dissertation, however, it is the low to intermediate frequency band, as represented in eqn. 2.15, that is of interest. Therefore, we are concerned here with the situation in which the magnitudes of k and ω are not large. In this case, it is possible to develop approximate solutions for the roots of eqn. 4.27.

Before proceeding with this analysis, it is worthwhile to review the importance of the dispersion equation to the wave solutions in eqns. 4.20 - 4.23. The role of the dispersion equation in the behaviour of these solutions is a crucial one. From each root of the dispersion equation there arises a set of wave solutions. Each set represents a particular mode of oscillation in the fluid-filled tube. The amplitude of the mode is determined by the arbitary constant a_1. The mode's velocity, and its rate of decay, depend upon the behaviour of that root of the dispersion equation generating the mode. Thus, it is evident that the relationship between k and ω implied by eqn. 4.27 is solely responsible for the propagation characteristics of the waves represented in eqns. 4.20 - 4.23. Now, we move on to a description of the method for obtaining approximate solutions for the roots of eqn. 4.27.

Analysis of the Dispersion Equation

It is convenient here to take the view that the dispersion equation provides solutions for k in terms of ω, where ω is real, as we are ultimately interested in using the wave solutions obtained in this chapter to study boundary-value problems. We begin the analysis by considering the symmetry exhibited by the roots of the dispersion equation. It follows from the properties of the modified Bessel functions I_0 and I_1 (Abramowitz and Stegun, 1972) that eqn. 4.27 is even in k. Hence, its solutions occur in pairs $\pm k$ for each ω. Further, it follows from the properties of I_0 and I_1, and those of κ evident from eqn. 4.13, that when ω is replaced by $-\omega$ and k is replaced by its complex conjugate k^* in eqn. 4.27, the result is the complex conjugate of the entire equation. Therefore, the complex conjugate k^* of any root of k of eqn. 4.27 is also a root, but corresponding to $-\omega$ in place of ω.

In view of the symmetry displayed by the roots k that is demonstrated above, we restrict our investigation of the dispersion equation to the region $\omega \geq 0$, $\text{Re } k \geq 0$. In addition, it is convenient in the subsequent analysis to pick that branch of κ for which $\text{Re } \kappa \geq 0$. It may be recalled that the problem is even in κ so the results are independent of this choice.

The dispersion equation (4.27) can be expressed more concisely as

$$\frac{kI_1(k)}{\omega^2}\left\{\left[1-i\omega\tau-\omega^2(\eta-\frac{1}{8})\right](1-F(k)/F(\kappa))-\omega^2\left[\frac{F(k)}{k^2}-\frac{1}{m\omega}(1-F(k)/F(\kappa))\right]\right\}=0. \tag{4.28}$$

Here, F is defined in terms of the modified Bessel functions as

$$F(z)=zI_0(z)/2I_1(z)\,. \tag{4.29}$$

From the structure of eqn. 4.27, it is clear the dispersion equation can possess a root at $k=0$ only if $\omega=0$ simultaneously. This possibility is discussed later. Otherwise, $kI_1(k)/\omega^2 \neq 0$, so it follows from eqn. 4.28 that

$$k^2\left[\frac{1}{F(k)}-\frac{1}{F(\kappa)}\right]\left[\Lambda(\omega)+\frac{1}{8}\omega^2+\frac{i\omega}{m}\right]=\omega^2\,, \tag{4.30}$$

where

$$\Lambda(\omega)=1-i\omega\tau-\omega^2\eta\,. \tag{4.31}$$

Alternatively, eqn. 4.30 can be written as

$$F(\kappa)\left[k^2\left(\Lambda(\omega)+\frac{1}{8}\omega^2+\frac{i\omega}{m}\right)-\omega^2F(k)\right]=k^2F(k)\left(\Lambda(\omega)+\frac{1}{8}\omega^2+\frac{i\omega}{m}\right). \tag{4.32}$$

Equation 4.32 is identical to the dispersion equation obtained by Rubinow and Keller (1978), if their equation is specialized to the case of an incompressible fluid and a tethered, incompressible tube wall

modelled as a Kelvin-Voigt linear viscoelastic solid.

We now analyse eqn. 4.32 by assuming that ω and $|k|$ remain small, and obtain asymptotic formulae for the roots k in terms of ω. To find solutions of eqn. 4.32 for which $|k|$ is small, we approximate $F(k)$ by its power series expansion. This expansion is computed in eqn. A.8 of the Appendix: thus,

$$F(k) = 1 + \frac{1}{8} k^2 - \frac{1}{192} k^4 + \ldots \qquad (4.33)$$

when $|k|$ is sufficiently small. The substitution of the expansion 4.33 into eqn. 4.32, and the subsequent neglect of the terms on each side of the equation of order $o(k^2)$ relative to the leading term on that side, yields the equation

$$F(\kappa)\left[k^2\left(\Lambda(\omega)+\frac{i\omega}{m}\right)-\omega^2\right] = k^2\left(\Lambda(\omega)+\frac{1}{8}\omega^2+\frac{i\omega}{m}\right)+\frac{1}{8}k^4 . \qquad (4.34)$$

In order to proceed further, $F(\kappa)$ must be approximated. It is clear from eqn. 4.13 that the appropriate approximation will depend upon the order of magnitude of $m\omega$. Typically, m is very large in large arteries or in the water-filled tubes used in experimental studies (Caro et al., 1978; Greenwald and Newman, 1982; Newman et al., 1983). For example, in Tube B of Newman et al. (1983), $R = 0.4$ cm and $c_0 = 833$ cm/s. Thus, if the liquid in the tube was whole blood with kinematic viscosity $\nu = 3.79\times10^{-2}$ cm^2/s (Patel and Vaishnav, 1980), m would be approximately 9000. For water, $\nu = 1\times10^{-2}$ cm^2/s so the

value of m is even higher, roughly 33000. Therefore, it is assumed in the sequel that

$$m \gg 1 . \tag{4.35}$$

As a consequence, the magnitude of $m\omega$ varies from much smaller than one to much greater than one, even though ω remains small. Hence, the size of ω is critical to determining a suitable approximation for $F(\kappa)$.

First of all, consider frequencies for which ω is small but $m\omega$ is large: that is, $\frac{1}{m} \ll \omega$. Then $|\kappa|$ is very large. As $|k|$ is assumed to be small, it is seen from eqn. 4.13 that κ can be expanded asymptotically as

$$\kappa = (-im\omega)^{1/2}\left[1+ \frac{ik^2}{2m\omega} + \ldots\right] . \tag{4.36}$$

Not only is $|\kappa|$ large, but $\mathrm{Re}\,\kappa$ and $-\mathrm{Im}\,\kappa$ are large as well. According to eqn. A.20 of the Appendix, the asymptotic expansion of $F(\kappa)$ when $\mathrm{Re}\,\kappa$ is large is

$$F(\kappa) \sim \frac{1}{2}\kappa\left(1 + \frac{1}{2\kappa} + \frac{3}{8\kappa^2} + \ldots\right) . \tag{4.37}$$

When the expansions 4.36 and 4.37 are substituted into eqn. 4.34, after first dividing the latter equation by $F(\kappa)$, and terms of order $o(k^4)$

are neglected, the approximate solution for k found from the resulting equation is, with the use of the power series expansion for $\Lambda^{-1/2}$,

$$k = \omega[1+ \frac{1}{2}(\eta - \frac{3}{4}\tau^2)\omega^2 + \frac{1}{2} i\omega\tau + (-im\omega)^{-1/2}(1+ \frac{1}{2} i\omega\tau)+(-im\omega)^{-1} +\ldots] . \tag{4.38}$$

The root 4.38 is the viscous correction, for large $m\omega$, to the inviscid root obtained by taking the limit in eqn. 4.38 as $\nu \to 0$, or $m \to \infty$, namely

$$k = \omega[1 + \frac{1}{2}(\eta - \frac{3}{4}\tau^2)\omega^2 + \frac{1}{2} i\omega\tau] + O(\omega^4) . \tag{4.39}$$

The inviscid result represented in eqn. 4.39 is equivalent to the one given by Moodie et al. (1985).

Next, consider frequencies so small that $m\omega$ is small: that is, $\omega \ll \frac{1}{m}$. Then $|\kappa|$ is small, so $F(\kappa)$ can be approximated by replacing k with κ in the power series expansion 4.33. When this expansion is substituted into eqn. 4.34, eqn. 4.13 used, and the terms of order $o(k^4)$ neglected, the approximate solution for k yielded by the resulting equation is

$$k = 2\left(\frac{2i\omega}{m}\right)^{1/2}[1 - \frac{1}{12} im\omega + \frac{1}{2} i\omega\tau + \ldots] , \tag{4.40}$$

upon employment of the power series expansion for $\Lambda^{-1/2}$. The leading

term in eqn. 4.40 is proportional to $\sqrt{\omega/m}$. Rubinow and Keller (1978) found the same behaviour near $\omega = 0$ for the corresponding root in an unconstrained tube.

Although the solution 4.40 is derived under the condition $\omega \neq 0$, it can be shown that this solution satisfies the dispersion equation 4.28 in the limit as $\omega \to 0$. Therefore, this root is valid not only near $\omega = 0$, but at $\omega = 0$ as well. On the other hand, the leading term in the inviscid root 4.39 is proportional to ω, so this root cannot be valid near $\omega = 0$. The behaviour of the inviscid root differs from that of its viscous counterpart 4.40 near $\omega = 0$ because viscosity becomes important there. Thus, the dependence of the dispersion equation on ω and ν is not uniform at $\omega = 0$, $\nu = 0$. As is noted in Chapter II, Rubinow and Keller (1978) were the first to recognize this.

It is evident from eqn. 4.40, on account of the assumption 4.35, that when ω is so small as to make $m\omega$ small, $|k^2|$ is much smaller than $m\omega$. For larger ω, $m\omega$ is no longer small but $|k|$ is still assumed to be. Hence, it remains true that $|k^2|$ is much smaller than $m\omega$. Thus,

$$|k^2| \ll m\omega \qquad (4.41)$$

through the entire range of values of $m\omega$. The inequality 4.41 implies that eqn. 4.36 represents a uniform asymptotic expansion for κ: that is, the expansion

$$\kappa = \kappa_0\left[1+\frac{1}{2}\frac{k^2}{\kappa_0^2}+O(k^4/\kappa_0^4)\right] , \qquad (4.42)$$

where

$$\kappa_0 = (-im\omega)^{1/2} = (m\omega)^{1/2}e^{-i\pi/4} , \qquad (4.43)$$

is uniformly valid unless $\omega \to 0$ and $m \to \infty$.

As a consequence, an approximation can be obtained for $F(\kappa)$ that is independent of the order of magnitude of $m\omega$. To see this, expand $F(\kappa)$ in a power series about $\kappa = \kappa_0$ as

$$F(\kappa) = F(\kappa_0) + F'(\kappa_0)(\kappa-\kappa_0) + O((\kappa-\kappa_0)^2) . \qquad (4.44)$$

Then, by calculating F' from eqn. 4.29 and making use of eqn. 4.42, the expansion for $F(\kappa)$ can be expressed as

$$F(\kappa) = F(\kappa_0) + F_1(\kappa_0)k^2 + O(k^4/\kappa_0^4) , \qquad (4.45)$$

where

$$F_1(\kappa_0) = \frac{F'(\kappa_0)}{2\kappa_0} = \frac{F(\kappa_0)}{\kappa_0^2}\left(1-1/F(\kappa_0)\right) + \frac{1}{4} . \qquad (4.46)$$

It follows from the definition 4.43 for κ_0, and the condition represented in 4.41, that the expansion 4.45 is uniformly valid provided $|F_1(\kappa_0)|$ is bounded for all κ_0. It is evident from the analysis presented in the Appendix that $|F_1(\kappa_0)|$ is indeed bounded for all κ_0. In fact, it is seen from Fig. A.2 of the Appendix that

the upper bound for $|F_1(\kappa_0)|$ is much less than one. Therefore, eqn. 4.45 does represent a uniform approximation of $F(\kappa)$.

This expansion for $F(\kappa)$ enables us to find an approximate solution k to eqn. 4.34, and hence to the full dispersion equation 4.28, that is uniformly valid. To this end, we insert eqn. 4.45 into eqn. 4.34 and neglect terms of order $o(k^4)$. After the resulting equation is divided by $F(\kappa_0)$, it can be expressed concisely as

$$A_1(\kappa_0)k^4 + B(\omega,\kappa_0)k^2 - \omega^2 = 0 , \tag{4.47}$$

where

$$A_1(\kappa_0) = \frac{F_1(\kappa_0) - \frac{1}{8}}{F(\kappa_0)} , \tag{4.48}$$

$$B(\omega,\kappa_0) = F_2(\kappa_0)\Lambda(\omega) - F_3(\kappa_0)\omega^2 , \tag{4.49}$$

and

$$F_2(\kappa_0) = \frac{F(\kappa_0) - 1}{F(\kappa_0)} , \tag{4.50}$$

$$F_3(\kappa_0) = \frac{F_1(\kappa_0) + \frac{1}{8}}{F(\kappa_0)} - \frac{F_2(\kappa_0)}{\kappa_0^2} . \tag{4.51}$$

Equation 4.47 has two solutions for k^2. They are

$$k^2 = \frac{1}{2A_1}\left\{-B \pm [B^2 + 4A_1\omega^2]^{1/2}\right\} . \tag{4.52}$$

This pair of solutions can be approximated by expanding the square root in eqn. 4.52 as

$$[B^2 + 4A_1\omega^2]^{1/2} = B\left[1 + \frac{2A_1\omega^2}{B^2} - \frac{2A_1^2\omega^4}{B^4} + O(A_1^3\omega^6/B^6)\right] . \qquad (4.53)$$

The expansion 4.53 is valid whenever

$$|A_1\omega^2/B^2| << 1 . \qquad (4.54)$$

It is clear from Fig. 4.1, in which $|A_1/B^2|$ is plotted against $|\kappa_0|$ for the typical parameter values $\eta = 0.173125$, $\tau = 0.15$, and $m = 8791$, that $|A_1/B^2|$ is bounded provided $|\kappa_0|$ is bounded away from zero. The behaviour of $|A_1/B^2|$ depicted in Fig. 4.1 is confirmed for large $|\kappa_0|$ by considering the asymptotic expansions for F_2, F_3, and A_1 derived in eqns. A.31 - A.33 of the Appendix. These expansions, when used in conjunction with eqn. 4.49, demonstrate that

$$|A_1/B^2| \sim \frac{1}{|4\kappa_0\Lambda^2|} + O(1/|\kappa_0^2|) << 1 .$$

Thus, condition 4.54 certainly holds when κ_0 is not near zero. To determine the behaviour of $|A_1/B^2|$ when $|\kappa_0|$ is small, we use the power series expansions from F_2, F_3, and A_1 given by eqns.

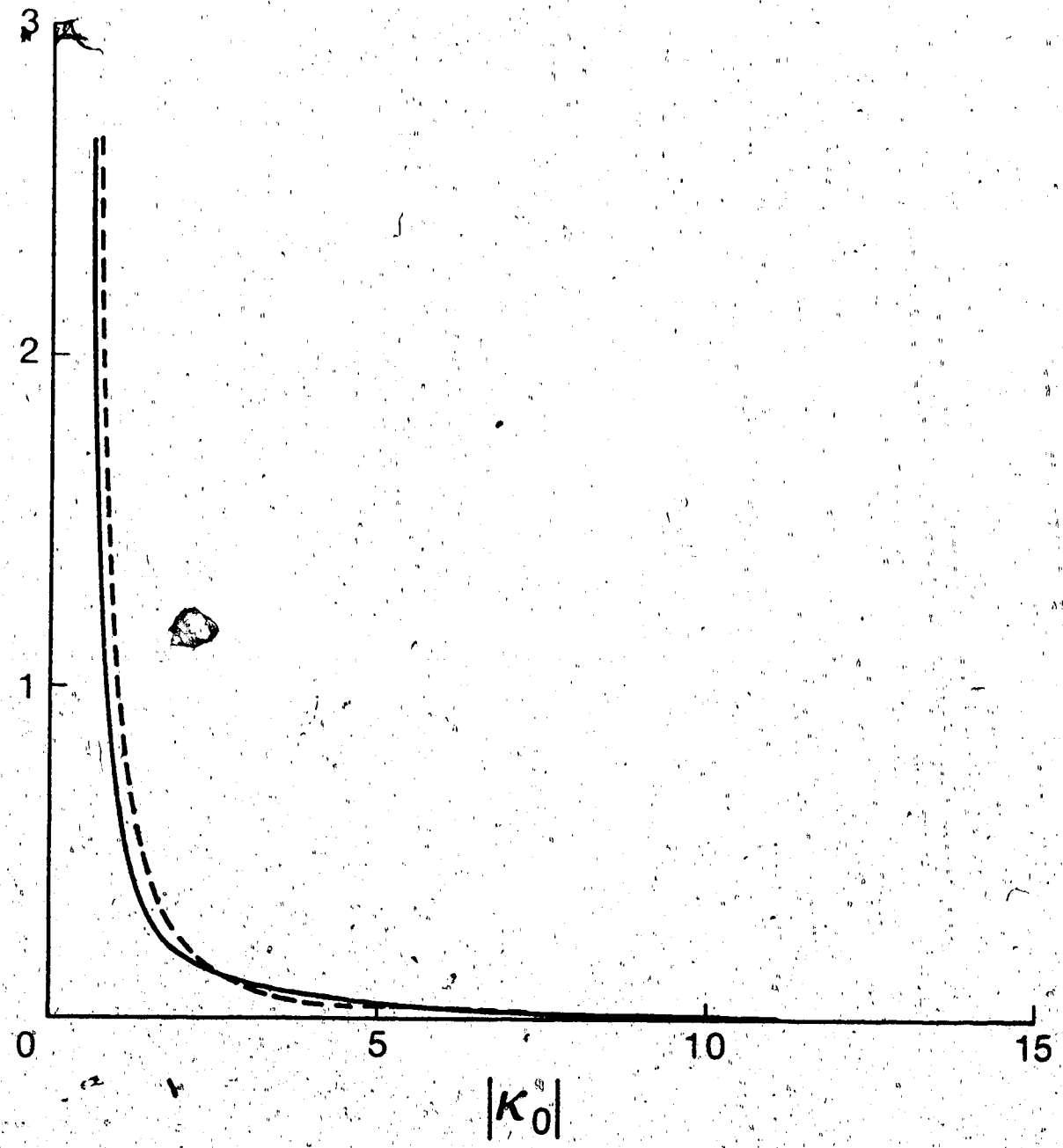

Fig. 4.1. $|A_1/B^2|$ (-) and $|F_3/F_2|$ (--) versus $|\kappa_0|$ for $n = 0.173125$, $\tau = 0.15$, $m = 8791$.

A.27 - A.29. These power series, together with eqn. 4.49, yield

$$|A_1/B^2| = \frac{2}{|3\kappa_0^2\Lambda^2|} + O(1) .$$

Hence, it follows from eqns. 4.31, 4.43, and condition 4.41 that the inequality 4.54 is satisfied when κ_0 is close to zero as well. Therefore, condition 4.54 holds for all κ_0. This implies that the expansion 4.53 is a uniform one.

This expansion can be inserted into eqn. 4.52 to obtain either

$$k^2 = \frac{\omega}{B}\left[1 - \frac{A_1\omega^2}{B^2} + O(A_1^2\omega^4/B^4)\right] , \qquad (4.55)$$

or

$$k^2 = -\frac{B}{A_1}\left[1 + \frac{A_1\omega^2}{B^2} + O(A_1^2\omega^4/B^4)\right] . \qquad (4.56)$$

Consider the conduct of this pair of approximate solutions to the dispersion equation in the limiting case of an inviscid fluid. As $m \to \infty$, the inviscid root 4.39 is recovered from the solution represented in eqn. 4.55 whereas the solution represented in eqn. 4.56 tends to infinity. Consequently, the latter solution is discarded as extraneous and only the former solution retained. In this solution $|k|$ remains small for all κ_0 as is confirmed by Fig. 4.2, in which $\omega/|B|^{1/2}$ is plotted against $|\kappa_0|$ for the pair of parameter values $m = 8791$ and 33088, with η and τ taking the same values as in Fig.

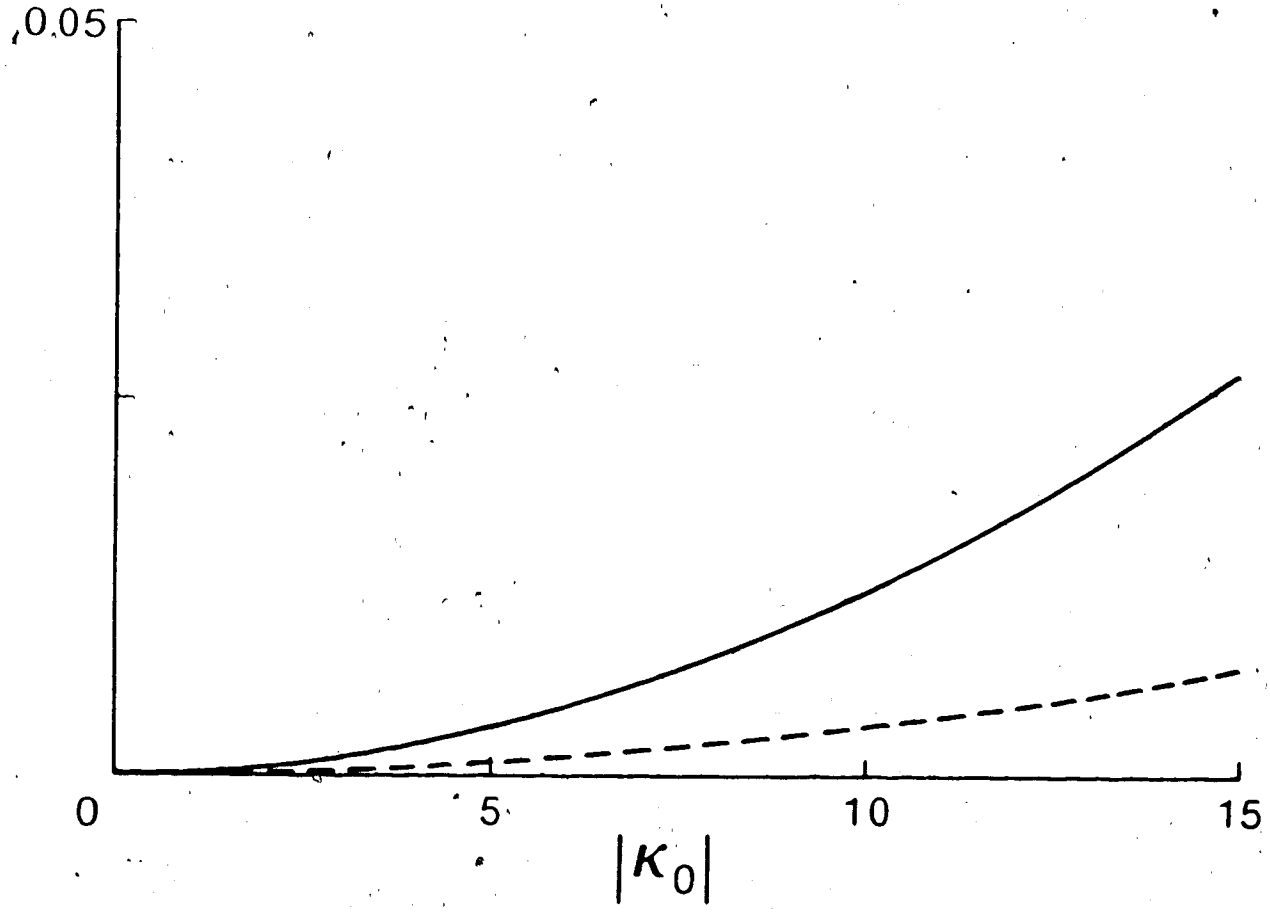

Fig. 4.2. $\omega/|B|^{1/2}$ versus $|\kappa_0|$ for $\eta = 0.173125$, $\tau = 0.15$, $m = 8791$ (-), 33088 (--).

4.1.

The root k with positive real part corresponding to eqn. 4.55 is

$$k = \omega B^{-1/2}\left[1 - \frac{A_1\omega^2}{2B^2} + O(A_1^2\omega^2/B^4)\right] . \qquad (4.57)$$

In eqn. 4.57 we have obtained an asymptotic expansion for the solutions $\pm k$ of the dispersion equation 4.27 that is valid when m is large and ω and $|k|$ are small. This approximation is uniformly valid unless $\omega \to 0$ and $m \to \infty$.

The root k in eqn. 4.57 can be approximated further by expanding $B(\omega,\kappa_0)$. By eqn. 4.49,

$$B = F_2\Lambda\left[1 - \frac{F_3\omega^2}{F_2\Lambda} + O(F_3^2\omega^4/F_2^2\Lambda^2)\right] . \qquad (4.58)$$

The expansion 4.58 is valid whenever

$$|F_3\omega^2/F_2\Lambda| \ll 1 . \qquad (4.59)$$

It can be demonstrated that condition 4.59 holds for all κ_0 by arguments similar to those used in connection with condition 4.54. From Fig. 4.1 it is seen that $|F_3/F_2|$ is bounded whenever $|\kappa_0|$ is bounded away from zero. In fact, for large $|\kappa_0|$,

$$|F_3/F_2| \sim \frac{1}{|4\kappa_0|} + O(1/|\kappa_0^2|) \ll 1 \ .$$

Thus, condition 4.59 is satisfied when $|\kappa_0|$ does not lie near the origin. On the other hand, when $|\kappa_0|$ is small,

$$|F_3/F_2| = \frac{1}{|\kappa_0^2|} + O(1) \ .$$

It then follows from eqns. 4.31, 4.43, and 4.41 that condition 4.59 is also true when κ_0 is in the neighbourhood of zero. Hence, the asymptotic expansion 4.58 for $B(\omega,\kappa_0)$ is a uniform one.

This expansion can be inserted into eqn. 4.57 to obtain another version of the uniform approximation of k, namely

$$k = \omega(F_2\Lambda)^{-1/2}\left[1 + \frac{1}{2}\left(\frac{F_3}{F_2\Lambda} - \frac{A_1}{(F_2\Lambda)^2}\right)\omega^2 + O\left(F_3^2\omega^4/F_2^2\Lambda^2\right)\right] \ . \qquad (4.60)$$

Equation 4.60 is a more convenient representation for k than eqn. 4.57 in that the dependence of k upon ω and κ_0 is separated in the former equation.

If the approximation process is continued, k can be written as an expansion in powers of ω, with coefficients that depend on κ_0. This is accomplished by expanding Λ^{-1} in a power series, via eqn. 4.31. The result is

$$k = \omega F_2^{-1/2}\left[1 + \frac{1}{2}\left(\eta - \frac{3}{4}\tau^2\right)\omega^2 + \frac{1}{2}\, i\omega\tau + \frac{1}{2}\left(F_3 - A_1/F_2\right)\omega^2/F_2 + \ldots\right] . \tag{4.61}$$

This asymptotic expansion for k is uniformly valid unless $\omega \to 0$ and $m \to \infty$. It is a viscous correction to the inviscid root 4.39, as is eqn. 4.38, but unlike eqn. 4.38 the approximation 4.61 is valid for all $m\omega$. It can be checked that eqn. 4.61 reduces to eqn. 4.38 when $m\omega$ is large, and to eqn. 4.40 when $m\omega$ is small.

Throughout the derivation of the various asymptotic formulae presented above for the root k of the dispersion equation, it is stated often that those formulae are valid when ω and $|k|$ are small. Such statements invite the following question: just how small must ω be for the formulae to be valid? In an attempt to answer this question, we inserted the expansion 4.60 for k into the original dispersion equation as represented by eqn. 4.30, and computed the difference in magnitude the approximation for k created between the two sides of this equation.

The results of these calculations are depicted in Figs. 4.3 and 4.4. It is evident from these graphs that the formula for k given in eqn. 4.60 is an excellent approximation when $0 \leq \omega \leq 1.0$, as the relative error generated in the dispersion equation is less than 1% throughout this frequency range. Surprisingly, the relative error does not even exceed 5% for values of ω as great as 1.5. It is only as ω increases beyond 1.5 that the error begins to grow dramatically. These

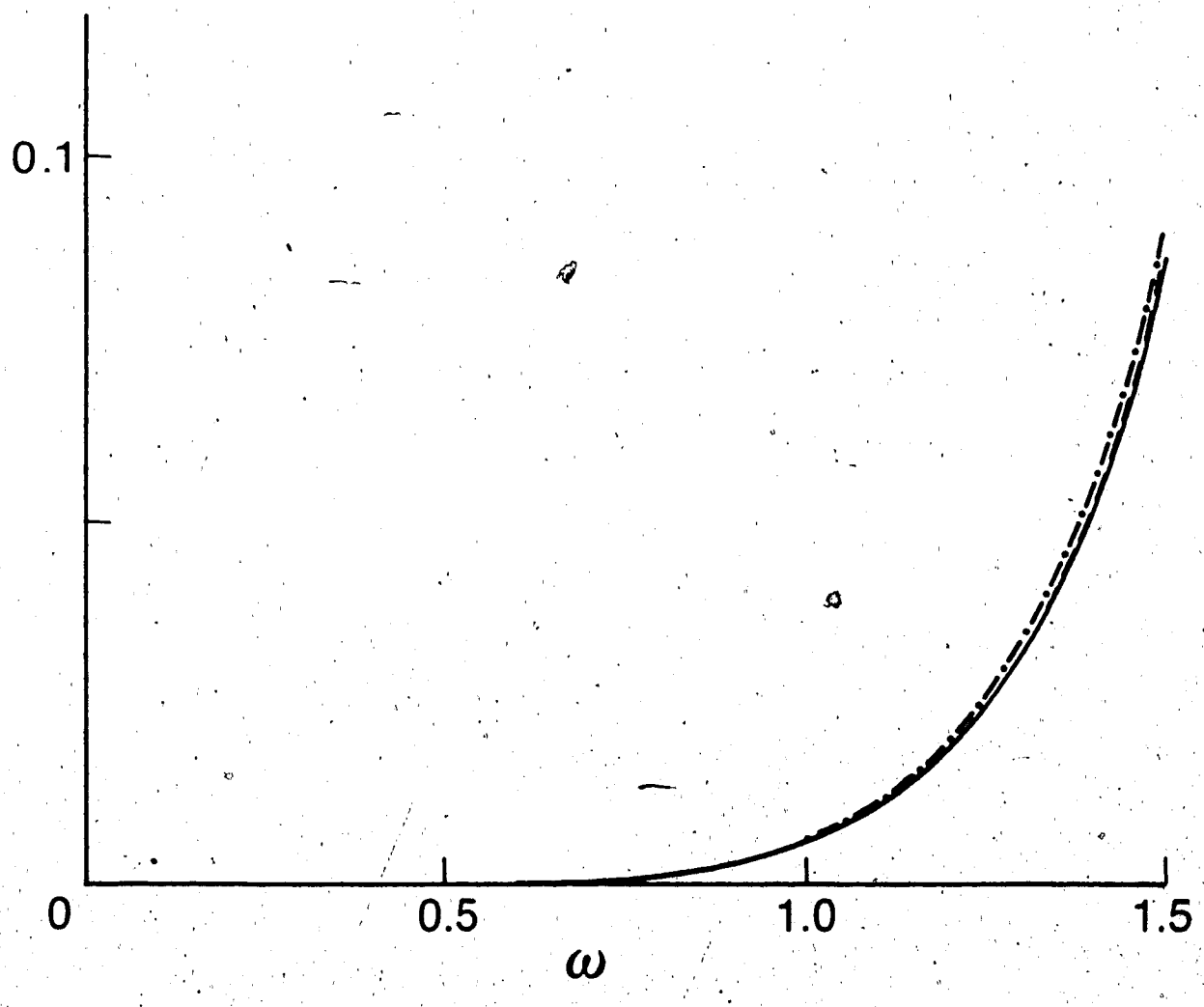

Fig. 4.3. Magnitude of error in dispersion equation as a function of ω for $\eta = 0.173125$, $\tau = 0.15$, $m = 33088$ (-), 8791 (--), 1666 (-·-).

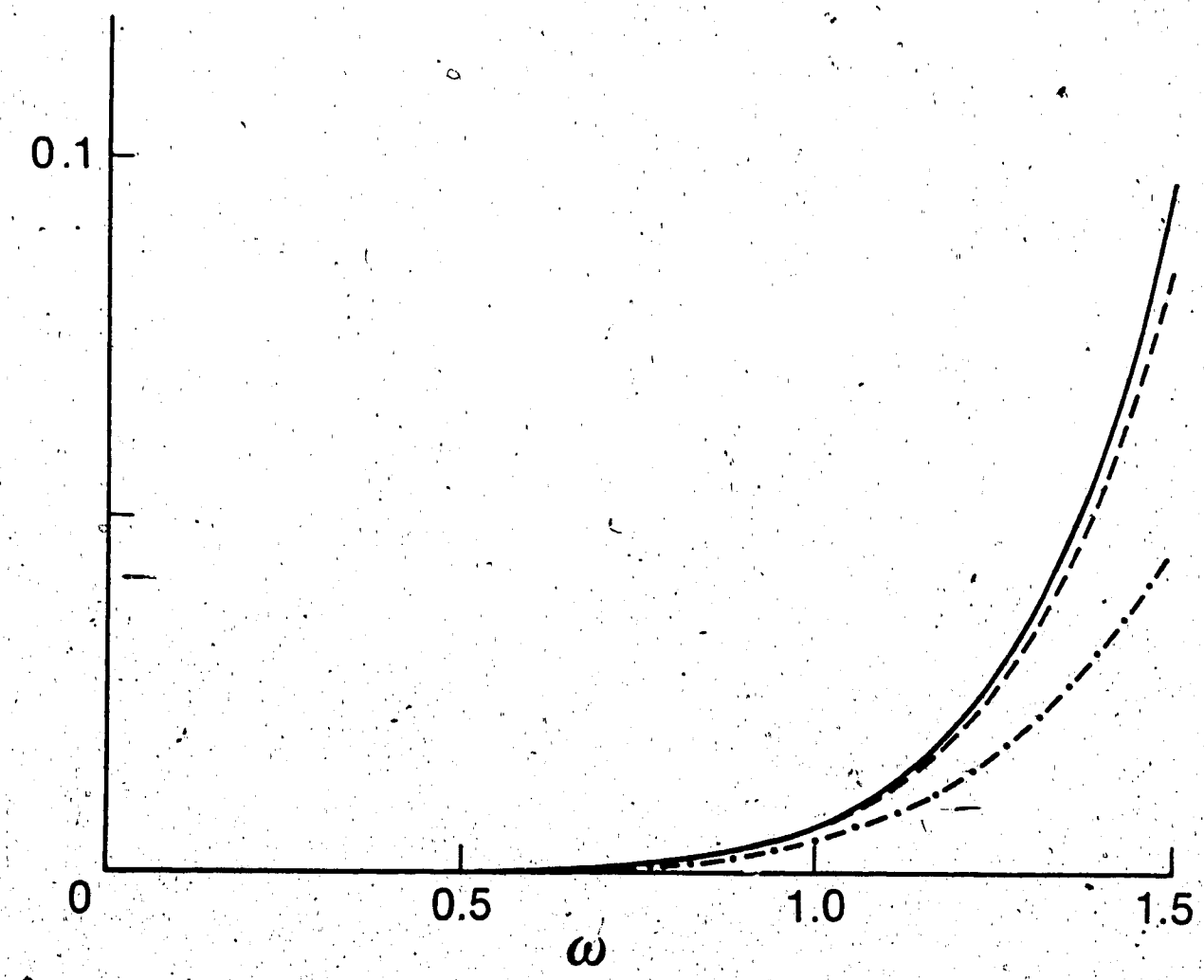

Fig. 4.4. Magnitude of error in dispersion equation as a function of ω for $\eta = 0.173125$, $m = 33088$, $\tau = 0$ (-), 0.15 (--), 0.5 (-·-).

results answer the question posed in the preceding paragraph. The asymptotic formula 4.60 is a reasonable approximation to the exact root k of the dispersion equation for $0 \leq \omega \leq 1.5$. In the interval $0 \leq \omega \leq 1.0$, the agreement between the asymptotic result and the exact one is very good.

Similar statements apply to the formulae in eqns. 4.57 and 4.61. The formula 4.57 produces values of k that on a graph, are indistinguishable from those produced by formula 4.60 over the interval $0 \leq \omega \leq 2.0$. Thus, the former formula provides an approximation for k that is as accurate as the latter. The values of k produced by eqn. 4.61 begin to depart from those produced by eqn. 4.60 as ω nears 1.0. This is a consequence of the expansion for Λ^{-1} in powers of ω used in eqn. 4.61. Hence, the formula in eqn. 4.61 is not as accurate as the formula in eqn. 4.60 when $\omega > 1.0$.

It is clear, then, that the asymptotic expansion 4.60 is better able to approximate k over the frequency band of interest to us, namely $0 \leq \omega \leq 1.5$, than the expansion 4.61. On the other hand, no clear-cut distinction exists between the results of formula 4.57 and those of 4.60 over this frequency range. The only difference between the two formulae is that eqn. 4.60 is a more convenient representation for k than eqn. 4.57, as noted earlier. For this reason, we choose to use eqn. 4.60, rather than eqn. 4.57, to approximate k in the rest of this thesis.

Now that we have developed an asymptotic solution for the root of k of the dispersion equation, the calculations for the set of wave solutions sought in eqn. 4.1 are complete. As is noted in the

introduction to this chapter, these wave solutions are the fundamental solutions to the equations forming the first part of the mathematical model considered in this dissertation. The problems of constructing general solutions from the fundamental ones, and developing particular solutions that satisfy those initial and boundary conditions forming the second part of the mathematical model, are addressed in Chapter V. Before turning to these problems, however, we discuss various features of the propagation process that can be ascertained from the behaviour of $k(\omega)$.

Phase Velocity and Wave Attenuation

The first thing to be observed about the propagation process is that only a single mode of propagation exists for pressure waves in the fluid-filled tube model considered here. This follows from the analysis of the preceding section. There, only the single pair of roots $\pm k$, as given by eqn. 4.60 for example, was found for the dispersion equation at each ω. Moreover, it is evident from the symmetry of this pair of roots that the solution $+k$ is associated with waves travelling in the positive x-direction whereas the solution $-k$ is associated with waves travelling in the negative x-direction. The waves travelling to the left, however, possess the same propagation characteristics as those travelling to the right. Thus, this pair of waves represents just one mode of propagation.

The characteristics of this mode can be identified by considering the root with positive real part, $+k(\omega)$. The qualities possessed by k that are important in wave propagation can be described by means of

two quantities: the phase velocity $c = \omega/\mathrm{Re}\, k$, and the transmission per unit distance $\exp[-\mathrm{Im}\, k]$. Here, the unit distance employed is the tube radius. These quantities, calculated from the approximation 4.60 for k, are plotted in Figs. 4.5 - 4.10 as functions of ω for various values of the viscosity parameter m and the viscoelasticity parameter τ. Note that the selections $m = 33088$ and $m = 8791$ are associated with water and whole blood respectively, while $\tau = 0$ represents the elastic case and $\tau = 0.15$ a typical viscoelastic one (Moodie, 1985).

It is evident from Figs. 4.5 - 4.7 that the dependence of the phase velocity upon ω is quite weak, except at very low frequencies. With fluid viscosity taken into account, it can be seen from Fig. 4.6, for example, that c rises rapidly to a level slightly below that of the Korteweg-Moens wave speed c_0. Throughout the interval $0.015 < \omega < 0.30$, the maximum variation of c from c_0 is less than 5% when $m = 33088$. On the other hand, at $\omega = 1.5$, c has decreased to a level roughly 20% lower than c_0. These results help to explain why Newman et al. (1983) were unable to detect any variation with frequency in their measurements of c. The range of frequencies monitored in their experiments was 5-100 Hz, corresponding to the dimensionless interval $0.015 < \omega < 0.30$. The predicted variation in c is too small to detect in this interval. However, these results do predict the possibility of detecting some variation in c with frequency in experiments producing pressure waves that contain frequencies in the range 300-500 Hz, corresponding to the dimensionless interval $0.9 < \omega < 1.5$. Over this interval, c should decrease from 10% to 20% below the value of c_0.

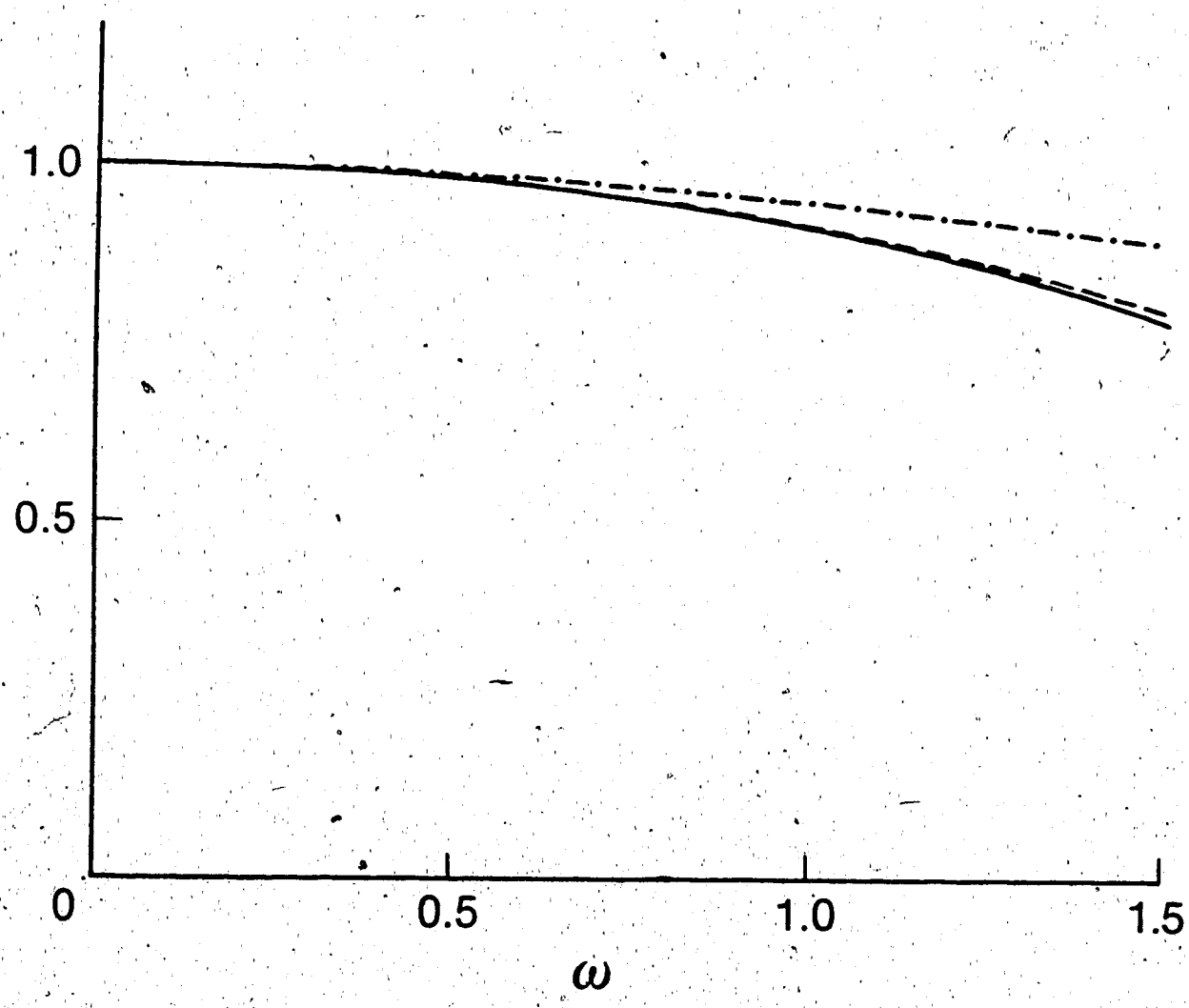

Fig. 4.5. Variation of nondimensional phase velocity c with nondimensional frequency ω for η = 0.173125, m → ∞, τ = 0 (-), 0.15 (--), 0.5 (-·-).

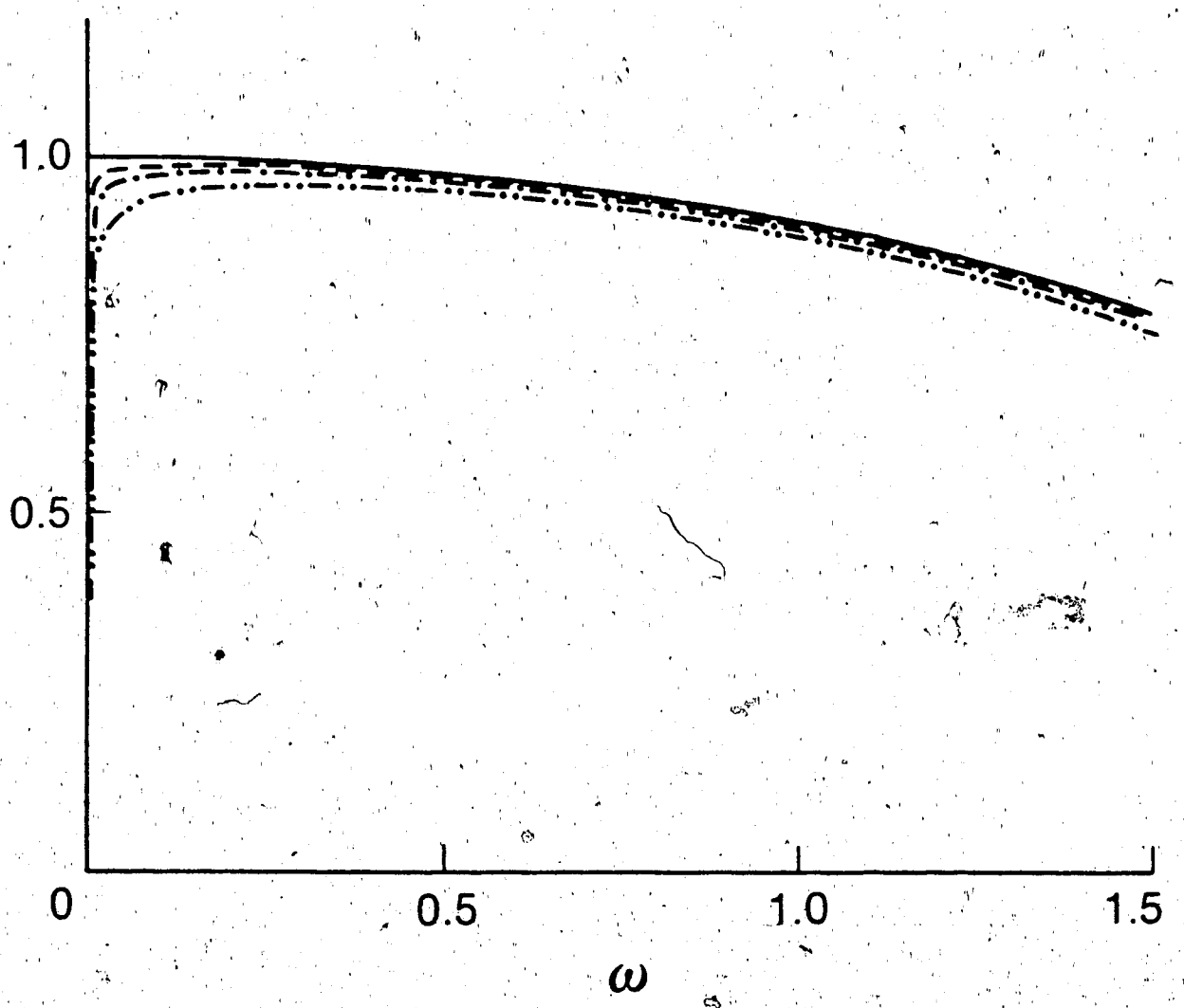

Fig. 4.6. Variation of nondimensional phase velocity c with nondimensional frequency ω for η = 0.173125, τ = 0.15, m → ∞ (-), 33088 (--), 8791 (-·-), 1666 (-···-).

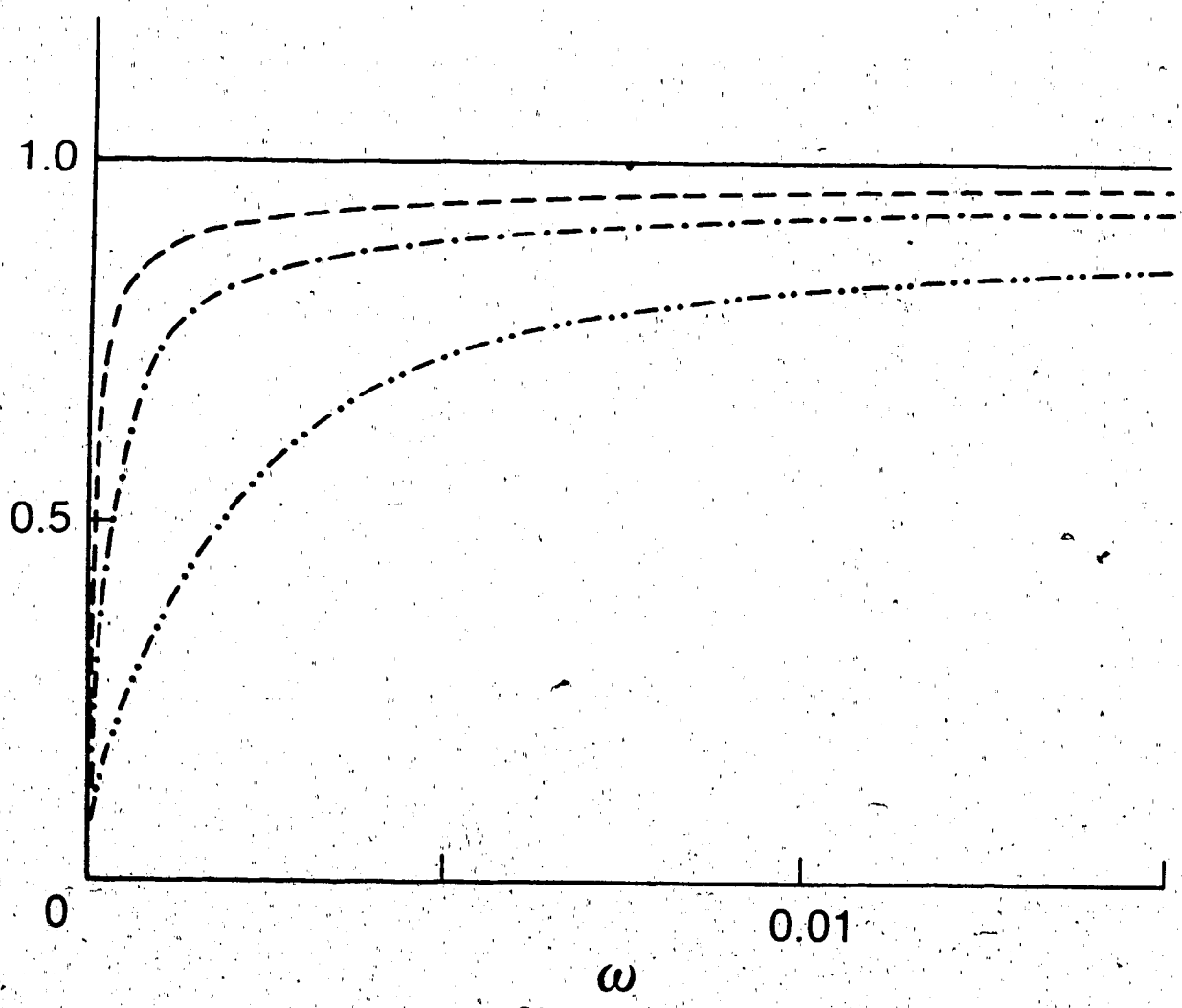

Fig. 4.7. Variation of nondimensional phase velocity c with nondimensional frequency ω on an enlarged scale for η = 0.173125, τ = 0.15, m → ∞ (-), 33088 (--), 8791 (-·-), 1666 (-···-).

The effect of wall viscoelasticity on the phase speed is demonstrated in Fig. 4.5. Evidently, changes in the viscoelastic parameter τ affect c marginally. As τ is increased, there is a small increase in c. This confirms a statement about the effect of viscoelasticity on the phase speed made in Chapter II. The magnitude of the increase in c brought about by increasing τ is sufficiently small, however, that it is unlikely to be detected experimentally. Surprisingly, the effect of viscoelasticity on the phase speed observed here is opposite to the effect produced when c is considered to be a function of the wave number k. In the latter case an increase in τ brings about a slight decrease in c (Moodie et al., 1985). This curious result is created by the higher order correction terms that modify the first order linear relationship between k and ω.

The influence of fluid viscosity on the phase speed is likewise depicted in Fig. 4.6. It is clear that in the case of fluids such as water or whole blood, viscosity has little impact on c when $\omega > 0.01$. An increase in viscosity leads to a slight decrease in phase speed. However, at very low frequencies, the impact of viscosity on c is enormous. The entire qualitative behaviour of c is altered near $\omega = 0$. When fluid viscosity is accounted for $c \to 0$ as $\omega \to 0$. In contrast, $c \to 1$ as $\omega \to 0$ in the inviscid case. This is clearly depicted in Fig. 4.7, where the curves in Fig. 4.6 are reproduced on an enlarged scale for ω. Thus, the dependence of c on m and ω is not uniform in the limit as $\omega \to 0$, $m \to \infty$, as is discussed in the previous section in connection with the solutions for k. Figure 4.7 also illustrates that the rate at which c rises from its value at

$\omega = 0$ is somewhat sensitive to the viscosity of the fluid.

The behaviour of the phase velocity as a function of ω is indicative of the dispersion inherent in the propagation process. It is seen from Figs. 4.5 and 4.6 that c is fairly flat over the interval $0.01 < \omega < 0.5$, implying that very little dispersion ought to occur over this interval. When $\omega > 0.5$, c begins a gentle decrease with ω, mainly on account of the combined radial inertia of the fluid and the wall, so some dispersion is probable here. Naturally, as c varies quite rapidly with ω in the interval $0 \leq \omega < 0.01$, considerable dispersion of wave components is expected to arise near $\omega = 0$.

The dissipation involved in the propagation process, on the other hand, can be inferred from the behaviour of the transmission per unit distance, $\exp[-\text{Im } k]$, as a function of ω. It is evident from Figs. 4.8 - 4.10 that very low frequency components are hardly damped at all. In fact, in the limit as $\omega \to 0$, these components remain undamped. The attenuation increases as ω increases, slowly at first, but then at an increasing rate. The degree of attenuation, however, depends on the source of the dissipation.

The effect of wall viscoelasticity on wave attenuation is illustrated in Fig. 4.8. It is observed that attenuation increases noticeably with frequency at the relatively higher frequencies. For $\omega < 0.3$, however, damping is virtually negligible. There is a marked increase in damping as τ is increased.

The influence of fluid viscosity on wave attenuation is depicted in Figs. 4.9 and 4.10. It is evident from Fig. 4.9 that the degree of

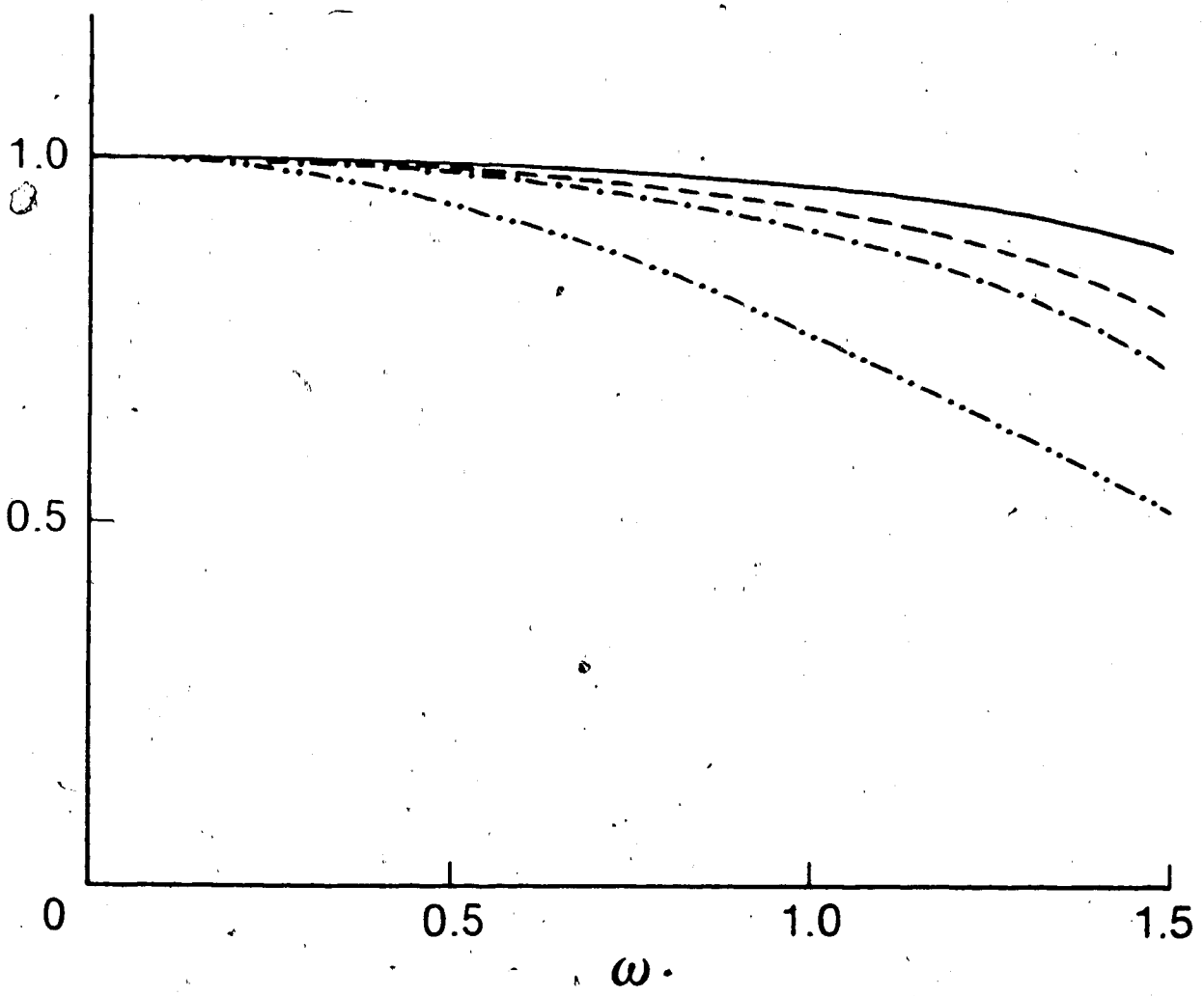

Fig. 4.8. Variation of transmission per unit distance exp[-Im k] with nondimensional frequency ω for $\eta = 0.173125$, $m = 33088$, $\tau = 0.05$ (-), 0.1 (--), 0.15 (-·-), 0.5 (-···-).

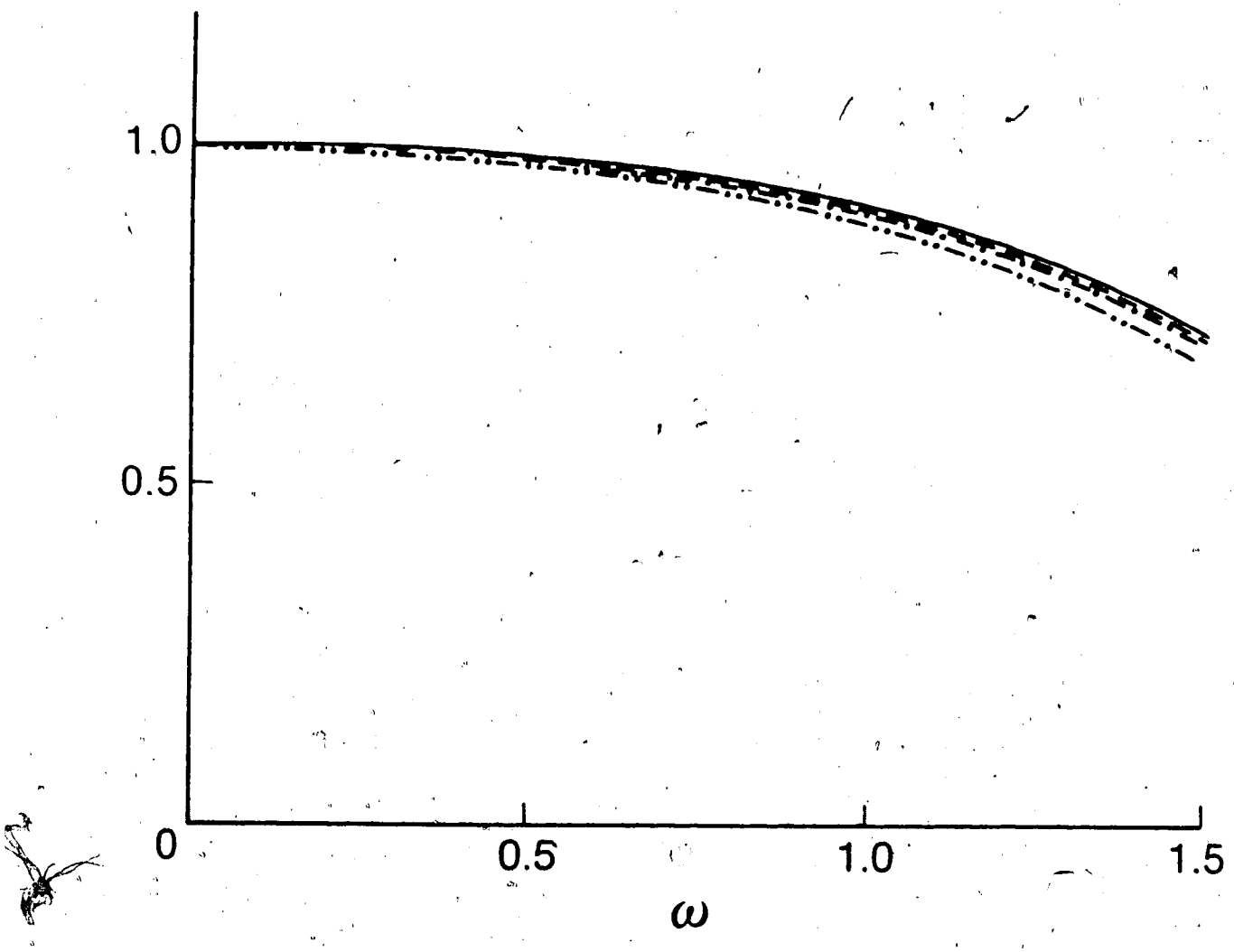

Fig. 4.9. Variation of transmission per unit distance exp[-Im k] with nondimensional frequency ω for $\eta = 0.173125$, $\tau = 0.15$, $m \to \infty$ (-), 33088 (--), 8791 (-·-), 1666 (-···-).

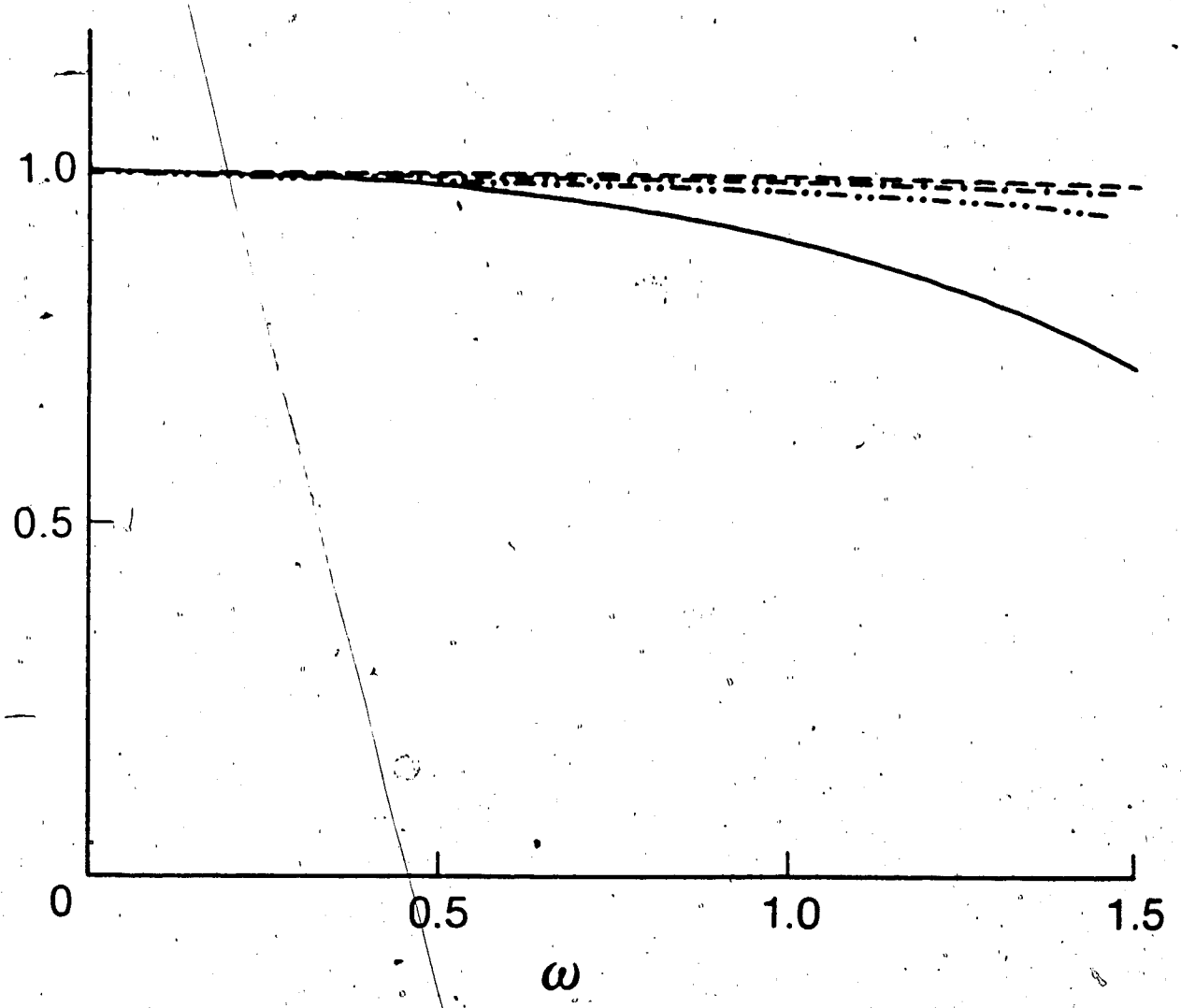

Fig. 4.10. Variation of transmission per unit distance exp[-Im k] with nondimensional frequency ω for $\eta = 0.173125$, $\tau = 0.15$, $m \to \infty$ (-), and $\tau = 0$, $m = 33088$ (--), 8791 (-·-), 1666(-···-).

damping is quite insensitive to m, and hence, to the viscosity. In fact, it is seen in Fig. 4.10 that viscosity produces very little damping over the entire interval $0 \leq \omega \leq 1.5$. The figure demonstrates that wall viscoelasticity rather than fluid viscosity is the chief source of dissipation for pressure waves in our fluid-filled distensible tube model. This point is in agreement with the opinion articulated by Caro et al. (1978).

Some conclusions about the propagation of disturbances contained in the frequency band considered here, namely the band associated with the dimensionless interval $0 \leq \omega \leq 1.5$, can be drawn from the preceding analysis of phase velocity and wave attenuation. It appears that very little dispersion is generated in the frequency band represented by the region $0.01 < \omega < 0.5$. Relatively high frequency components contained in the interval $0.5 < \omega < 1.5$ do display some dispersive qualities, and very low frequency waves in the narrow band $0 \leq \omega < 0.01$ will be dispersed considerably through the action of fluid viscosity. The effects of dissipation over the frequency band under consideration are also preferential. Waves in the interval $0 \leq \omega < 0.3$ should suffer very little attenuation. At higher frequencies, significant damping occurs by virtue of wall viscoelasticity. Thus, if most of the energy in a given disturbance is concentrated within the interval $0.01 < \omega < 0.3$, it is predicted that the disturbance will manifest few signs of dispersion or dissipation as it propagates along the tube.

Whether the conclusions described above do, in fact, accurately represent the propagation characteristics of a pulse composed of a

continuous spectrum of frequency components awaits the results of an investigation into the transient response of the fluid-filled tube model used here. This investigation is pursued in the following chapter, where the boundary-value problem posed in Chapter III is solved. If the observations in the experiments of Newman et al. (1983) are any guide, the pressure pulses computed in Chapter V will display greater evidence of dispersion and dissipation than the analysis of phase velocity and wave attenuation presented above predicts.

CHAPTER V

Pulse Propagation

In the preceding chapter, certain conclusions were reached regarding various aspects of the wave propagation process in the fluid-filled tube model derived in Chapter III. These conclusions were based on an analysis of the behaviour of the phase velocity and the transmission per unit distance as functions of frequency. In Chapter II, however, we had issued a warning about the dangers of relying too heavily on graphs of phase velocities and transmission coefficients to give a complete description of the features of pulse propagation. While the pattern of propagation for the pulse as a whole is determined, in principle, solely from the propagation characteristics of its frequency components, it is not an easy feat in practice to predict exactly how the contribution of each component affects the shape of the pulse. For example, some signs of dispersion or dissipation manifested by the pulse in its travel down the tube are not apparent *apriori* in the plots of the frequency spectra.

Therefore, in this chapter, we examine the propagation of pulses directly by investigating the transient response of our fluid-filled tube model. To do this, we compute solutions for the boundary-value problem forming the second part of the mathematical model developed in Chapter III, and compare the behaviour of these solutions with the predictions based on the roots of the dispersion equation given in Chapter IV.

Fourier Integral Solutions

The first step in solving the boundary-value problem under consideration here is to construct general solutions to the fluid-filled tube model from the wave solutions calculated in Chapter IV. As the boundary condition 3.51 is formulated in terms of the averaged fluid pressure p_m, we focus particular attention on this variable, as well as on the other averaged variable, the averaged axial component of fluid velocity v_m, and on the radial wall displacement w.

The averaged pressure p_m associated with the set of wave solutions represented by eqns. 4.20 - 4.23 is calculated in eqn. 4.24. For convenience, we repeat the formula here:

$$p_m = \frac{2I_1(k)}{k} a_1 \exp[i(kx-\omega t)] \ . \qquad (5.1)$$

Similarly, the averaged axial velocity v_m associated with the wave solutions in eqns. 4.20 - 4.23 is represented in eqn. 4.25. With the use of eqn. 4.29, the formula for v_m can be written as

$$v_m = \frac{2I_1(k)}{k} (1-F(k)/F(\kappa))a_1 \exp[i(kx-\omega t)] \ . \qquad (5.2)$$

The wave solution for the radial wall displacement w is given by eqn. 4.23. It too can be expressed in terms of the function F defined in eqn. 4.29: that is,

$$w = \frac{kI_1(k)}{\omega^2}\,(1-F(k)/F(\kappa))a_1\exp[i(kx-\omega t)] \quad . \tag{5.3}$$

General solutions for p_m, v_m, and w can be constructed directly from eqns. 5.1 - 5.3 by means of Fourier integrals. As it is found in Chapter IV that the dispersion equation possesses the pair of roots $\pm k$, as approximated by eqn. 4.60 for example, the Fourier integrals will contain two terms corresponding to the two roots. Thus, the general representation for p_m is

$$p_m(x,t) = \frac{1}{2\pi}\int_{-\infty}^{\infty}\left[P^+(\omega)e^{ikx} + P^-(\omega)e^{-ikx}\right]e^{-i\omega t}d\omega \quad , \tag{5.4}$$

where k is selected to be that function of ω given by eqn. 4.60. Similarly, the formulae for v_m and w are

$$v_m(x,t) = \frac{1}{2\pi}\int_{-\infty}^{\infty}\frac{k}{\omega}\,(1-F(k)/F(\kappa))\left[P^+(\omega)e^{ikx} - P^-(\omega)e^{-ikx}\right]e^{-i\omega t}d\omega \quad , \tag{5.5}$$

$$w(x,t) = \frac{1}{2\pi}\int_{-\infty}^{\infty}\frac{k}{2\omega^2}\,(1-F(k)/F(\kappa))\left[P^+(\omega)e^{ikx} + P^-(\omega)e^{-ikx}\right]e^{-i\omega t}d\omega \quad . \tag{5.6}$$

Now that general solutions to the fluid-filled tube model have been developed, particular solutions can be extracted from them to satisfy the given boundary-value problem. The general solution 5.4 for

p_m can be specialized to satisfy the boundary condition 3.51 by taking the coefficients P^+ and P^- to be

$$P^+(\omega) = \bar{\varphi}(\omega) \ , \ P^-(\omega) = 0 \ , \tag{5.7}$$

where $\bar{\varphi}(\omega)$ is the Fourier transform of $\varphi(t)$, namely

$$\bar{\varphi}(\omega) = \int_0^\infty \varphi(t) e^{i\omega t} dt \ . \tag{5.8}$$

The choices for P^+ and P^- represented in eqns. 5.7 and 5.8 ensure that the corresponding constructions for p_m , v_m , and w satisfy the rest of the conditions posed in Chapter III as well: namely, the quiescent initial conditions and the regularity conditions imposed as $x \to \infty$ or $t \to \infty$. Hence, the given boundary-value problem is solved.

To recapitulate, we have obtained the transient response of the fluid-filled distensible tube model derived in Chapter III to a disturbance in averaged fluid pressure generated at one end of a semi-infinite tube. The response is characterized by solutions giving the averaged fluid pressure p_m , the averaged axial component of fluid velocity v_m , and the radial wall displacement w. These solutions are, respectively,

$$p_m(x,t) = \frac{1}{2\pi} \int_{-\infty}^{\infty} \bar{\varphi}(\omega) \exp[i(kx-\omega t)] d\omega \ , \tag{5.9}$$

$$\bar{v}_m(x,t) = \frac{1}{2\pi}\int_{-\infty}^{\infty} \frac{k\bar{\varphi}(\omega)}{\omega}\,(1-F(k)/F(\kappa))\exp[i(kx-\omega t)]d\omega\ , \qquad (5.10)$$

$$w(x,t) = \frac{1}{2\pi}\int_{-\infty}^{\infty} \frac{k^2\bar{\varphi}(\omega)}{2\omega^2}\,(1-F(k)/F(\kappa))\exp[i(kx-\omega t)]d\omega\ , \qquad (5.11)$$

where $\bar{\varphi}$ is given by eqn. 5.8, F by eqn. 4.29, κ by eqn. 4.13, κ_0 by eqn. 4.43, and k by eqn. 4.60.

It is evident from the solutions represented in eqns. 5.9 - 5.11 that the disturbance generated at the end of the tube is able to travel in only one direction, namely the positive x-direction. This hardly comes as a great shock. However, aside from this superficial observation, very little can be inferred from the content of the Fourier integrals above. This is typical in wave propagation problems (Whitham, 1974). Consequently, the behaviour of the solutions contained in eqns. 5.9 - 5.11 is analysed in detail by resorting to numerical integration.

Numerical Computation

The solutions given in the preceding section as a description of the transient response of the fluid-filled tube uniformly appear in the following integral form:

$$s(x,t) = \int_{-\infty}^{\infty} S(\omega,x)e^{-i\omega t}\,d\omega\ . \qquad (5.12)$$

Integrals of this sort can be evaluated numerically by means of the

discrete Fourier transform. In this procedure, an approximation to $s(x,t)$ is calculated for a fixed value of x at the discrete values of t given by

$$t_j = \frac{\pi}{N\Delta\omega} j \quad , \quad j = -N,-N+1,\ldots,N-1 \quad , \tag{5.13}$$

according to the formula

$$s(x,t_j) = \left[\sum_{n=-N}^{N-1} S(n\Delta\omega,x)\exp(-in\pi j/N) \right]\Delta\omega \quad , \tag{5.14}$$

where $\Delta\omega$ is a suitably chosen increment of the circular frequency ω.

This discretization produces values of a function that is periodic with period $2\pi/\Delta\omega$ and approximates $s(x,t)$ at $2N+1$ equally-spaced points in the interval $-\frac{\pi}{\Delta\omega} \leq t \leq \frac{\pi}{\Delta\omega}$. In the problems considered here, we are only interested in the values of the approximants when $t \geq 0$. Hence, the function values corresponding to $t < 0$ can be discarded as extraneous. Care must be taken in the approximating formula 5.14 to choose N and $\Delta\omega$ in such a way that $S(\omega,x)$ is negligible when $\omega > N\Delta\omega$, and $s(x,t)$ is negligible when $t > \pi/\Delta\omega$. The consequences of failing to obey this injunction are discussed by Brigham (1974).

The discrete Fourier transform can be computed efficiently by using one of a number of variations of a basic algorithm known as the

Fast Fourier Transform (FFT). The subroutine used to perform the calculations presented in this thesis implements the algorithm of Cooley, Lewis, and Welch quoted by Dahlquist and Björck (1974). The speed of the FFT algorithm makes it ideal for use in a situation such as ours, where it is necessary to evaluate the solutions 5.9 - 5.11 at various stations along the tube, as well as for many combinations of the parameter pair τ and m.

The integrands in eqns. 5.9 - 5.11 depend on three dimensionless parameters, namely η, τ, and m. It is natural, then, to expect that the appropriate values of N and $\Delta\omega$ to be used in the discrete transform will depend on these parameters. For the particular function $\varphi(t)$ employed here to represent the pressure input at $x = 0$, however, it was found by conducting numerical experiments that N and $\Delta\omega$ can be chosen independent of not only η, τ, and m for the range of values of these parameters under investigation, but also of the axial position x for $0 \leq x \leq 50$. Therefore, N and $\Delta\omega$ do not have to be changed each time η, τ, m, or x are changed. Good results were obtained by setting $N = 2^{11}$ and the product $N\Delta\omega = 16\pi/t_0$, where t_0 is the dimensionless time at which $\varphi(t)$ attains a maximum.

It is evident from the preceding discussion that in order to compute any one of the solutions 5.9 - 5.11, the associated integrand has to be evaluated as a function of ω at a very large number of points, $N = 2^{11}$ for example. It would be an even greater number, namely $2N$ points, but for the symmetry of the integrands. When ω is replaced by $-\omega$, the corresponding integrand takes the complex

conjugate of its original value. This, at least, saves evaluation at half of the $2N$ points. Thus, k must be calculated as a function of ω for N values of ω. It is clear, then, why an analytic formula for $k(\omega)$ is so desirable. The cost of solving the dispersion equation, as given by eqn. 4.32 for example, at N values of ω is astronomical since eqn. 4.32 is a transcendental equation. The use of an explicit formula to evaluate k is considerably cheaper. The fact that we have, in eqn. 4.60, an approximation for k that is uniformly valid in ω is an added convenience. This allows us to avoid the use of separate expansions for k, where each expansion is valid in only a part of the domain for ω, and the attendant problems involved in connecting these expansions.

The numerical computation of the solutions contained in eqns. 5.9 - 5.11 is based on a semi-infinite tube whose physical parameters are those of tube B in Newman et al. (1983). Thus $h = 0.035$ cm, $R = 0.4$ cm, and $c_0 = 833$ cm/s. As the tube is slightly more dense than the fluid it contains, we take $\gamma/\rho = 1.1$. The kinematic viscosity is chosen to be $\nu = 1.007\times10^{-2}$ cm^2/s, corresponding to that of water at 20°C (Patel and Vaishnav, 1980). According to Moodie et al. (1985), an appropriate choice for the viscoelastic parameter τ associated with this latex rubber tube is $\tau = 0.15$ (7.2×10^{-5} s).

The pressure input at $x = 0$ shown in Fig. 5.1 is

$$\varphi(t) = \frac{1}{2}\,[1 + \cos(\pi(t-t_0)/t_0)](H(t)-H(t-2t_0)) \,, \qquad (5.15)$$

The function $\varphi(t)$ is an idealization of the pressure input in the

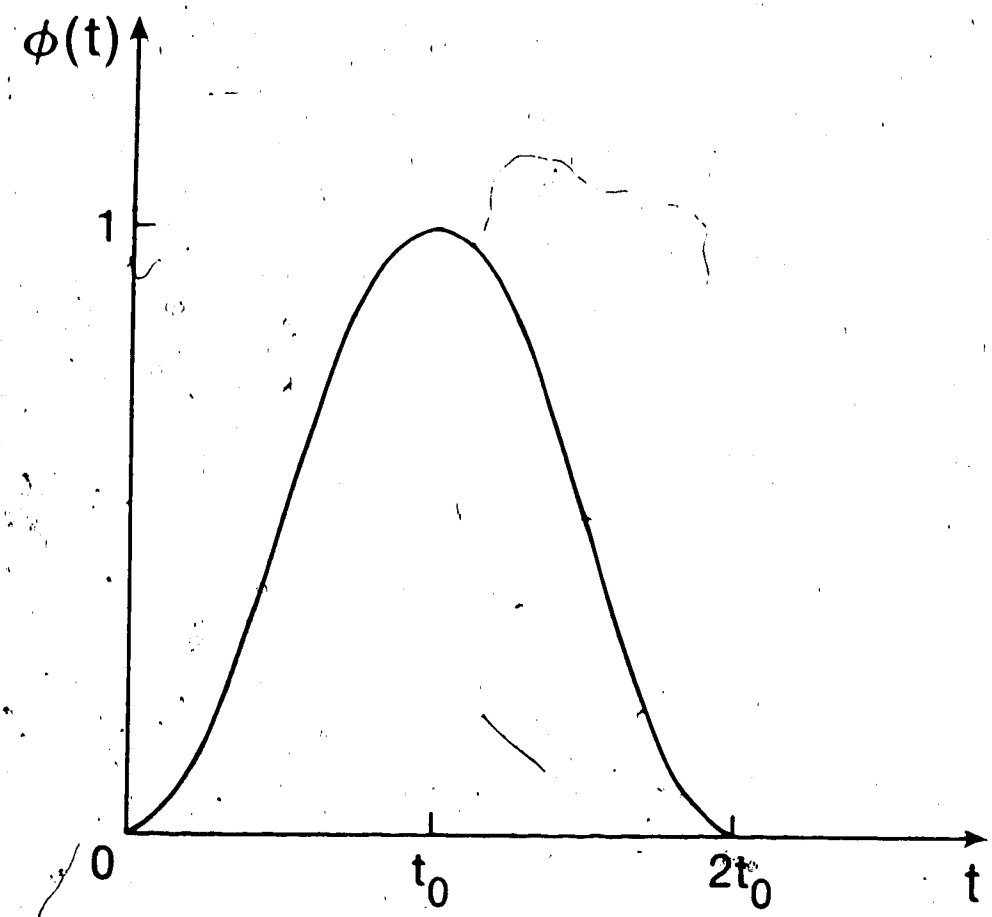

Fig. 5.1. Input function ϕ specifying averaged pressure p_m at $x = 0$.

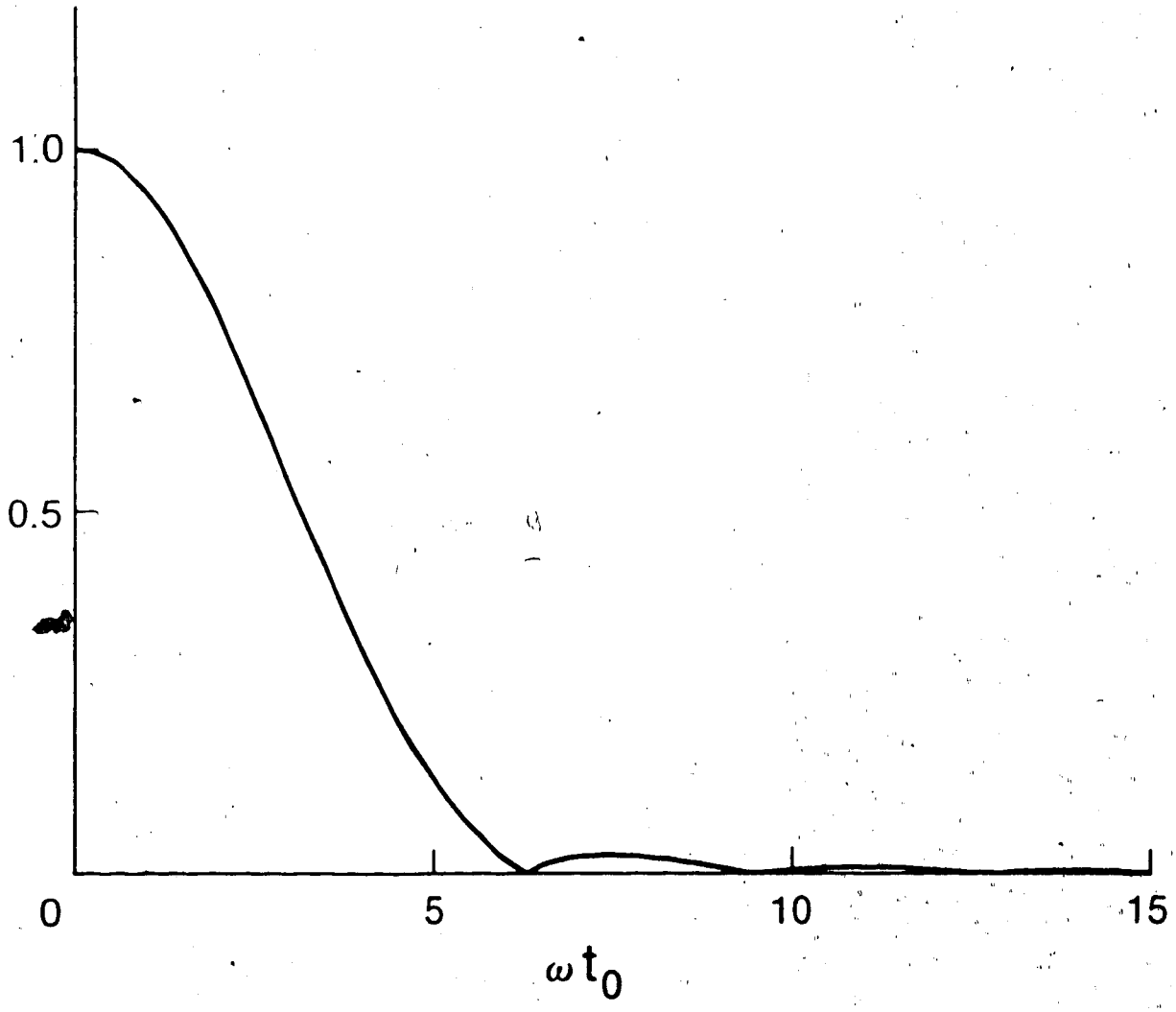

Fig. 5.2. The absolute value of $\bar{\phi}/t_0$ as a function of ωt_0.

experiments reported by Greenwald and Newman (1982) and Newman et al. (1983). In those experiments, the input pressure was at a maximum in 3 ms, which translates to 6.25 in our nondimensional scheme. Hence, we take $t_0 = 6$ as the dimensionless peak time. The Fourier transform of $\varphi(t)$ is

$$\bar{\varphi}(\omega) = \frac{1}{2}\left[\frac{(\pi/t_0)^2}{i\omega\left([\pi/t_0]^2 - \omega^2\right)}\right](1-e^{2t_0\omega i}) . \qquad (5.16)$$

The modulus of the transform is depicted in Fig. 5.2. It is clear that when $t_0 = 6$ virtually all of the energy contained in the pressure input lies in the interval $0 \leq \omega \leq 1.5$.

The averaged fluid pressure corresponding to the input pressure given in eqn. 5.1 is plotted in Fig. 5.3 at various stations along the tube. The corresponding graphs of averaged axial velocity and radial wall displacement were found to be indistinguishable in shape from the graph of averaged pressure, so they are not presented here. The pressure p_m in Fig. 5.3 agrees well with solutions to similar boundary-value problems obtained from an inviscid theory (Moodie et al., 1984; Moodie et al., 1985; Moodie et al., 1986). The pulse broadens, is attenuated, and its oscillatory tail is damped as the wave travels down the tube. As is noted in Chapter II, the same general pattern of pulse propagation is observed in the experiments of Newman et al. (1983).

In Fig. 5.4, the pressure p_m is plotted for the same parameter

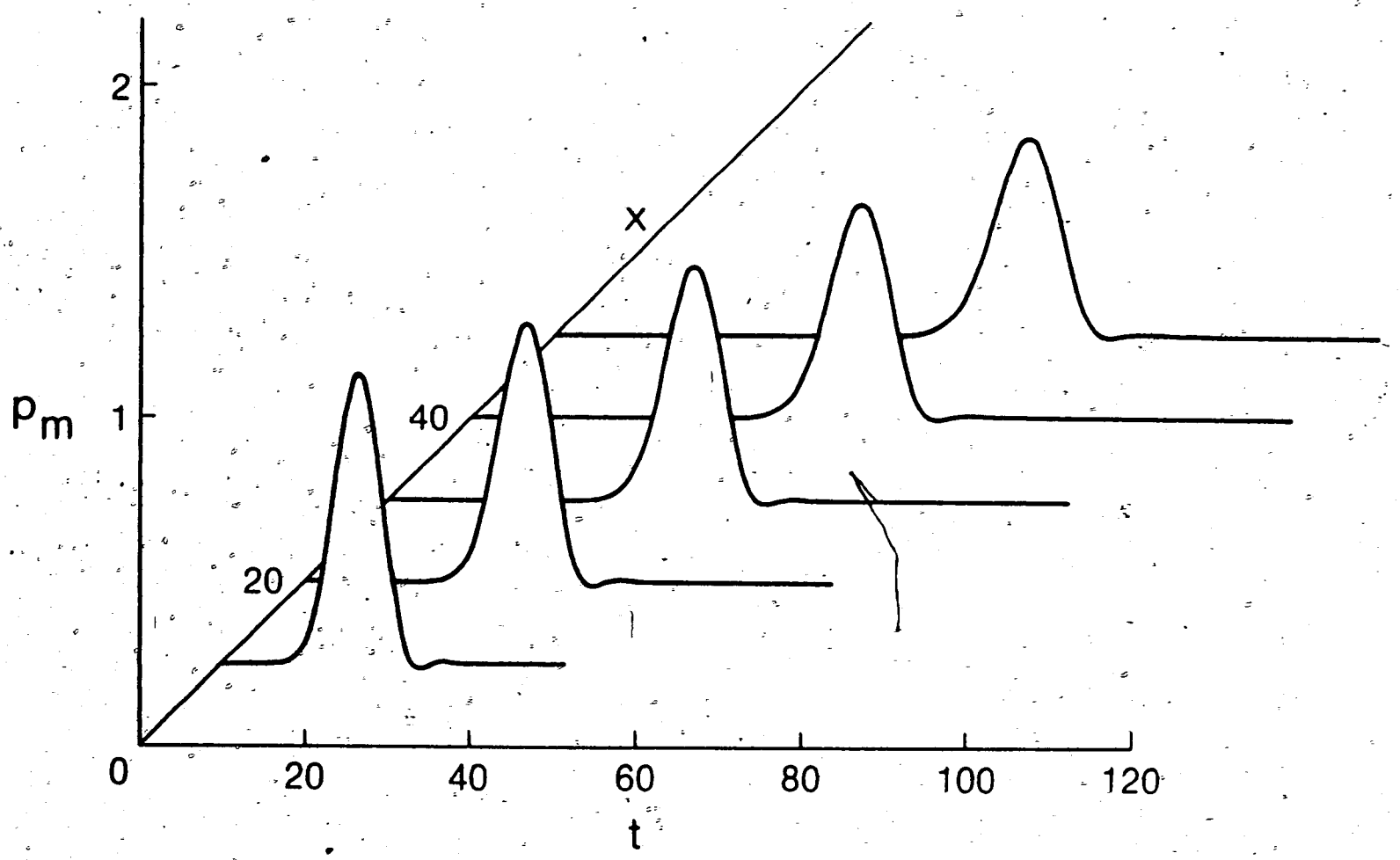

Fig. 5.3. Variation of nondimensional averaged pressure p_m with nondimensional time at the nondimensional stations x = 10, 20, 30, 40, 50 for Γ = 0.173125, τ = 0.15, m = 33088.

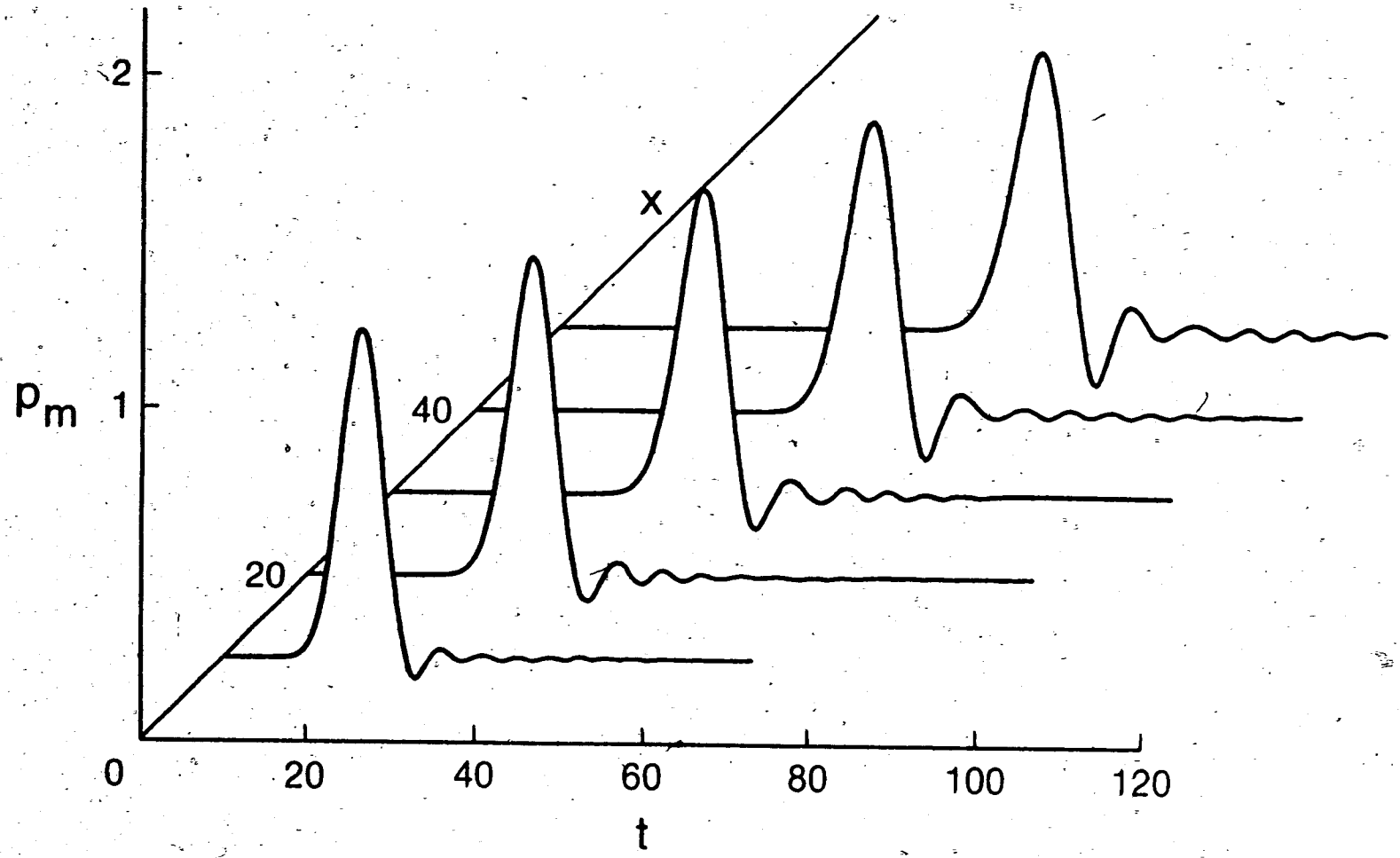

Fig. 5.4. Variation of nondimensional averaged pressure p_m with nondimensional time at the nondimensional stations x = 10, 20, 30, 40, 50 for $\eta = 0.173125$, $\tau = 0$, m = 33088.

values as in Fig. 5.3, except that in the former figure we take $\tau = 0$ to represent an elastic, rather than a viscoelastic, tube. It is obvious that the pulse depicted in Fig. 5.4 does not share the same propagation characteristics with the pulse in Fig. 5.3. The pulse in Fig. 5.4 is damped and its peak is attenuated, but the wave train following the main part of the pulse grows in amplitude from one station to the next. This feature is magnified in Fig. 5.5 where p_m is plotted for $t_0 = 3$ with the other parameters unchanged from Fig. 5.4. When the parameter value $\tau = 0$ is replaced by $\tau = 0.15$, the wave train following the pulse reverts to the state depicted in Fig. 5.3: that is, it is annihilated. Figure 5.6 demonstrates this result. Although some of the energy in the pressure input falls in the region $\omega > 1.5$ for the choice $t_0 = 3$, the bulk of the energy in the pulse remains in the interval $0 \leq \omega \leq 1.5$, so the behaviour of the pulse when $t_0 = 3$ is useful in confirming characteristics detected when $t_0 = 6$.

A likely explanation for the presence of the wave train described in the preceding paragraph is based on the weakness of fluid viscosity as an agent of attenuation. As a consequence of the dispersive character of the propagation process, the higher frequency components in the pulse fall behind the lower frequency components as the wave travels down the tube. This is evident from the variation in c with ω depicted in Fig. 4.6, for example. These components are not observed in Figs. 5.3 and 5.6, where $\tau = 0.15$, as they are attenuated far more severely than the lower frequency components for this value of the viscoelastic parameter. Figure 4.8 supports this argument. On the

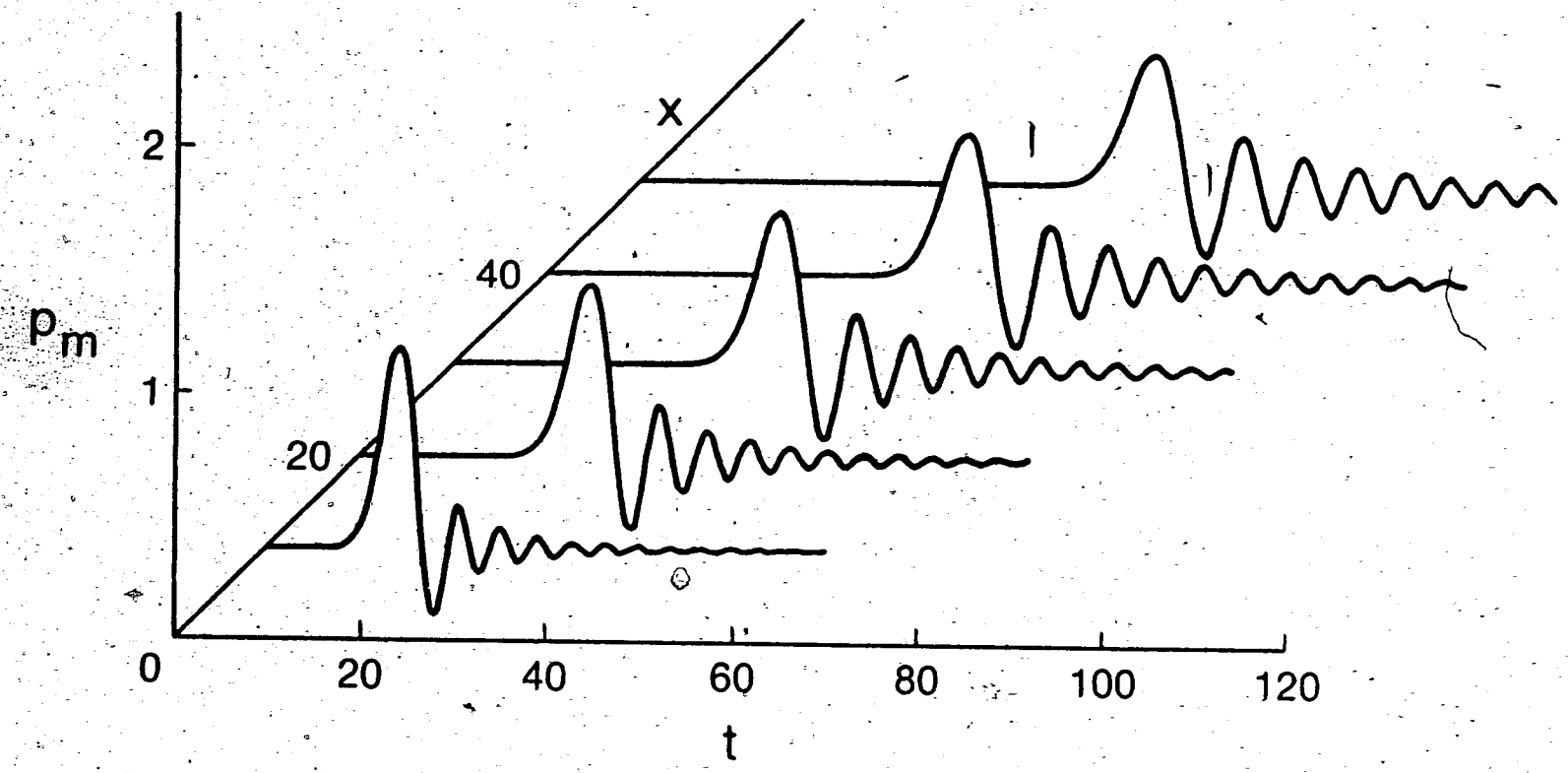

Fig. 5.5. Variation of nondimensional averaged pressure p_m with nondimensional time at the nondimensional stations x = 10, 20, 30, 40, 50 for $\eta = 0.173125$, $\tau = 0$, m = 33088, and $t_0 = 3$.

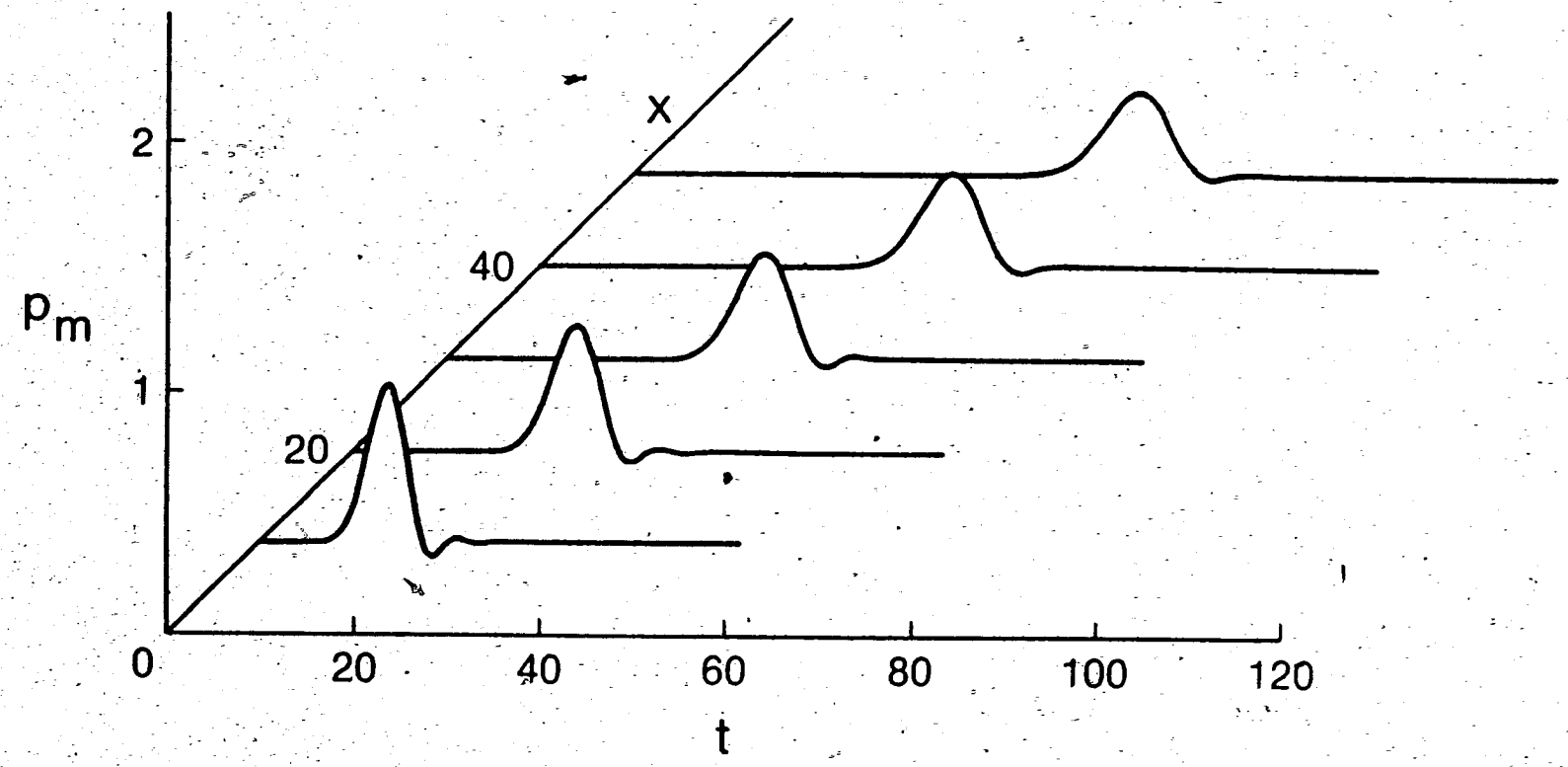

Fig. 5.6. Variation of nondimensional averaged pressure p_m with nondimensional time at the nondimensional stations $x = 10, 20, 30, 40, 50$ for $\eta = 0.173125$, $\tau = 0.15$, $m' = 33088$, and $t_0 = 3$.

other hand, when $\tau = 0$, the higher frequency components are not damped any more than the lower frequency ones, according to Fig. 4.10. Thus, as the attenuation produced by fluid viscosity is quite weak, the wave train following the pulse does not disappear in Figs. 5.4 and 5.5.

In fact, the wave train grows, rather than decays, from one station to the next. This is not a manifestation of an instability in the propagation process. It simply reflects the fact that energy is shifted from lower frequency components in the main part of the pulse to higher frequency components in the wave train, on account of the aforementioned dispersive qualities of these waves, at a faster rate than it can be dissipated by the effects of fluid viscosity. The production of wave trains behind the main part of the pulse is far more dramatic in fluid-filled tubes in which all dissipative effects have been ignored, as can be seen clearly in the papers by Moodie and Haddow (1978, 1980).

In the impulses generated by Newman et al. (1983), wave trains do not develop behind the main part of the pulse. It is clear from the preceding discussion, then, that fluid viscosity alone cannot account for the dissipative effects observed in these pulses. On the other hand, the use of wall viscoelasticity in the fluid-filled tube model produces pulses that agree well with the ones generated in the experiments cited above. Thus, wall viscoelasticity must be the chief source of dissipation in these fluid-filled tubes. This conclusion, based on considerations of the propagation properties of the entire pulse, demonstrates that the view espoused in Caro et al. (1978), where only the propagation characteristics of individual frequency components

were examined, is an accurate one. A more detailed comparison of the respective roles of wall viscoelasticity and fluid viscosity in the dissipation and dispersion of pressure pulses follows in the next section.

The Role of Dissipative Mechanisms

In Chapter IV, we compared the influence of wall viscoelasticity with that of fluid viscosity on the propagation of individual frequency components within a pulse by analysing the respective contributions of the two dissipative mechanisms to the behaviour of the phase velocity c and the transmission per unit distance $\exp[-\mathrm{Im}\, k]$ as functions of ω. Here, we discuss the impact that wall viscoelasticity and fluid viscosity have on the propagation of the pulse as a whole.

The quantitative effect of wall viscoelasticity on the average pressure is illustrated in Fig. 5.7, where p_m is plotted at $x = 30$ for three different values of τ. It is seen in this graph that the peak of the pulse occurs slightly earlier in time as τ is increased. This implies that the velocity of the main part of the pulse increases as the viscoelasticity of the wall increases. The same conclusion was reached in Chaper IV on the basis of the frequency spectra plots. Figure 5.7 also shows that part of the wave train behind the pulse remains when $\tau = 0.05$, but as τ is increased, only a single oscillation in this wave train is retained. Finally, the attenuation in the peak of the pulse produced by wall viscoelasticity is very clearly indicated in Fig. 5.7. This attenuation is discussed in greater detail below in connection with the attenuation plots shown in

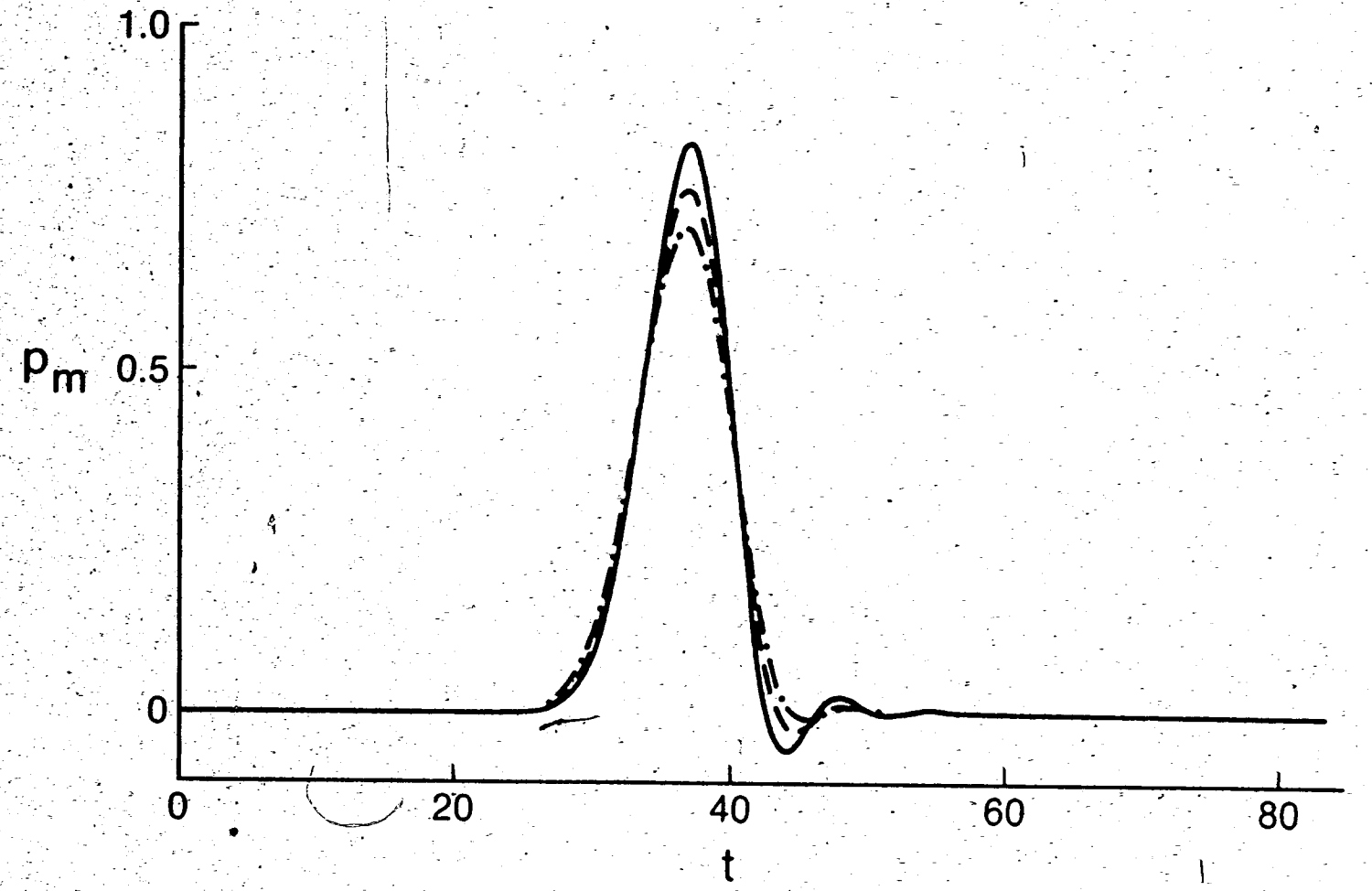

Fig. 5.7. Variation of nondimensional averaged pressure p_m with nondimensional time at the nondimensional station $x = 30$ for $n = 0.173125$, $m = .33088$, $\tau = 0.05$ (-), 0.10 (--), 0.15 (-·-).

Figs. 5.10 - 5.13.

The effect of fluid viscosity on the pressure pulse is depicted in Fig. 5.8, where p_m is plotted at $x = 30$ for the values of m associated with an inviscid fluid, water, and whole blood. It is seen in this graph that fluid viscosity affects the velocity of the pulse in a way opposite to that of the wall viscoelasticity. The peak pressure occurs later in time as fluid viscosity is increased. This, too, is consistent with the predictions in Chapter IV. As $\tau = 0.15$ for the graphs plotted in Fig. 5.8, only the first oscillation in the wave train behind the pulse is observed. For a sufficiently large increase in fluid viscosity, even this overshoot in pressure disappears. The attenuation in the peak of the pulse caused by fluid viscosity is not great, but it is much larger than is predicted from Fig. 4.9 in Chapter IV. We return to this point later when discussing Figs. 5.10 - 5.13.

The contributions of wall viscoelasticity and fluid viscosity to the shape of the pressure pulse are compared in Fig. 5.9. There, p_m is plotted at $x = 30$ for the case of an elastic tube containing whole blood or a fluid whose kinematic viscosity is twenty times that of water, and for the case of a viscoelastic tube containing an inviscid fluid. It is seen that a fluid much more viscous than blood is required to attenuate the peak of the pulse to the same degree as is done by the particular viscoelastic tube represented in this graph, and that even a fluid of such great viscosity cannot annihilate the train of oscillations trailing the main pulse. These observations agree with the predictions in Chapter IV based on Figs. 4.9 and 4.10. Thus, Fig. 5.9 provides further evidence that it is wall viscoelasticity, rather

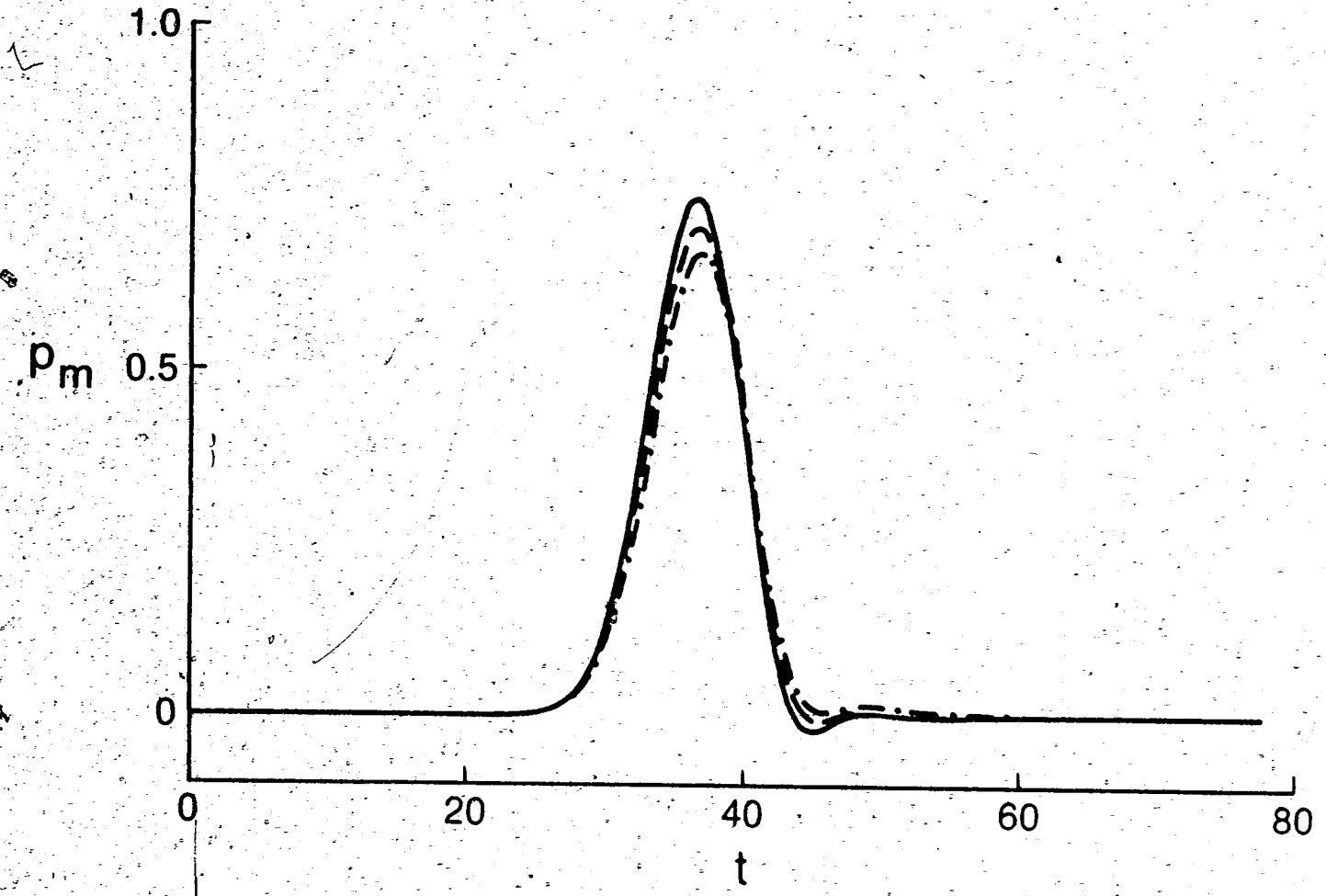

Fig. 5.8. Variation of nondimensional averaged pressure p_m with nondimensional time at the nondimensional station $x = 30$ for $\eta = 0.173125$, $\tau = 0.15$, $m \to \infty$ (-), 33088 (--), 8791 (-·-).

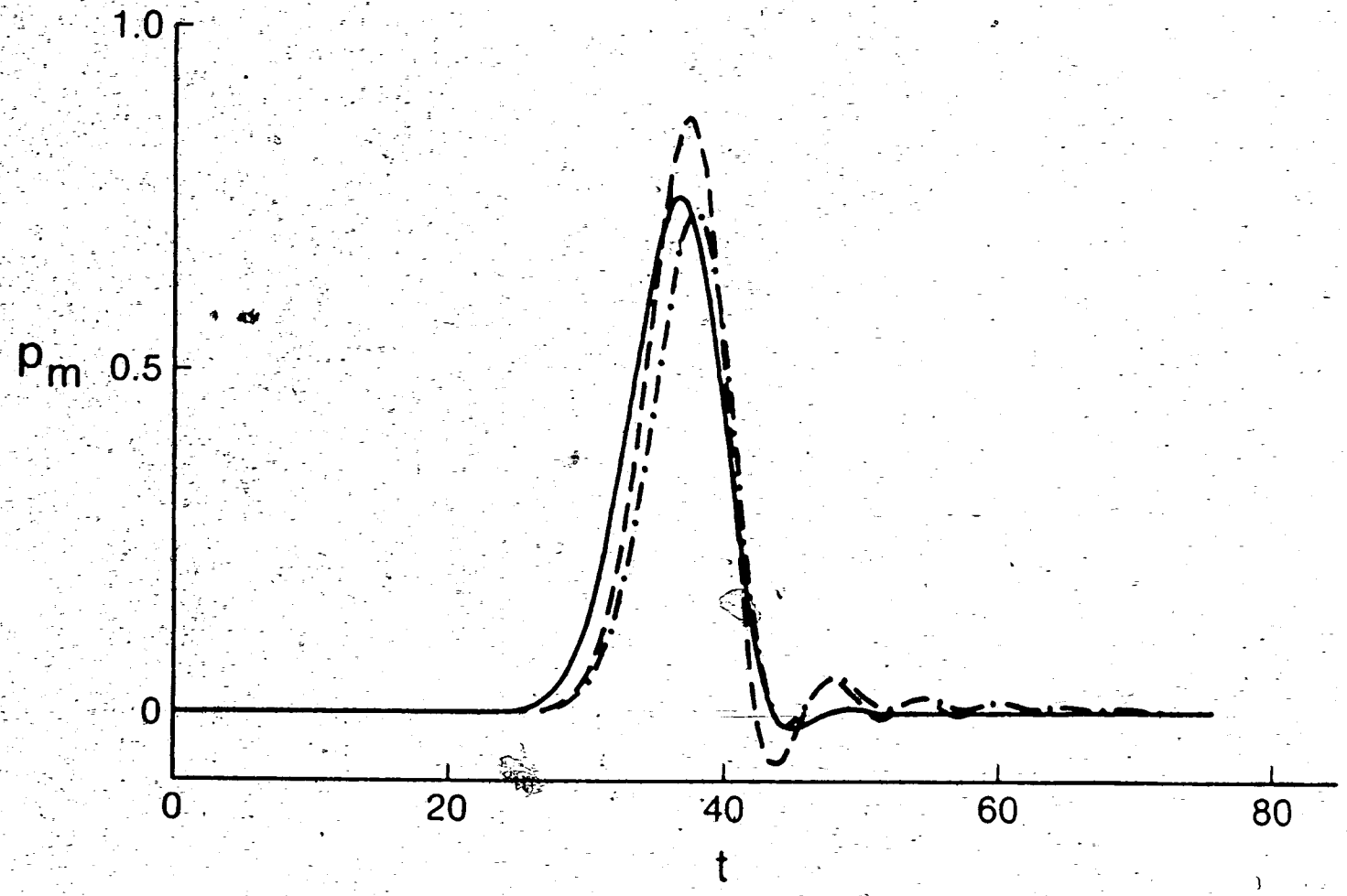

Fig. 5.9. Variation of nondimensional averaged pressure p_m with nondimensional time at the nondimensional station $x = 30$ for $\eta = 0.173125$, $\tau = 0.15$, $m \to \infty$ (-), and $\tau = 0$, $m = 8791$ (--), 1666 (-·-).

than fluid viscosity, that is the chief source of the damping observed in pressure pulses in large arteries and in water-filled latex tubes.

The decay in peak pressure observed in the pulses considered in this chapter is subjected to closer scrutiny in Figs. 5.10 - 5.13. In these figures, the maximum amplitude of p_m is plotted at successive stations along the tube for a variety of values of τ and m. With certain exceptions, these graphs display the same concave behaviour in the vertical direction that is observed in the attenuation plots depicted in Greenwald and Newman (1982). The exceptions to the general pattern occur for cases where there is little or no dissipation. Even in these situations the peak pressure eventually starts to decrease from station to station, but this is caused more by the dispersion of the main part of the pulse than by any dissipation of the pulse. Otherwise, the general pattern in the attenuation plots does not change. The peak amplitude of the pulse decays rapidly at first, but the decrease in amplitude diminishes at each successive station.

These plots affirm what has been repeated regularly throughout this dissertation: that the attenuation produced by wall viscoelasticity when τ lies between 0.1 and 0.15 is much greater than the attenuation produced by fluid viscosity when m takes the values associated with water or whole blood. This is not to say that the damping produced by fluid viscosity is insignificant, however. It is much greater than the graphs in Fig. 4.9 predict it should be. In fact, Figs. 5.10 - 5.13 demonstrate that the attenuation of pressure pulses is far more sensitive to τ or m than is indicated by the frequency spectra in Figs. 4.9 and 4.10.

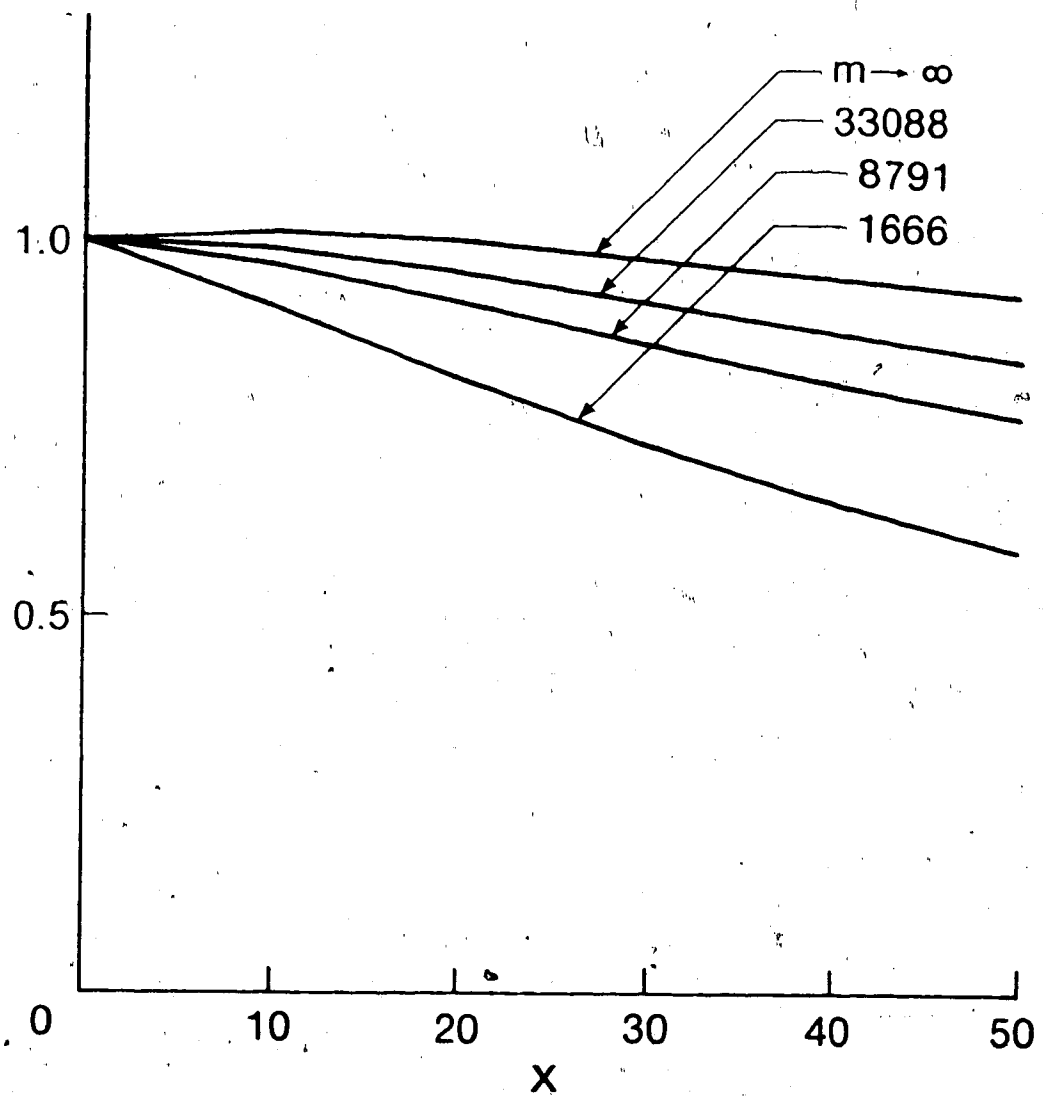

Fig. 5.10. Peak nondimensional averaged pressure versus nondimensional distance along the tube axis for $\eta = 0.173125$, $\tau = 0$, $m \to \infty$, 33088, 8791, 1666.

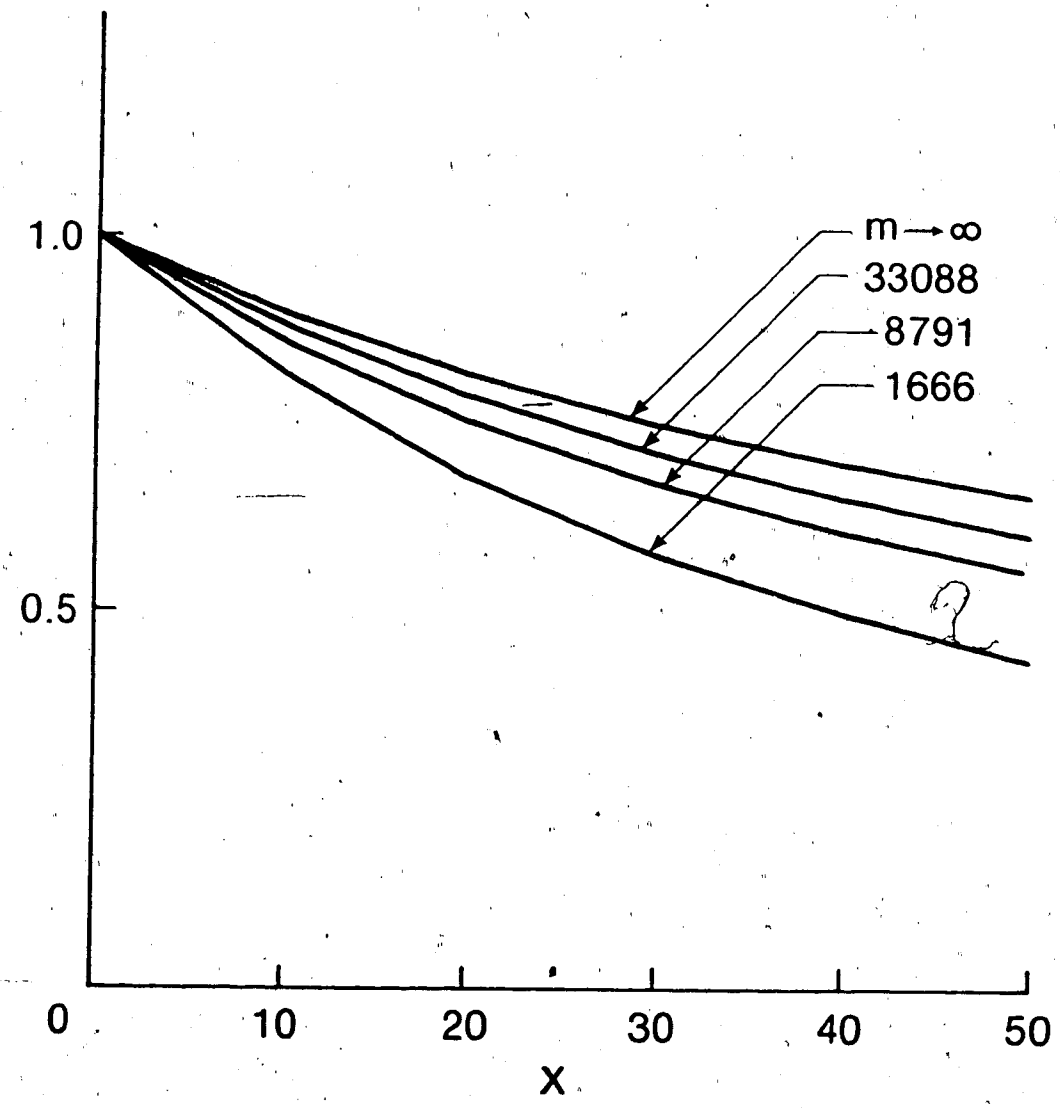

Fig. 5.11. Peak nondimensional averaged pressure versus nondimensional distance along the tube axis for $\eta = 0.173125$, $\tau = 0.15$, $m \to \infty$, 33088, 8791, 1666.

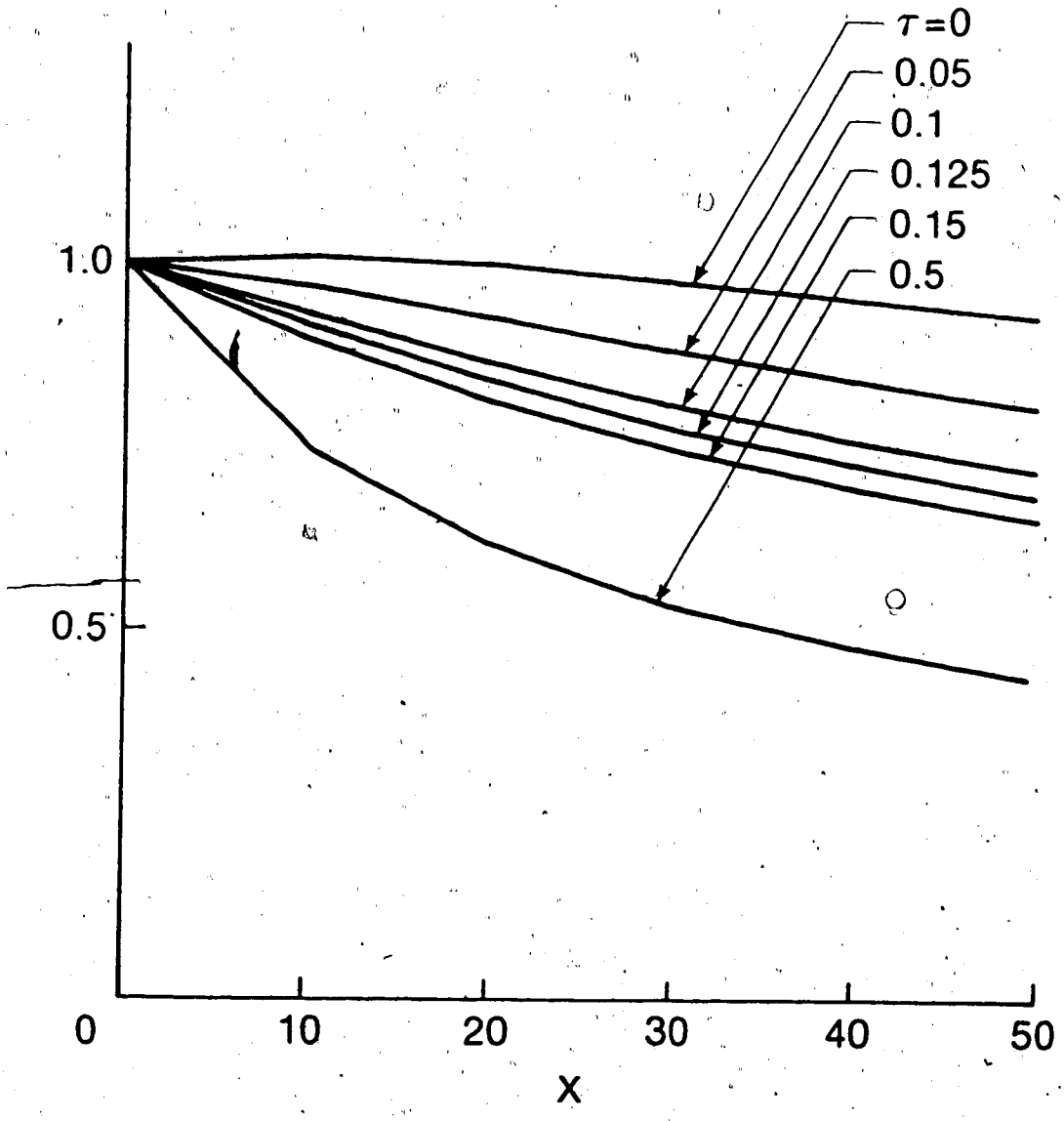

Fig. 5.12. Peak nondimensional averaged pressure versus nondimensional distance along the tube axis for $\eta = 0.173125$, $m \to \infty$, $\tau = 0, 0.05, 0.10, 0.125, 0.15, 0.50$.

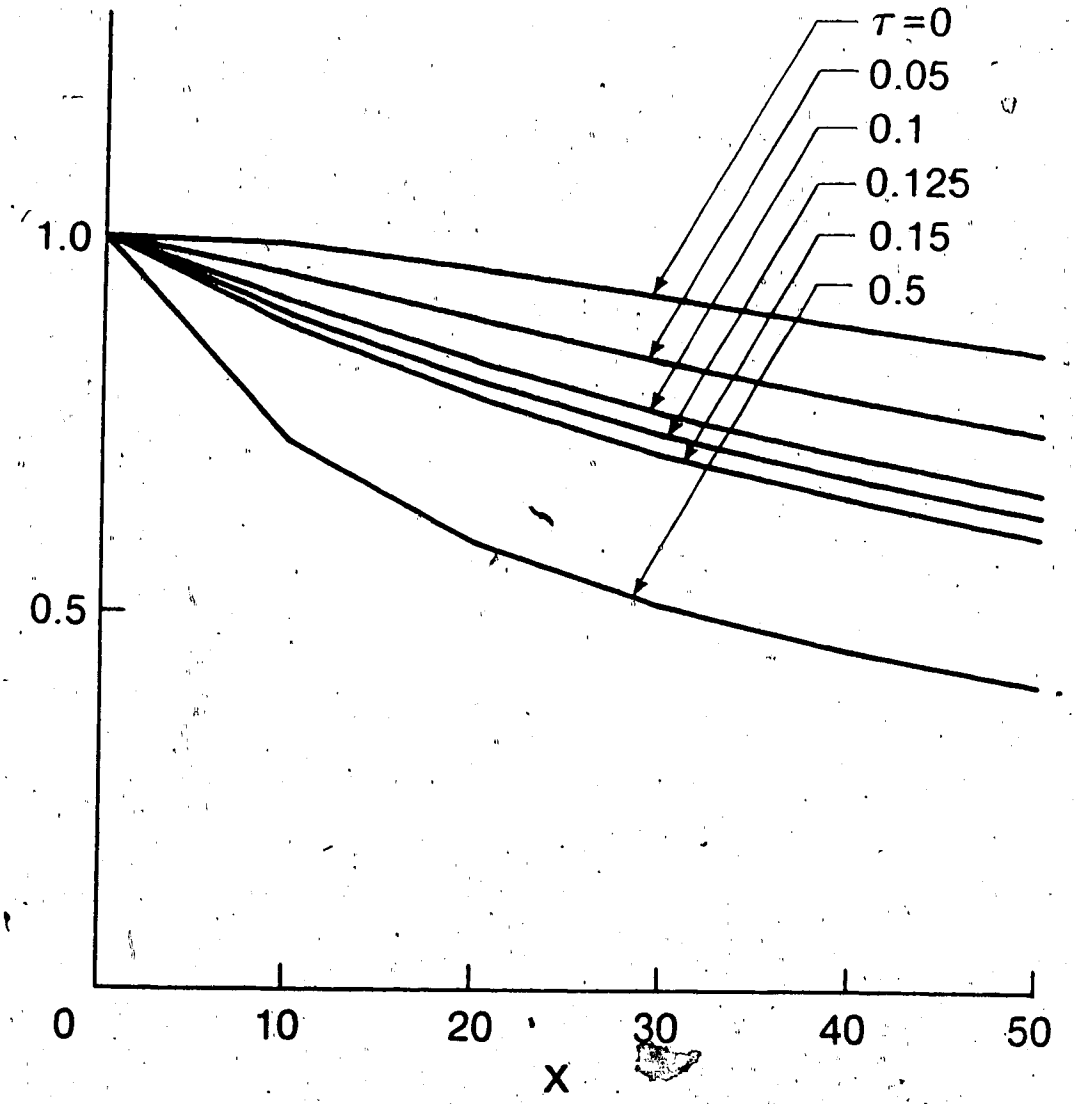

Fig. 5.13. Peak nondimensional averaged pressure versus nondimensional distance along the tube axis for $\eta = 0.173125$, $m = 33088$, $\tau = 0, 0.05, 0.10, 0.125, 0.15, 0.50$.

This suggests that there is a better approach to assessing the dissipation inherent in pressure wave propagation through fluid-filled distensible tubes than the common practice of measuring the loss in amplitude from peak to peak of steady-state sinusoidal variations in pressure. As is evident in Figs. 4.8 - 4.10, the damping of individual frequency components is not very sensitive to the strength of the dissipative processes until one reaches larger frequencies. In contrast, the attenuation of the peak averaged pressure for the type of pressure pulses analysed in this chapter is very sensitive to the degree of dissipation, according to Figs. 5.10 - 5.13. Thus, by measuring the maximum amplitude attained by pressure impulses of the sort generated by Greenwald and Newman (1982) at successive stations along the tube, it ought to be possible to identify the values of the parameters representing the dissipative mechanisms involved.

It is clear, then, from the analysis presented in this chapter, that there are many features of pressure pulse propagation in fluid-filled distensible tubes that are not obvious when considering solely the properties of the phase velocity c and the transmission per unit distance $\exp[-\mathrm{Im}\, k]$ as functions of frequency. The analysis in Chapter IV, based on the behaviour of c and $\exp[-\mathrm{Im}\, k]$, indicates that a disturbance with most of its energy concentrated in the interval $0.01 < \omega < 0.3$ should manifest few signs of dispersion or dissipation as it propagates along the tube. However, the direct computation of pulse propagation performed in this chapter, with an initial impulse whose energy is concentrated mainly in the interval $0.01 < \omega < 0.3$, demonstrates that some signs of dispersion and dissipation do appear as

the disturbance travels down the tube. The pulse broadens, its peak attenuates, and a wave train is created behind the main part of the pulse. As is noted in Chapter II, the same features are encountered in the impulses generated in the experiments of Greenwald and Newman (1982) and Newman et al. (1983). There, too, Fourier analysis of the pressure pulses did not confirm these characteristics of dispersion and dissipation.

Certainly, some aspects of the propagation process can be anticipated from plots of the frequency spectra. It is evident from Figs. 5.7 and 5.8 that the velocity of the main part of the pulse is affected very little by wall viscoelasticity or fluid viscosity. Moreover, it is clear from Fig. 5.3 that the pulse velocity is independent of either dispersive or dissipative mechanisms, as the speed of the peak of the pulse remains virtually constant throughout the period of propagation depicted in this graph. These results are consistent with the analysis in Chapter IV. Further, they demonstrate that the prediction there regarding the influence of fluid viscosity on the pulse velocity is accurate, despite the fact that fluid velocity has a great effect on the phase speed at very low frequencies. The pulse does not possess enough energy at these frequencies for the variation in c to make any difference to the overall speed of the disturbance.

The wave trains that appear behind the main part of the pulse, depicted in Figs. 5.3 - 5.6 for example, can also be predicted from plots of the frequency spectra as is seen in the discussion presented earlier in this chapter, although the assistance of hindsight in this

explanation should not go unnoticed. The broadening exhibited by the pulse, however, is not obvious from the frequency dependence of phase velocity and wave attenuation described in Chapter IV, even though the insensitivity of this broadening to changes in τ or m is. More importantly, the sensitivity of the attenuation in the peak pulse pressure to changes in τ or m, as demonstrated in Figs. 5.10 - 5.13, is not in any way evident from the frequency plots of $\exp[-\mathrm{Im}\, k]$.

The main difficulty in using plots of phase speed and wave attenuation to predict the properties of a propagating pulse occurs with those aspects of dispersion and dissipation that manifest themselves gradually as the pulse travels down the fluid-filled tube. This is not surprising when one considers that small differences in c and $\exp[-\mathrm{Im}\, k]$ are magnified in the evolution of an impulse consisting of a range of frequency components. For example, if the phase speed of two different frequencies differs by 5%, their respective components become separated by a distance equal to 2 tube radii in the time it takes the pulse to travel a distance of 40 tube radii. This separation is not large, but it will lead to alterations in the shape of the pulse. Where the difference in velocity between components is greater, the separation distance will be increased and a wave train will develop behind the main part of the pulse.

The effects of small differences in the wave attenuation between components are even greater. For example, if the difference in attenuation between two components is just 1%, their respective amplitudes will differ by 40% when the pulse has travelled 50 tube radii. This distinction in amplitude occurs after only 10 tube radii

when the difference in attenuation is 5%, and after merely 5 tube radii, or 2 cm with the dimensions used here, when the difference in attenuation is 10%. This explains the great sensitivity of the peak in the pressure pulse to changes in τ or m.

Thus, it is clear that plots of frequency spectra can be used successfully to explain qualitative features of the propagation of a pulse composed of a spectrum of frequency components. However, it is not as easy to anticipate the properties of the pulse from the behaviour of c and exp[-Im k]. The evidence of dispersion and dissipation in the pulses computed in this chapter is certainly greater than that predicted in Chapter IV. Further, it is not possible to predict the quantitative changes that variations in the physical parameters, particularly variations in the parameters representing the two dissipative mechanisms considered here, engender in the pulse as a whole on the basis of the frequency plots. These quantitative changes in the shape of the pulse can be determined only by computing the solutions for the pulse directly as is done in this chapter.

This completes the present analysis of pressure pulse propagation. It is appropriate for wave propagation in a vessel sufficiently long that reflections can be ignored, as it is based on computing solutions to the boundary-value problem formulated in Chapter III for a semi-infinite tube. It is our conclusion from this investigation that, in the absence of geometric or mechanical discontinuities, the dominant dissipative mechanism involved in the evolution of pressure pulses through large arteries or water-filled latex tubes is that of wall viscoelasticity. The part played by fluid viscosity is secondary. It

remains to be seen in Chapter VI whether this is also the case for a system of fluid-filled tubes containing junctions and other discontinuities.

CHAPTER VI

Wave Reflection

The analysis in the preceding three chapters provides a complete description of pressure pulse propagation in fluid-filled distensible tubes that are straight, uniform, and very long. The latex rubber tubes used in laboratory experiments on pressure wave propagation usually possess these properties. As is noted in Chapter II, however, the geometry of the circulatory system is not that of a straight, uniform, circular cylinder. There are bends and bifurcations, aneurysms and stenoses. Nevertheless, these features can be viewed as short geometric and mechanical transitions between straight, uniform segments.

The analysis of pulse propagation presented in this dissertation, then, can be applied to the cardiovascular system as well, provided the theory is modified to account for reflections at sites of abrupt geometric and mechanical change in the arterial tree. The model studied here adapts well to the inclusion of wave reflection at sites geometric and mechanical discontinuity in a system of uniform tubes. The necessary modifications can be made in the same way as those to the LLW theory and Womersley's theory mentioned in Chapter II. The present chapter provides a description of the details concerning these alterations and an analysis of the reflection phenomena predicted by the model.

Conditions at a Discontinuity

The abrupt changes in geometric and mechanical properties that can

occur in a system of uniform tubes obviously do not alter the equations of motion for each tube. These discontinuities merely require new boundary conditions to be added to the set of equations governing the system. Thus, the details concerning the nature of the boundary conditions appropriate for the model presented in Chapter III, and the solution of the associated pulse propagation problem, can be illustrated by the simple example of two dissimilar tubes joined together. The principles employed in solving this canonical problem can be extended directly to cover more complicated systems of tubes.

Consider, then, two dissimilar vessels connected at $x = L$. The tube occupying $x < L$ is labelled Tube 1 and the tube occupying $x > L$ Tube 2. The geometric properties of the two tubes are denoted by $h^{(i)}$ and $R^{(i)}$, where $i = 1$ indicates Tube 1 and $i = 2$ indicates Tube 2. Similarly, the mechanical properties of the two tubes are denoted by $\gamma^{(i)}$, $G_e^{(i)}$, and $\tau^{(i)}$. Consequently, the derived parameters are $c_0^{(i)}$, $\eta^{(i)}$, and $m^{(i)}$. As the two tubes are filled with the same liquid, the fluid density ρ is identical in both.

Now, suppose that a pressure pulse similar to those computed in Chapter V is generated in Tube 1 and propagates toward the junction at $x = L$. When the pulse arrives at the junction, part of it is reflected back into Tube 1 and part is transmitted into Tube 2. The relationship between the incident, reflected, and transmitted waves is determined by the boundary conditions at the junction. These conditions are prescribed later. First, we obtain the general solutions for the pulses in the two tubes.

The solutions for the incident, reflected, and transmitted pulses are nothing more than particular cases of the general solutions for p_m, v_m, and w given in eqns. 5.4 - 5.6. To maintain consistency, it is necessary to make all the variables nondimensional with respect to the parameters of one of the tubes: arbitrarily, the parameters used are those of Tube 1. Then, the respective solutions of the nondimensional dispersion equations for Tubes 1 and 2 are, according to eqn. 4.60,

$$k = \pm\omega(F_2^{(1)}\Lambda^{(1)})^{-1/2}\left[1 + \frac{1}{2}\left(\frac{F_3^{(1)}}{F_2^{(1)}\Lambda^{(1)}} - \frac{A_1^{(1)}}{(F_2^{(1)}\Lambda^{(1)})^2}\right)\omega^2\right] = \pm k^{(1)}(\omega) , \tag{6.1}$$

$$k = \pm\omega \frac{c_0^{(1)}}{c_0^{(2)}} (F_2^{(2)}\Lambda^{(2)})^{-1/2} \times\left[1 + \frac{1}{2}\left(\frac{F_3^{(2)}}{F_2^{(2)}\Lambda^{(2)}} - \frac{A_1^{(2)}}{(F_2^{(2)}\Lambda^{(2)})^2}\right)\omega^2\left[\frac{R^{(2)}c_0^{(1)}}{R^{(1)}c_0^{(2)}}\right]^2\right] = \pm k^{(2)}(\omega) , \tag{6.2}$$

where

$$\Lambda^{(1)} = 1 - i\omega\tau^{(1)} - \omega^2\eta^{(1)} , \tag{6.3}$$

$$\Lambda^{(2)} = 1 - i\omega\tau^{(2)} - \omega^2\left[\frac{R^{(2)}c_0^{(1)}}{R^{(1)}c_0^{(2)}}\right]^2\eta^{(2)} , \tag{6.4}$$

$$\{F_2^{(i)}, F_3^{(i)}, A_1^{(i)}\} \equiv \{F_2(\kappa_0^{(i)}), F_3(\kappa_0^{(i)}), A_1(\kappa_0^{(i)})\} , \quad i = 1,2 , \tag{6.5}$$

and

$$\kappa_0^{(1)} = (m^{(1)}\omega)^{1/2} e^{-i\pi/4}, \tag{6.6}$$

$$\kappa_0^{(2)} = \left(m^{(2)}\omega \left[\frac{R^{(2)} c_0^{(1)}}{R^{(1)} c_0^{(2)}} \right] \right)^{1/2} e^{-i\pi/4}. \tag{6.7}$$

It follows from eqn. 5.4, then, that the solutions for p_m^i, p_m^r, and p_m^t, respectively the incident, reflected, and transmitted pressure pulses, take the form

$$p_m^i = \frac{1}{2\pi} \int_{-\infty}^{\infty} \bar{\varphi}(\omega) \exp\{i[k^{(1)}x - \omega t]\} d\omega = \frac{1}{2\pi} \int_{-\infty}^{\infty} \bar{p}_m^i(x,\omega) e^{-i\omega t} d\omega, \tag{6.8}$$

$$p_m^r = \frac{1}{2\pi} \int_{-\infty}^{\infty} \bar{a}^r(\omega) \exp\{i[-k^{(1)}x - \omega t]\} d\omega = \frac{1}{2\pi} \int_{-\infty}^{\infty} \bar{p}_m^r(x,\omega) e^{-i\omega t} d\omega, \tag{6.9}$$

$$p_m^t = \frac{1}{2\pi} \int_{-\infty}^{\infty} \bar{a}^t(\omega) \exp\{i[k^{(2)}x - \omega t]\} d\omega = \frac{1}{2\pi} \int_{-\infty}^{\infty} \bar{p}_m^t(x,\omega) e^{-i\omega t} d\omega, \tag{6.10}$$

wherein $\bar{\varphi}(\omega)$ is determined by the incident waveform and $\bar{a}^r(\omega)$, $\bar{a}^t(\omega)$ are determined from the boundary conditions at the junction.

Similarly, the solutions for the incident, reflected, and transmitted velocity pulses are

$$v_m^i = \frac{1}{2\pi}\int_{-\infty}^{\infty} \frac{k^{(1)}}{\omega}\,\bar{\varphi}(\omega)\left[1-F(k^{(1)})/F(\kappa^{(1)})\right]\exp\{i[k^{(1)}x-\omega t]\}\,d\omega$$

$$= \frac{1}{2\pi}\int_{-\infty}^{\infty} \bar{v}_m^i(x,\omega)e^{-i\omega t}\,d\omega\,, \tag{6.11}$$

$$v_m^r = -\frac{1}{2\pi}\int_{-\infty}^{\infty} \frac{k^{(1)}}{\omega}\,\bar{a}^r(\omega)\left[1-F(k^{(1)})/F(\kappa^{(1)})\right]\exp\{i[-k^{(1)}x-\omega t]\}\,d\omega$$

$$= \frac{1}{2\pi}\int_{-\infty}^{\infty} \bar{v}_m^r(x,\omega)e^{-i\omega t}\,d\omega\,, \tag{6.12}$$

$$v_m^t = \frac{1}{2\pi}\int_{-\infty}^{\infty} \frac{k^{(2)}}{\omega}\,\bar{a}^t(\omega)\left[1-F(k^{(2)}[\frac{R^{(2)}}{R^{(1)}}])/F(\kappa^{(2)})\right]\exp\{i[k^{(2)}x-\omega t]\}\,d\omega\,.$$

$$= \frac{1}{2\pi}\int_{-\infty}^{\infty} \bar{v}_m^t(x,\omega)e^{-i\omega t}\,d\omega\,, \tag{6.13}$$

respectively, where

$$\kappa^{(1)} = [(k^{(1)})^2 - im^{(1)}\omega]^{1/2}\,, \tag{6.14}$$

$$\kappa^{(2)} = \left[(k^{(2)})^2[\frac{R^{(2)}}{R^{(1)}}]^2 - im^{(2)}\omega[\frac{R^{(2)}c_0^{(1)}}{R^{(1)}c_0^{(2)}}]\right]^{1/2}\,, \tag{6.15}$$

It is convenient in the subsequent analysis to use those branches of $\kappa^{(1)}$ and $\kappa^{(2)}$ with positive real parts, but the results are

independent of this choice as is noted in Chapter IV.

Finally, the solutions for the incident, reflected, and transmitted waveforms of radial wall displacement can also be represented in the same fashion as those above for averaged pressure and averaged axial velocity. However, as the solutions for w are not directly involved in the boundary conditions at the junction, they are not given here.

The boundary conditions are based on two physical principles: both the averaged normal stress in the axial direction, and the volume flow, must be continuous across the junction. As the averaged normal stress in the axial direction is $p_m - \frac{2}{m}\frac{\partial v_m}{\partial x}$, the continuity of this quantity across the junction yields the condition

$$p_m^i(L,t) - \frac{2}{m(1)}\frac{\partial v_m^i(L,t)}{\partial x} + p_m^r(L,t) - \frac{2}{m(1)}\frac{\partial v_m^r(L,t)}{\partial x} = p_m^t(L,t) - \frac{2}{m(1)}\frac{\partial v_m^t(L,t)}{\partial x} . \tag{6.16}$$

It is common practice for the normal stress in eqn. 6.16 to be approximated by the fluid pressure (Womersley, 1957b; Cox, 1969). This approximation is very accurate for the waveforms discussed in this thesis, as the magnitude of the stress induced by the axial velocity component is quite small for such disturbances. Nevertheless, for the sake of completeness, we express the continuity of normal stress across

the junction in its exact form here. The continuity of volume flow through the junction produces the condition

$$\pi[R^{(1)}]^2[v_m^i(L,t) + v_m^r(L,t)] = \pi[R^{(2)}]^2 v_m^t(L,t) \ , \qquad (6.17)$$

as the volume flow through any vessel is simply $\pi R^2 v_m$.

The boundary conditions prescribed in eqns. 6.16 and 6.17 enable us to determine the solutions for averaged pressure and averaged velocity in Tubes 1 and 2, as the incident waveform in Tube 1 is assumed to be known. These details form the contents of the next section. The calculation of p_m and v_m in each vessel completes the solution to the problem. In a more complicated system of tubes, the procedure outlined here must be repeated at each junction.

Reflection and Transmission Coefficients

The boundary conditions given in eqns. 6.16 and 6.17 are satisfied in a straightforward manner by the solutions provided in eqns. 6.8 - 6.13 that describe the incident, reflected, and transmitted waveforms of p_m and v_m . The latter equations can be inserted into the former to obtain

$$\bar{p}_m^i(L,\omega) - \frac{2ik^{(1)}}{m^{(1)}} \bar{v}_m^i(L,\omega) + \bar{p}_m^r(L,\omega) + \frac{2ik^{(1)}}{m^{(1)}} \bar{v}_m^r(L,\omega)$$

$$= \bar{p}_m^t(L,\omega) - \frac{2ik^{(2)}}{m^{(1)}} \bar{v}_m^t(L,\omega) \ , \qquad (6.18)$$

$$\pi[R^{(1)}]^2[\bar{v}_m^i(L,\omega) + \bar{v}_m^r(L,\omega)] = \pi[R^{(2)}]^2\bar{v}_m^t(L,\omega) \ . \qquad (6.19)$$

It follows from eqns. 6.8 - 6.13 that the ratios of $\bar{v}_m$ to $\bar{p}_m$ in the incident, reflected, and transmitted waveforms are

$$\beta^{(1)} \equiv \frac{\bar{v}_m^i(L,\omega)}{\bar{p}_m^i(L,\omega)} = -\frac{\bar{v}_m^r(L,\omega)}{\bar{p}_m^r(L,\omega)} = \frac{k^{(1)}}{\omega}\left[1-F(k^{(1)})/F(\kappa^{(1)})\right] \ , \qquad (6.20)$$

$$\beta^{(2)} \equiv \frac{\bar{v}_m^t(L,\omega)}{\bar{p}_m^t(L,\omega)} = \frac{k^{(2)}}{\omega}\left[1-F(k^{(2)}[\frac{R^{(2)}}{R^{(1)}}])/F(\kappa^{(2)})\right] \ , \qquad (6.21)$$

respectively. Consequently, it is possible to express the pair of equations 6.18 and 6.19 in terms of the two unknown ratios

$$R_c = \frac{\bar{p}_m^r(L,\omega)}{\bar{p}_m^i(L,\omega)} \ , \quad T_c = \frac{\bar{p}_m^t(L,\omega)}{\bar{p}_m^i(L,\omega)} \ , \qquad (6.22)$$

where R_c is the ratio of the amplitude of the reflected pressure wave to that of the incident pressure wave at $x = L$ and T_c is the corresponding ratio of the amplitude of the transmitted to the incident pressure wave. Thus, eqns. 6.18 and 6.19 become

$$\left[1 - \frac{2ik^{(1)}}{m^{(1)}}\beta^{(1)}\right](1+R_c) = \left[1 - \frac{2ik^{(2)}}{m^{(1)}}\beta^{(2)}\right]T_c \ , \qquad (6.23)$$

$$\beta^{(1)}(1-R_c) = \left[\frac{R^{(2)}}{R^{(1)}}\right]^2 \beta^{(2)} T_c \quad . \tag{6.24}$$

The solution of eqns. 6.23 and 6.24 is

$$R_c = \frac{1-\lambda_c}{1+\lambda_c} \quad , \tag{6.25}$$

$$T_c = \frac{\left[1- \frac{2ik^{(1)}}{m^{(1)}} \beta^{(1)}\right]}{\left[1- \frac{2ik^{(2)}}{m^{(1)}} \beta^{(2)}\right]} \frac{2}{1+\lambda_c} \quad , \tag{6.26}$$

where

$$\lambda_c = \left[\frac{R^{(2)}}{R^{(1)}}\right]^2 \left[\left[\frac{\beta^{(2)}}{\beta^{(1)}}\right] \frac{1- \frac{2ik^{(1)}}{m^{(1)}} \beta^{(1)}}{1- \frac{2ik^{(2)}}{m^{(1)}} \beta^{(2)}}\right] \tag{6.27}$$

is the discontinuity coefficient. The coefficients R_c and T_c depend on the change in geometric and mechanical properties at the junction but are independent of the junction's location. Therefore they completely characterize the reflection and transmission of pressure waves at any site where there is a geometric or mechanical discontinuity.

The rate of energy transfer in the reflected wave relative to that in the incident wave is R_c^2 while the rate of energy transfer in the

transmitted wave compared with that in the incident wave is

$$\lambda_c \left[\frac{1 - \frac{2ik^{(2)}}{m^{(1)}} \beta^{(2)}}{1 - \frac{2ik^{(1)}}{m^{(1)}} \beta^{(1)}} \right]^2 T_c^2 .$$

Thus, the latter quantity is called the transmission coefficient and R_c^2 the reflection coefficient. It is observed from eqns. 6.25 and 6.26 that

$$R_c^2 + \lambda_c \left[\frac{1 - \frac{2ik^{(2)}}{m^{(1)}} \beta^{(2)}}{1 - \frac{2ik^{(1)}}{m^{(1)}} \beta^{(1)}} \right]^2 T_c^2 = 1. \qquad (6.28)$$

This confirms that no energy is lost at a discontinuity under the boundary conditions imposed here.

The reflection and transmission coefficients derived in this chapter can be expressed in terms of the characteristic impedance Z in the same way as the coefficients in eqns. 2.10 - 2.13 that are based on the LLW theory. For a tube containing a viscous fluid, Z is defined as the ratio of the averaged normal stress in the axial direction to the volume flow: that is,

$$Z = \frac{\left[p_m - \frac{2}{m}\frac{\partial v_m}{\partial x}\right]}{\pi R^2 v_m} . \qquad (6.29)$$

Therefore, it follows from eqns. 4.24 and 4.25 that

$$Z(\omega) = \frac{\rho c_0\left[1 - \frac{2ik^2}{m\omega}\left[1-F(k)/F(\kappa)\right]\right]}{\pi R^2 \frac{k}{\omega}\left[1-F(k)/F(\kappa)\right]} . \qquad (6.30)$$

Consequently, the discontinuity coefficient λ_c given in eqn. 6.27 is simply

$$\lambda_c = Z^{(1)}/Z^{(2)} , \qquad (6.31)$$

as

$$Z^{(1)} = \frac{\rho c_0^{(1)}\left[1 - \frac{2ik^{(1)}}{m^{(1)}}\beta^{(1)}\right]}{\pi\left[R^{(1)}\right]^2\beta^{(1)}} , \quad Z^{(2)} = \frac{\rho c_0^{(1)}\left[1 - \frac{2ik^{(2)}}{m^{(1)}}\beta^{(2)}\right]}{\pi\left[R^{(2)}\right]^2\beta^{(2)}} . \qquad (6.32)$$

Thus, λ_c takes exactly the same form here as in the LLW theory.

This means that the coefficient R_c in eqn. 6.25 possesses the same structure as its counterpart in eqn. 2.11. This is not true for the coefficient T_c, however. There is a factor in eqn. 6.26 that is missing in eqn. 2.12. Nevertheless, these coefficients would be formally identical if T_c in eqn. 6.26 was defined to be the ratio of the transmitted normal stress to the incident normal stress, instead of

the ratio of the transmitted pressure to the incident pressure. Under these conditions, the factor $[1- \frac{2ik^{(1)}}{m^{(1)}} \beta^{(1)}]/[1- \frac{2ik^{(2)}}{m^{(1)}} \beta^{(2)}]$ would disappear from eqn. 6.26, making this equation identical to eqn. 2.12. In this case, the energy equation 6.28 reduces to the form of the energy equation in the LLW theory, eqn. 2.13, as well.

The reflection and transmission coefficients for an inviscid fluid can be recovered from those for a viscous fluid as represented in eqns. 6.25 - 6.27 by letting $m^{(1)} \to \infty$ in these equations. Thus,

$$R_c = \frac{1-\lambda_c}{1+\lambda_c} \quad , \quad T_c = \frac{2}{1+\lambda_c} \quad , \tag{6.33}$$

in this instance, where

$$\lambda_c = [\frac{R^{(2)}}{R^{(1)}}]^2 \frac{k^{(2)}}{k^{(1)}} \quad , \tag{6.34}$$

$$k^{(1)} = \omega[\Lambda^{(1)}]^{-1/2} \quad , \quad k^{(2)} = \omega[\frac{c_0^{(1)}}{c_0^{(2)}}][\Lambda^{(2)}]^{-1/2} \quad , \tag{6.35}$$

with $\Lambda^{(1)}$ and $\Lambda^{(2)}$ given in eqns. 6.3 and 6.4 respectively. The coefficients in eqns. 6.33 - 6.35 reduce to the ones of the LLW theory in the limit as $\omega \to 0$.

This is not the case, however, for the coefficients associated with a viscous fluid. It is evident from eqn. 6.27 that as $\omega \to 0$,

$$\lambda_c = \left[\frac{R^{(2)}}{R^{(1)}}\right]^3 \left[\frac{c_0^{(1)}}{c_0^{(2)}}\right] . \qquad (6.36)$$

The corresponding coefficient in the LLW theory is

$$\lambda_c = \left[\frac{R^{(2)}}{R^{(1)}}\right]^2 \left[\frac{c_0^{(1)}}{c_0^{(2)}}\right] . \qquad (6.37)$$

Thus, the limiting value of λ_c at $\omega = 0$ that is connected with the viscous theory does not agree with the corresponding value of λ_c from the inviscid theory. Disagreement between the viscous and inviscid theories as $\omega \to 0$ is also a feature of the behaviour of the phase velocity c, as is noted in Chapter IV. There, the discrepancy in the respective limiting values of c at $\omega = 0$ was blamed on the nonuniform dependence of the dispersion equation on ω and ν at $\omega = 0$, $\nu = 0$. This is the reason for the different limiting values of λ_c at $\omega = 0$ as well. The nonuniform dependence of λ_c on ω and ν at $\omega = 0$, $\nu = 0$ has not been acknowledged in the literature, unlike that of c. The influence of Womersley's work, where the range of ω considered did not include the region associated with frequencies lower that 1 Hz, bears much of the responsibility for this omission.

In contrast to the constancy of the coefficients R_c and T_c that arise in the LLW theory, the coefficients R_c and T_c presented

in eqns. 6.25 and 6.26 are functions of frequency. This is due mainly to the frequency dependence of the discontinuity coefficient λ_c in eqn. 6.27. The variation of λ_c with ω can be deduced approximately from the variation of the functions $k^{(1)}(\omega)$ and $k^{(2)}(\omega)$ in eqns. 6.1 and 6.2, as the other factors involved in λ_c depend only weakly on ω unless ω is very close to zero. Initially, as ω increases from zero, λ_c moves from its limiting value $[R^{(2)}/R^{(1)}]^3[c_0^{(1)}/c_0^{(2)}]$ at $\omega = 0$ toward the corresponding limiting value for λ_c in the inviscid case, namely $[R^{(2)}/R^{(1)}]^2[c_0^{(1)}/c_0^{(2)}]$. Thereafter, with further increases in ω, the higher order terms in $k^{(1)}(\omega)$ and $k^{(2)}(\omega)$ start to have an effect. It is evident that the ratio $[R^{(2)}c_0^{(1)}/R^{(1)}c_0^{(2)}]$ is important in these higher order terms, instead of the ratio $[(R^{(2)})^2c_0^{(1)}/(R^{(1)})^2c_0^{(2)}]$ that dominates the lowest order term.

The degree to which R_c and T_c vary with frequency can be seen exactly by plotting them as a functions of ω. The dependence of $|R_c|$ and arg $R_c = \varphi_R$ on ω is displayed in Figs. 6.1 - 6.6. As the frequency dependence of $|T_c|$ and arg $T_c = \varphi_T$ respectively is nearly identical to that of $|R_c|$ and φ_R, graphs of the former quantities are not depicted here. In order to make the choice of parameters for Figs. 6.1 - 6.6 as simple as possible, we have taken $h^{(1)} = h^{(2)}$ and $\gamma^{(1)} = \gamma^{(2)}$ in these figures. Further, it is assumed that the nondimensional relaxation time for Tube 1 is identical to the nondimensional relaxation time for Tube 2, when the former time is made dimensionless with respect to the parameters of Tube 1 and the latter

time is made dimensionless with respect to the parameters of Tube 2. This means that the viscoelastic damping in each tube is the same. As a consequence of these decisions regarding the physical properties of the two tubes, the geometric discontinuity at the junction is represented solely by the ratio $R^{(2)}/R^{(1)}$ and the mechanical discontinuity solely by the ratio $c_0^{(2)}/c_0^{(1)}$. Therefore, the dimensionless parameters η, τ, and m for Tube 2 are related to their counterparts for Tube 1 by the formulae

$$\left.\begin{aligned} \eta^{(2)} &= \frac{1}{8} + (\eta^{(1)} - \frac{1}{8}) \frac{R^{(1)}}{R^{(2)}}, \quad \tau^{(2)} = \tau^{(1)} \frac{R^{(2)} c_0^{(1)}}{R^{(1)} c_0^{(2)}}, \\ m^{(2)} &= m^{(1)} \frac{R^{(2)} c_0^{(2)}}{R^{(1)} c_0^{(1)}}. \end{aligned}\right\} \tag{6.38}$$

The variation of $|R_c|$ and φ_R with frequency near $\omega = 0$ is shown in Figs. 6.1 and 6.2 for the case $R^{(2)}/R^{(1)} = 2$, $c_0^{(1)}/c_0^{(2)} = 1$. The nonuniform behaviour of $|R_c|$ at $\omega = 0$, $\nu = 0$ is illustrated in Fig. 6.1. As is discussed earlier in this section, $|R_c|$ moves from the value $[R^{(2)}/R^{(1)}]^3[c_0^{(1)}/c_0^{(2)}]$ at $\omega = 0$ toward the value $[R^{(2)}/R^{(1)}]^2[c_0^{(1)}/c_0^{(2)}]$ as ω increases. The transition becomes less abrupt as $m^{(1)}$ is decreased, but it remains confined to a region of ω very near the origin even when the viscosity is relatively large. It is seen in Fig. 6.2 that the phase angle φ_R also behaves very

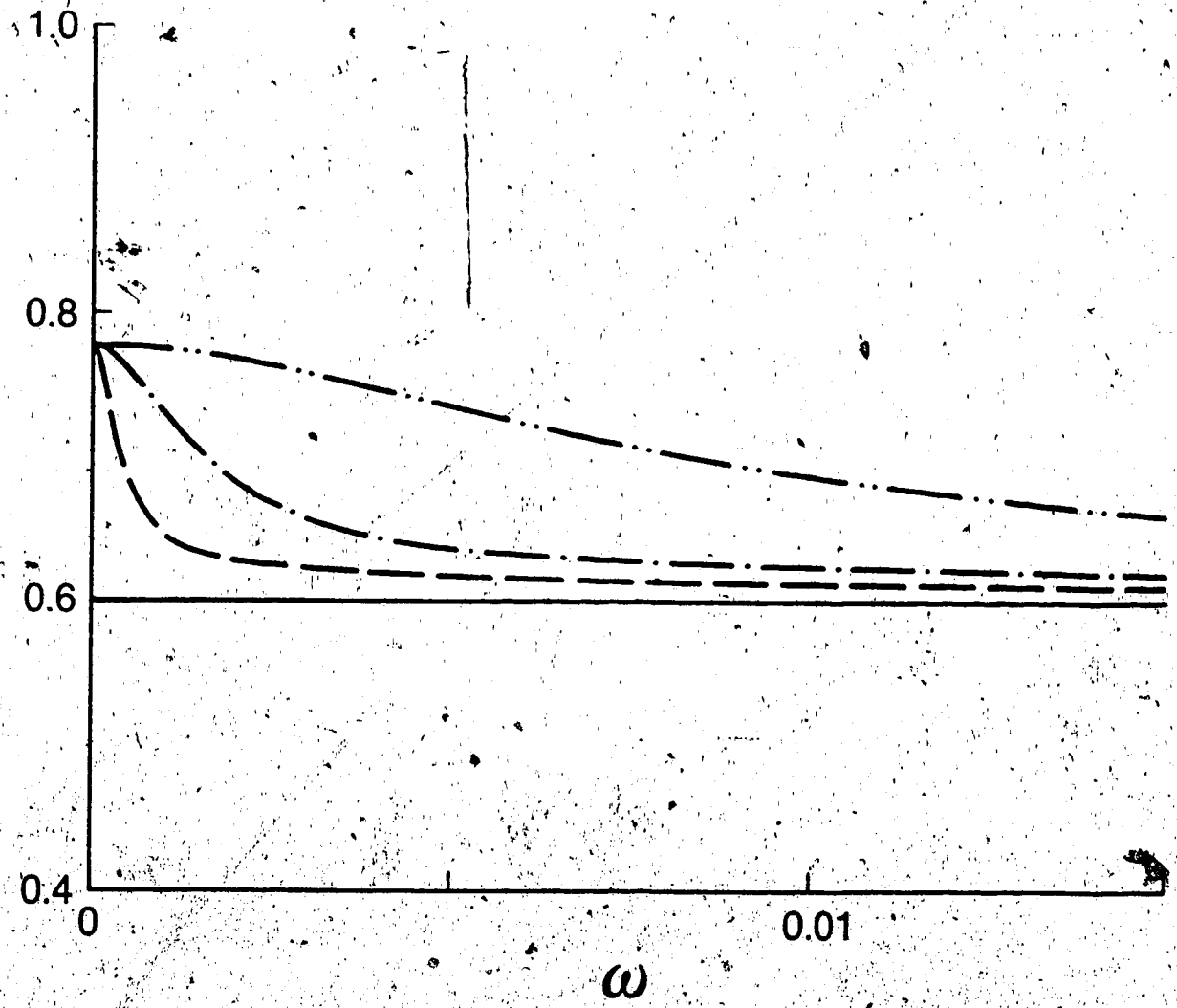

Fig. 6.1. Variation with ω of $|R_c|$ on an enlarged scale for $R^{(2)}/R^{(1)} = 1/2$, $c_0^{(1)}/c_0^{(2)} = 1$, and $\eta^{(1)} = 0.173125$, $\tau^{(1)} = 0.15$, $m^{(1)} \to \infty$ (-), 33088 (--), 8791 (-·-), 1666 (-···-).

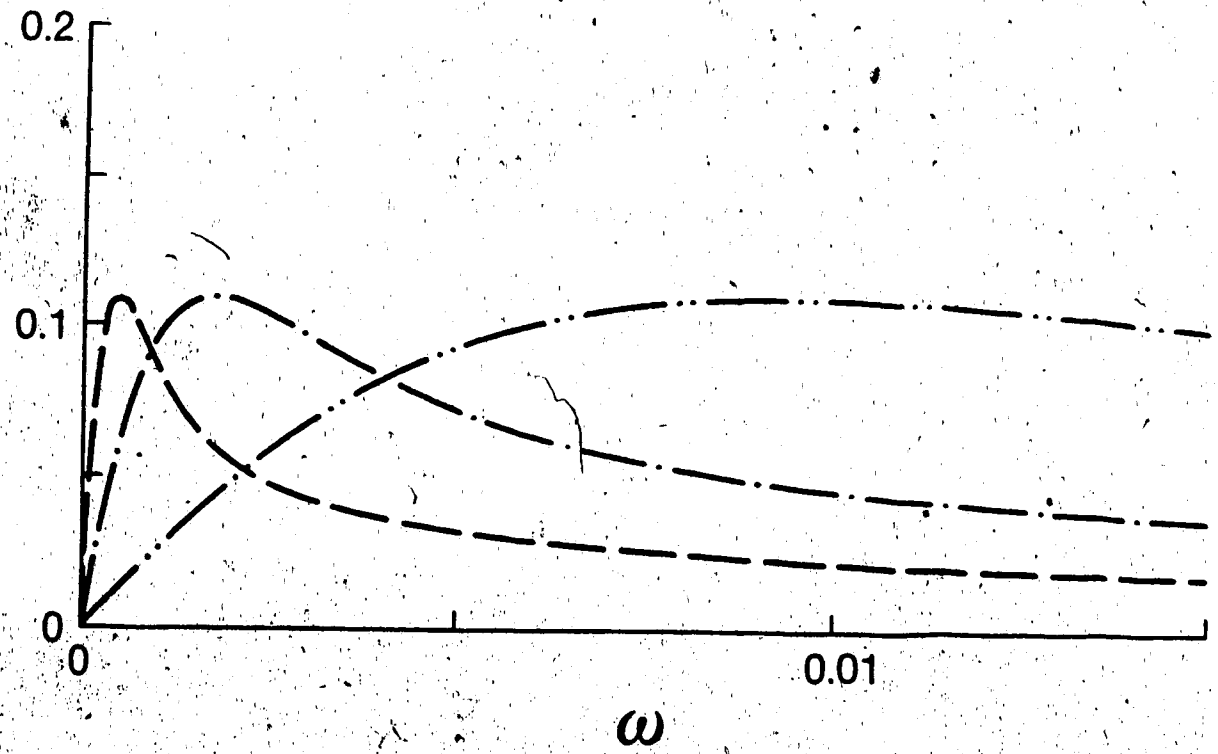

Fig. 6.2. Variation with ω of φ_R (in radians) on an enlarged scale for $R^{(2)}/R^{(1)} = 1/2$, $c_0^{(1)}/c_0^{(2)} = 1$, and $\eta^{(1)} = 0.173125$, $\tau^{(1)} = 0.15$, $m^{(1)} \to \infty$ (-), 33088 (--), 8791 (-·-), 1666 (-···-).

differently in the viscous case than in the inviscid one when ω' is near zero. For an inviscid fluid, φ_R is indistinguishable from zero over the frequency interval depicted in Fig. 6.2. When viscosity is taken into account, on the other hand, φ_R starts at zero, reaches a maximum of roughly 0.1 radians, and then descends asymptotically to zero. These effects of viscosity on R_c would be extremely difficult to detect in experiments, as they occur over such a narrow frequency band.

The dependence of R_c on ω over a much broader frequency band is illustrated in Figs. 6.3 - 6.6 for the cases $R^{(2)}/R^{(1)} = 1$, $c_0^{(1)}/c_0^{(2)} = \frac{1}{2}$, and $R^{(2)}/R^{(1)} = 1$, $c_0^{(1)}/c_0^{(2)} = 2$. At low frequencies, the dependence of R_c on frequency is quite weak. For example, the variation of $|R_c|$ and φ_R from their respective limits at $\omega = 0$ is less than 2% throughout the interval $0.015 < \omega < 0.30$ in Figs. 6.3 - 6.6 when $\tau^{(1)} = 0.15$. On the other hand, at $\omega = 1.5$, R_c is substantially different from its limit at $\omega = 0$. For the $c_0^{(1)}/c_0^{(2)} = \frac{1}{2}$, $|R_c|$ is 20% greater at $\omega = 1.5$ than at $\omega = 0$ and φ_R increases from 0 at $\omega = 0$ to 0.1 at $\omega = 1.5$ when $\tau^{(1)} = 0.15$. The change in R_c is even more striking in the case $c_0^{(1)}/c_0^{(2)} = 2$. There, $|R_c|$ doubles from $\omega = 0$ to $\omega = 1.5$ and φ_R increases from $-\pi$ at $\omega = 0$ to roughly -2.35 at $\omega = 1.5$ when $\tau^{(1)} = 0.15$. This change in phase is almost 45°.

These results help to explain why Newman et al. (1983) were unable to detect much variation with frequency in their measurements of the ratio of the amplitudes of the reflected and incident pressure waves

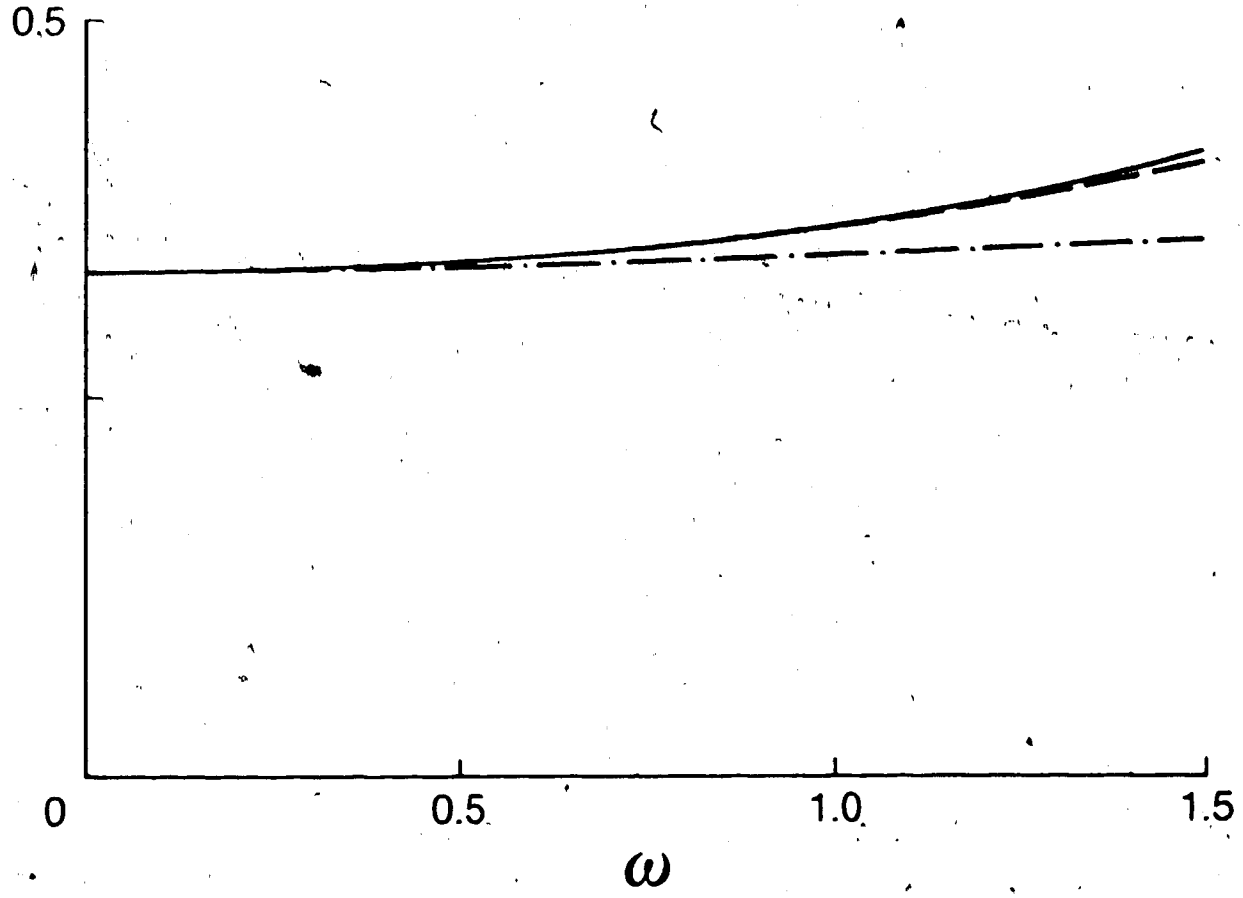

Fig. 6.3. Variation with ω of $|R_c|$ for $R^{(2)}/R^{(1)} = 1$, $e_0^{(1)}/c_0^{(2)} = 1/2$, and $\eta^{(1)} = 0.173125$, $m^{(1)} = 33088$, $\tau^{(1)} = 0.05$ (-) , 0.15 (--), 0.5 (-·-).

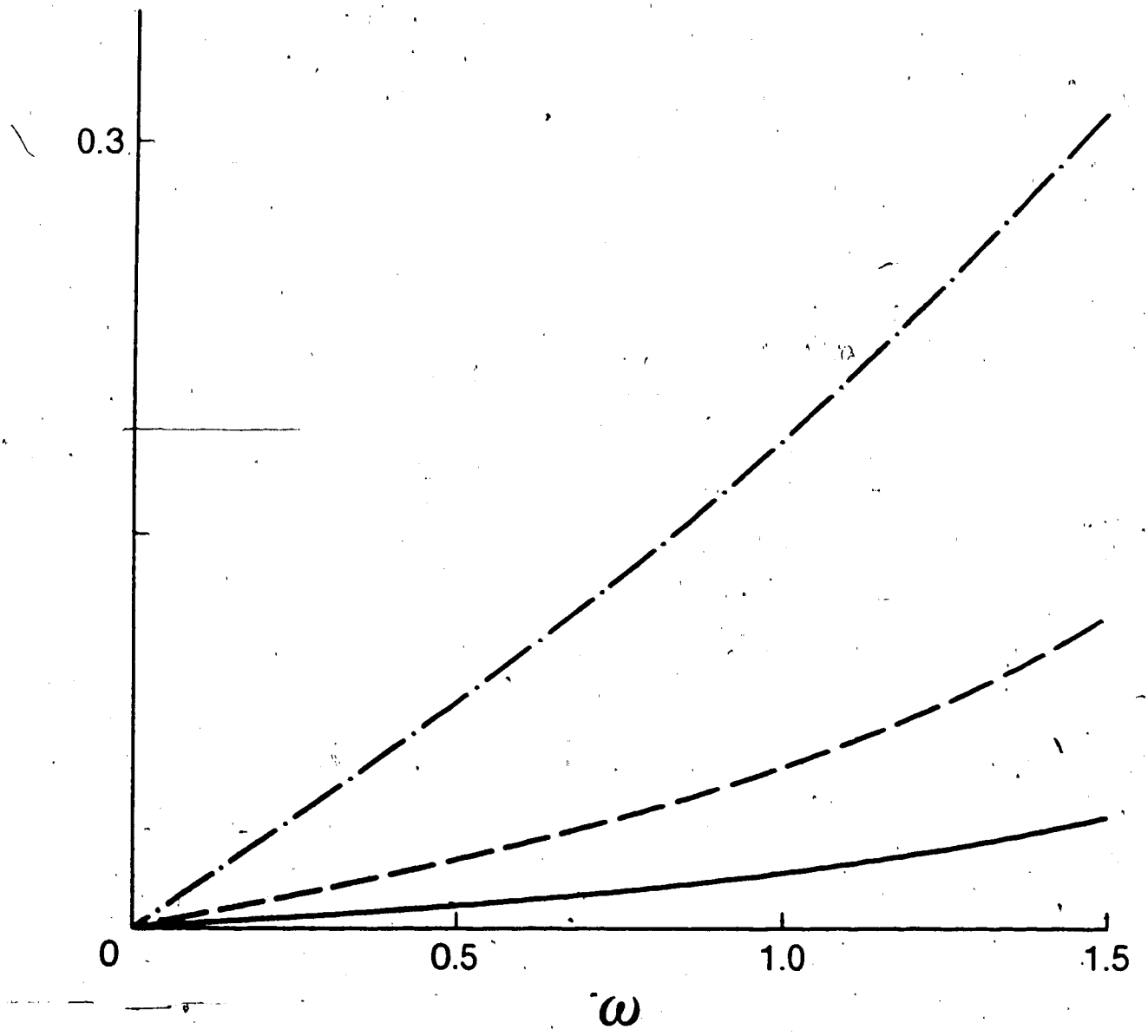

Fig. 6.4. Variation with ω of φ_R (in radians) for $R^{(2)}/R^{(1)} = 1$, $c_0^{(1)}/c_0^{(2)} = 1/2$, and $\eta^{(1)} = 0.173125$, $m^{(1)} = 33088$, $\tau^{(1)} = 0.05$ (-) , 0.15 (--), 0.5(-·-).

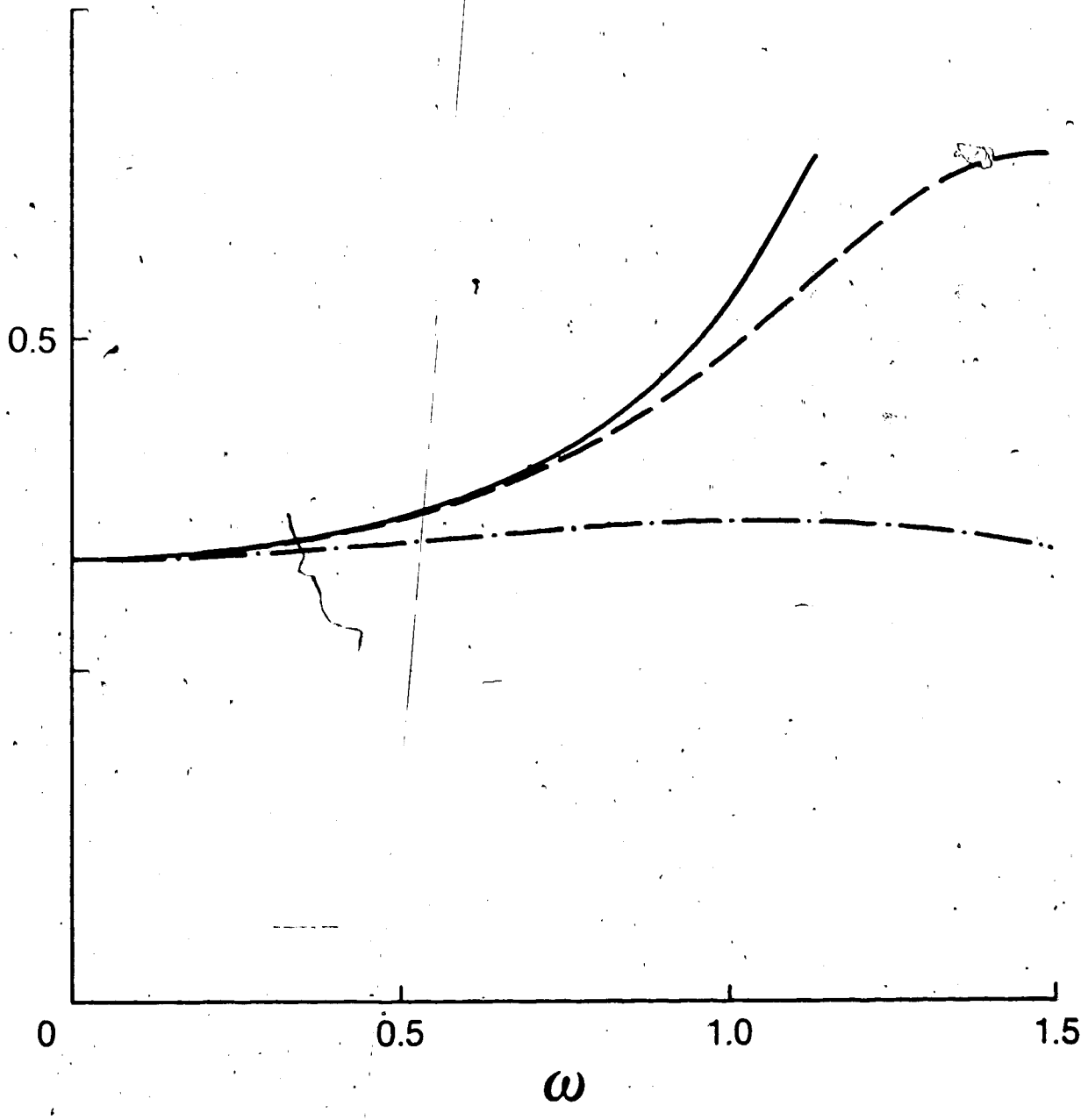

Fig. 6.5. Variation with ω of $|R_c|$ for $R^{(2)}/R^{(1)} = 1$, $c_0^{(1)}/c_0^{(2)} = 2$, and $\eta^{(1)} = 0.173125$, $m^{(1)} = 33088$, $\tau^{(1)} = 0.05$ (-), 0.15 (--), 0.5 (-·-).

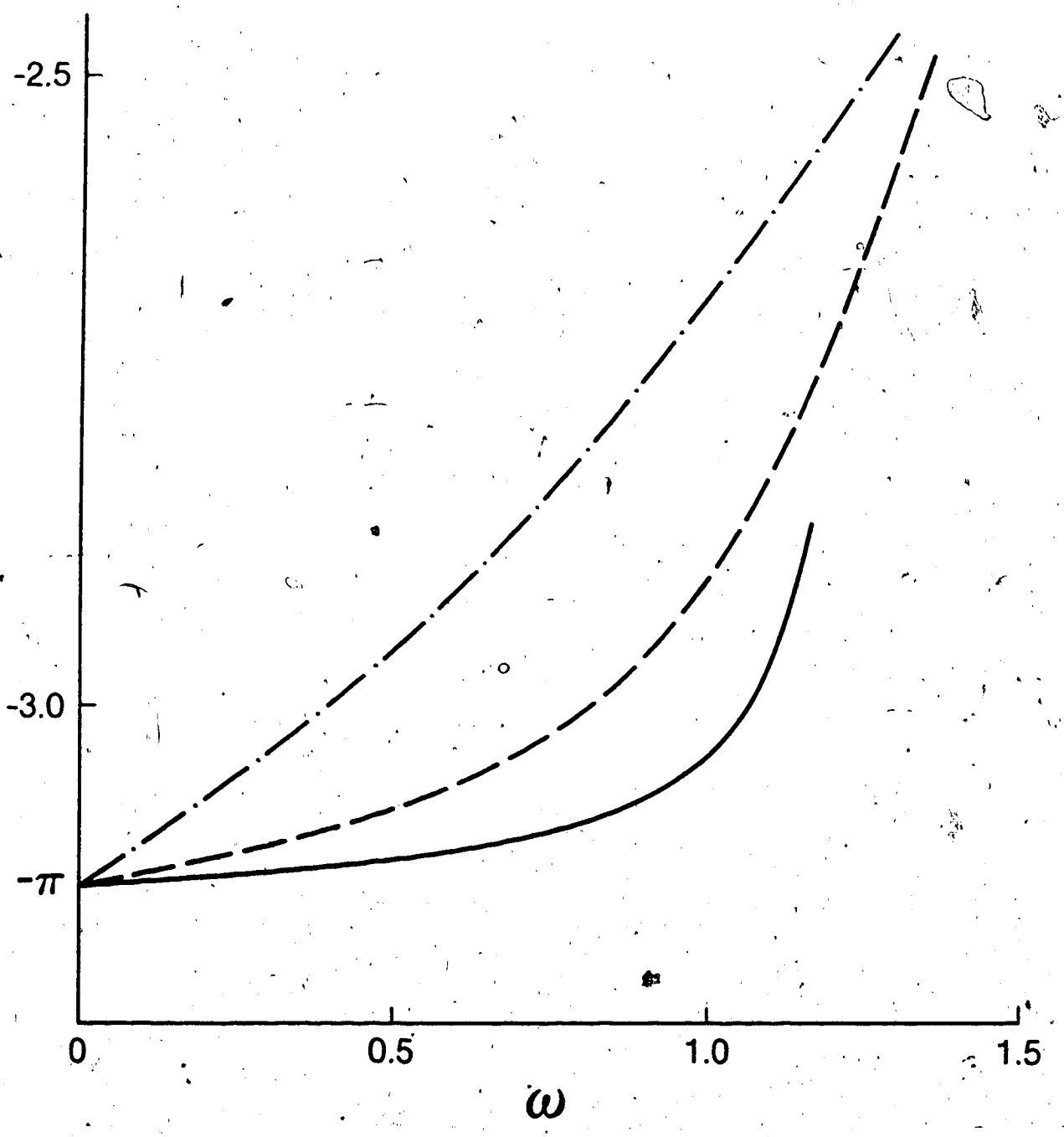

Fig. 6.6. Variation with ω of φ_R (in radians) for $R^{(2)}/R^{(1)} = 1$, $c_0^{(1)}/c_0^{(2)} = 2$, and $\eta^{(1)} = 0.173125$, $m^{(1)} = 33088$, $\tau^{(1)} = 0.05$ (-), 0.15 (--), 0.5 (-·-).

generated at a mechanical discontinuity. The range of frequencies monitored in their reflection experiments is the same as that of their impulse propagation studies, namely 5-100 Hz. This corresponds to the dimensionless interval $0.015 < \omega < 0.30$. The predicted variation in R_c, like that of the phase velocity c, is too small to detect in this interval. However, these results do predict that some variation in R_c would be observed in experiments that use pressure waves containing frequencies in the band 300-500 Hz, corresponding to the dimensionless interval $0.9 < \omega < 1.5$. Over this interval, R_c should vary from its limit at $\omega = 0$ in the manner outlined in the preceding paragraph.

It is evident from Figs. 6.3 - 6.6 that R_c is fairly sensitive to changes in $\tau^{(1)}$. As $\tau^{(1)}$ increases, the increase in $|R_c|$ with frequency diminishes, according to Figs. 6.3 and 6.5. In fact, when $\tau^{(1)} = 0.5$, $|R_c|$ is virtually flat over the interval $0 \leq \omega \leq 1.5$. In this case, the effects of wall viscoelasticity offset the frequency dependence in $|R_c|$ induced by the combined radial inertia of the fluid and the vessel wall. On the other hand, the increase in φ_R with frequency is enhanced by increasing $\tau^{(1)}$, as is clear from Figs. 6.4 and 6.6.

This sensitivity of R_c to change in $\tau^{(1)}$ is in sharp contrast to the insensitivity of R_c to change in $m^{(1)}$. Graphs of $|R_c|$ and φ_R as functions of ω are altered very little by varying $m^{(1)}$. When $c_0^{(1)}/c_0^{(2)} = \frac{1}{2}$, in fact, changes in $m^{(1)}$ cannot be observed in the plots of $|R_c|$ and φ_R. For this reason, graphs depicting the

effects of fluid viscosity on R_c are not shown here.

The dependence of R_c on $\tau^{(1)}$ and $m^{(1)}$ that is described in the preceding paragraph indicates that the influence of wall viscoelasticity is much greater than the influence of fluid viscosity on the reflection and transmission of pressure waves at a junction between two dissimilar tubes. Hence, wall viscoelasticity predominates over fluid viscosity not only in the propagation of pressure waves through a tube, but also in the reflection of these waves at a site of geometric or mechanical discontinuity.

Some conclusions about the reflection of an entire pulse at a junction between two tubes can be drawn from the analysis of the frequency dependence of the reflection and transmission coefficients presented in this section. In the first place, the reflected and transmitted pulses are not much different from predictions based on the LLW theory. When $[(R^{(2)})^2 c_0^{(1)}/(R^{(1)})^2/c_0^{(2)}] < 1$, a 'closed' reflection occurs: that is, the reflected pressure pulse is positive and the transmitted pulse is greater in amplitude than the incident pulse. Conversely, when $[(R^{(2)})^2 c_0^{(1)}/(R^{(1)})^2/c_0^{(2)}] > 1$, a 'positive' reflection occurs: the reflected pressure pulse is negative and the transmitted pulse is smaller in amplitude than the incident pulse.

Secondary changes do occur in the shape of the reflected and transmitted pulses as a result of the frequency dependence of the reflection and transmission coefficients. That part of the pulse represented by frequencies in the interval $0.01 < \omega < 0.30$ Is affected very little, as R_c and T_c depend weakly on ω throughout

this interval. However, the higher frequency components contained in the interval $0.5 < \omega < 1.5$ are altered in magnitude and phase. In the case of a closed reflection, the magnitude and phase of both the reflected and transmitted waves are greater over this frequency range than their predicted values based on the LLW theory. In the case of an open reflection, the magnitude and phase of the reflected waves are greater than those of their LLW theory counterparts, whereas the magnitude and phase of the transmitted waves are smaller. Similarly, the very low frequency components in the interval $0 \leq \omega \leq 0.01$ are modified in magnitude and in phase at the junction in the manner illustrated in Figs. 6.1 and 6.2.

The impact of the aforementioned frequency dependence in the reflection and transmission coefficients on the shape of reflected and transmitted pressure pulses at a site of geometric or mechanical discontinuity is likely to be quite small, however. Most of the energy in a typical disturbance is concentrated in the interval $0.01 < \omega < 0.30$, where the dependence of R_c and T_c on ω is weak. Not as much energy is available at other frequencies, where the variation of R_c and T_c is greater. The frequency band associated with the interval $0 \leq \omega \leq 0.01$ is simply too narrow for the energy there to be large relative to the energy in the rest of the pulse. Throughout the interval $0.5 < \omega < 1.5$, on the other hand, pressure waves are attenuated considerably as they propagate along a fluid-filled distensible tube: this is demonstrated in Chapter IV. Consequently, even if some energy is deposited in this frequency band initially, most of this energy is dissipated before the pulse can

travel far. Therefore, under most circumstances, a pressure pulse propagating from the end of one tube contains relatively little energy outside the range $0.01 < \omega < 0.30$ by the time it meets another tube.

Moreover, the time scale involved in the reflection and transmission process at a junction is not long. Reflection and transmission continues only for as long as it takes the entire pulse to arrive at the junction. Therefore, small variations in the frequency dependence of R_c and T_c cannot have an amplified effect on the reflection and transmission of a pulse. There are no surprises, then, in the changes wrought in the shapes of the reflected and transmitted pulses by frequency dependence, as there were in the case of a propagating pulse.

The arguments produced above demonstrate that any changes in the shapes of the reflected and transmitted pressure pulses from the shape of the incident pulse at a junction between two dissimilar tubes are minor. These predictions are confirmed by the direct computations done, for an inviscid fluid, in the pair of papers by Moodie and Barclay (1985, 1986). In these articles, there is little change from the shape of the incident pulse observed in the reflected and transmitted pulses, beyond that predicted by the LLW theory. Naturally, in a more complicated system of tubes, it is not as easy to determine the shapes of reflected and transmitted pulses from the frequency dependence of the reflection and transmission coefficients. This is particularly true when two sites of geometric and/or mechanical transition appear close together, as is the case in models of stenoses and aneurysms. The direct calculation of pressure pulses reflected and

transmitted through such tube systems can be accomplished with the use of the analysis presented in this chapter.

CHAPTER VII

Summary and Conclusions

In this dissertation, the results of an investigation of the mechanics of wave propagation in fluid-filled distensible tubes are presented. The distensible tubes in question are modelled on the latex rubber tubes used by researchers studying wave propagation in the cardiovascular system. The modelling performed here is also applicable to the large arteries themselves. It is primarily with the propagation of pressure pulses containing frequencies in the range 0-500 Hz that this thesis is concerned. This frequency band is much broader than that considered in most previous research on theories of wave propagation in fluid-filled distensible tubes applied to the large arteries. In the past, attention has been focused mainly on the natural arterial pulse, where the frequency content is limited to the range 1-10 Hz in humans, and 2-20 Hz in dogs. Disturbances of the sort analysed here have been artificially generated in experiments studying wave propagation in water-filled latex tubes and large arteries, for example by Greenwald and Newman (1982).

The problem central to this dissertation is the following one: what is the role of fluid viscosity in pressure pulses whose energy resides in the frequency band 0-500 Hz, and how does this role compare with that of wall viscoelasticity? In order to answer this question, the influence of viscosity and viscoelasticity is investigated not only with regard to the evolution of a pressure pulse as it travels down a tube, but also with regard to the reflection and transmission of the

pulse at discontinuities in the tube.

The role of dissipative mechanisms in the propagation of pressure pulses through fluid-filled distensible tubes is explored by studying the transient response of an appropriate fluid-filled tube model. The model employed in this thesis is the same one developed by Moodie and his colleagues (Moodie et al., 1982; Moodie et al., 1985), except that their model is extended here to include a viscous fluid. The theory is a linear one: the main contributors to pulse propagation are the pressure difference across the vessel wall, the circumferential stiffness of the vessel wall, and the combined radial inertia of the fluid and the vessel wall. Energy dissipation is provided by the viscoelasticity of the wall and the viscosity of the fluid. The viscoelastic response of the tube is modelled as a Kelvin-Voigt solid, as any linear viscoelastic solid tends to behave as a Kelvin-Voigt material at low frequencies. Our analysis is not restricted to a particular viscoelastic model, however, in that more elaborate ones can be handled with minor alterations.

The transient response of this fluid-filled distensible tube model is examined by considering two boundary-value problems. One is posed to describe the propagation of an impulse along a tube in the absence of reflections, the other to describe the reflection and transmission of an impulse at a junction between two dissimilar tubes. The solutions to both problems are constructed by means of Fourier integrals. In the course of the analysis an approximate solution to the dispersion equation is obtained, yielding an asymptotic formula for the dimensionless wave number k in terms of the dimensionless

circular frequency ω. This approximation is uniformly valid throughout the range of interest in ω and the kinematic fluid viscosity ν, except at the point $\omega = 0$, $\nu = 0$ where the dependence of k upon ω and ν is nonuniform. The approximate solution of the dispersion equation derived in this dissertation is the first one to be uniformly valid over the entire frequency range considered here, namely the range associated with the dimensionless interval $0 \leq \omega \leq 1.5$. This formula is not only of intrinsic value. It is also of benefit in the numerical calculations of the Fourier integral solutions to the two boundary-value problems, as it leads to greater computational efficiency.

Some conclusions about the propagation of pressure disturbances contained in the frequency band investigated in this thesis can be inferred by examining the frequency dependence of four functions related to $k(\omega)$: that is, the phase velocity $c = \omega/\mathrm{Re}\, k$, the transmission per unit distance $\exp[-\mathrm{Im}\, k]$, the reflection factor R_c, and the transmission factor T_c. The first two quantities in the list are connected with the pulse's evolution along a tube, the last two with its reflection and transmission at a junction. The dependence of these functions on ω is illustrated here through frequency plots.

In each case, the dependence of the function on ω is weak throughout the interval $0.01 < \omega < 0.30$. There is, however, marked variation with frequency in the range $0.5 < \omega < 1.5$. Furthermore, some of the functions vary rapidly with frequency in the neighbourhood of $\omega = 0$, as a consequence of the nonuniformity in $k(\omega)$ at $\omega = 0$, $\nu = 0$. The nonuniformity in k produces a corresponding

nonuniformity in c, Im k, R_c, and T_c. This lack of uniformity in the behaviour of R_c and T_c at $\omega = 0$, $\nu = 0$, has not been acknowledged previously.

These results are consistent with the observations reported in the experiments of Greenwald and Newman (1982) and Newman et al. (1983). In these experiments the frequency dependence of c and R_c measured over the range 5-100 Hz, or over the interval $0.015 < \omega < 0.30$ according to our nondimensional scheme, was very weak. Nevertheless, our results do predict that it is possible to detect frequency dependence in c and R_c outside this frequency range. Although the interval in the neighbourhood of $\omega = 0$ may be too small to measure the frequency dependence therein, some variation in c and R_c with frequency ought to be observed in experiments producing pressure waves that contain frequencies in the range 300-500 Hz, corresponding to the dimensionless interval $0.9 < \omega < 1.5$.

It is evident from the frequency plots of c, $\exp[-\text{Im } k]$, R_c, and T_c that these quantities depend more heavily on wall viscoelasticity than on fluid viscosity. The value of m, the parameter representing viscosity, affects these plots significantly only in the neighbourhood of $\omega = 0$ where the nonuniformity in k dominates events. Elsewhere, the sole effect of m is a slightly vertical shift in the graphs. On the other hand, the value of the viscoelastic parameter τ has a more noticeable effect on the frequency plots. Its influence throughout the frequency band considered here is preferential. At lower frequencies, roughly up to $\omega = 0.3$, the graphs are virtually independent of τ. As ω increases from this point, the presence of τ is felt more

strongly. Therefore, these frequency spectra plots indicate that wall viscoelasticity rather than fluid viscosity is the chief source of energy dissipation for pressure waves in fluid-filled distensible tubes. This conclusion agrees with the one reached in Caro et al. (1978).

It is apparent, then, that if most of the energy in a given disturbance is concentrated within the interval $0.01 < \omega < 0.30$, the propagation and reflection characteristics of the individual waves in the disturbance imply that the pulse as a whole will manifest few signs of dispersion or dissipation as it propagates along a tube, or is reflected at a junction. Whether this is, in fact, true for a pulse composed of a continuous spectrum of frequency components can be tested directly by computing the Fourier integral solutions to the two boundary-value problems posed in this dissertation. The computations of pulse propagation depicted in the articles by Moodie and Barclay (1985, 1986) demonstrate that in the case of an inviscid fluid the shapes of the reflected and transmitted pulses at a junction are almost identical to the shape of the incident pulse, apart from the uniform changes in amplitude predicted by the LLW theory. This must also be true when the viscosity of the fluid is taken into account, as the dependence of R_c and T_c on fluid viscosity is very weak and the time scale involved in the reflection process at a junction is not long enough for small changes in the values of R_c and T_c to have much effect on the shape of the reflected or transmitted pulses.

On the other hand, as a pulse travels along a tube its shape is modified by the effects of dispersion and dissipation. The pulse

broadens, is attenuated, and its oscillatory tail is damped as the wave travels down the tube. This is clear not only in the computations for a viscous fluid presented in this thesis, but also in the calculations for an inviscid fluid in the articles by Moodie and his colleagues (Moodie et al., 1984; Moodie et al., 1985; Moodie et al., 1986). The evidence of dispersion and dissipation displayed in these pressure pulses is greater than that indicated in the frequency plots of c and exp[-Im k]. Our explanation for this apparent paradox is based on the time scale involved in the passage of a pulse along a tube. For example, the time required for a pulse to travel 50 tube radii, in contrast to the time required for a pulse to reflect at a junction, is sufficiently long that small variations in phase velocity and wave attenuation with frequency accumulate to give an effect substantially larger than anticipated from the frequency spectra plots. This is particularly true with regard to the attenuation of the pulse. The recordings of pressure impulses in the experiments of Greenwald and Newman (1982) and Newman et al. (1983) confirm the dispersive and dissipative character displayed by pulses travelling along a tube, and the lack of it in reflections at a junction.

The computations of pressure pulse propagation performed in this dissertation are the first to take into account the influence of fluid viscosity. Therefore, it is possible for the first time to compare the role of fluid viscosity with that of wall viscoelasticity in the propagation of these pulses. Both viscosity and viscoelasticity have a minor effect on the velocity of the main part of the pulse. The viscoelasticity of the wall hastens the arrival of the peak in the

pressure pulse slightly whereas the viscosity of the fluid causes a small delay. The principal importance of these dissipative mechanisms, however, arises from their attenuation of the peak in the pulse. While fluid viscosity causes a modest reduction in the amplitude of the pressure pulse, wall viscoelasticity attenuates the pulse to a far greater degree. The attenuation produced by both dissipative processes, though, is very sensitive to changes in the dissipation parameters τ and m. For the reasons mentioned above, this sensitivity is not revealed in the frequency spectra plots. This suggests that a good experimental approach to assessing the dissipation inherent in pressure wave propagation through fluid-filled distensible tubes is to measure the attenuation in pressure impulses of the sort generated by Greenwald and Newman (1982).

In conclusion, then, we have succeeded in answering the query posed in the introduction to this dissertation. The dominant dissipative mechanism involved in the propagation of the pressure pulses under consideration here through large arteries or water-filled latex tubes is that of wall viscoelasticity. The part played by fluid viscosity, both in the pulse's passage along a tube and in its reflection at a junction, is secondary.

BIBLOGRAPHY

Abramowitz, M. and Stegun, I.A. Handbook of Mathematical Functions. New York: Dover, 1972.

Anliker, M., Histand, M.B. and Ogden, E. Dispersion and attenuation of small artificial pressure waves in the canine aorta. Circ. Res. 23, 539-551 (1968).

Anliker, M., Rockwell, R.L. and Ogden, E. Nonlinear analysis of flow pulses and shock waves in arteries. Part I: Derivation and properties of mathematical model. Z. Angew. Math. Phys. 22, 217-246 (1971).

Atabek, H.B. Wave propagation through a viscous fluid contained in a tethered, initially stressed, orthotropic elastic tube. Biophys. J. 8, 626-649 (1968).

Atabek, H.B. and Lew, H.S. Wave propagation through a viscous incompressible fluid contained in an initially stressed elastic tube. Biophys. J. 6, 481-503 (1966).

Barnard, A.C.L., Hunt, W.A., Timlake, W.P. and Varley, E. A theory of fluid flow in compliant tubes. Biophys. J. 6, 717-724 (1966).

Barnard, A.C.L., Hunt, W.A., Timlake, W.P. and Varley, E. Peaking of the pressure pulse in fluid-filled tubes of spatially varying compliance. Biophys. J. 6, 735-746 (1966).

Brigham, E.O. The Fast Fourier Transform. Englewood Cliffs, N.J.: Prentice-Hall, 1974.

Caro, C.G., Pedley, T.J., Schroter, R.C. and Seed, W.A. The Mechanics of the Circulation. Oxford: Oxford University Press, 1978.

Chow, J.C.F. and Apter, J.T. Wave propagation in a viscous incompressible fluid contained in flexible viscoelastic tubes. J. Acoust. Soc. Am. 44, 437-443 (1968).

Christensen, R.M. Theory of Viscoelasticity: an Introduction, Second Edition. New York: Academic Press, 1982.

Cox, R.H. Comparison of linearized wave propagation models for arterial blood flow analysis. J. Biomechanics 2, 251-265 (1969).

Cox, R.H. A model for the dynamic mechanical properties of arteries. J. Biomechanics 5, 135-152 (1972).

Cox, R.H. Physiology and hemodynamics of the macrocirculation. In Hemodynamics and the Blood Vessel Wall, ed. W.E. Stehbens. Springfield, Illinois: Charles C. Thomas, 1979, pp. 75-156.

Dahlquist, G. and Björck, A. Numerical Methods. Englewood Cliffs, N.J.: Prentice-Hall, 1974.

Euler, L. Principia pro motu sanguins per arterias determinado. In Opera Postuma Mathematica et Physica, Vol. 2, ediderunt P.H. Fuss et N. Fuss. Petropoli: 1862. Reprinted Nendeln, Liechtenstein: Kraus, 1969, pp. 814-823.

Goedhard, W.J.A. and Knoop, A.A. A model of the arterial wall. J. Biomechanics 6, 281-288 (1973).

Goodman, F.O. and Imaeda, K. On empirical linear response models of arterial walls. J. Biomechanics 10, 283-288 (1977).

Greenwald, S.E. and Newman, D.L. Impulse propagation through junctions. Med. & Biol. Eng. & Comput. 20, 343-350 (1982).

Greenwald, S.E., Newman, D.L. and Moodie, T.B. Impulse propagation in rubber-tube analogues of arterial stenoses and aneurysms. Med. & Biol. Eng. & Comput. 23, 150-154 (1985).

Herrman, G. and Mirsky, I. Three-dimensional and shell-theory analysis of axially symmetric motions of cylinders. J. Appl. Mech. 23, 563-568 (1956).

Holenstein, R., Niederer, P. and Anliker, M. A viscoelastic model for use in predicting arterial pulse waves. J. Biomech. Engng. 102, 318-325 (1980).

Lamb, H. On the velocity of sound in a tube, as affected by the elasticity of the walls. Manchester Lit. Phil. Society. Memoirs Proc. 42, 1-16 (1898).

Lambert, J.W. On the nonlinearities of fluid flow in nonrigid tubes. J. Franklin Institute 266, 83-102 (1958).

Learoyd, B.M. and Taylor, M.G. Alterations with age in the viscoelastic properties of human arterial walls. Circ. Res. 18, 278-292 (1966).

Leitzmann, A. (ed.) Georg Christoph Lichtenbergs Aphorismen, Vol. 2. Berlin: 1904. Reprinted in Deutsche Literaturdenkmale des 18. und 19. Jahrhunderts, No. 131. Nendeln, Liechtenstein: Kraus, 1968.

Lighthill, M.J. Waves in Fluids. Cambridge: Cambridge University Press, 1978.

Maxwell, J.A. and Anliker, M. The dissipation and dispersion of small waves in arteries and veins with viscoelastic wall properties. Biophys. J. 8, 920-950 (1968).

McDonald, D.A. Blood Flow in Arteries, Second Edition. London: Edward Arnold, 1974.

Mills, C.J., Gabe, I.T., Gault, J.H., Mason, D.T., Ross, J., Braunwald, E. and Shillingford, J.P. Pressure-flow relationships and vascular impedance in man. Cardiovasc. Res. 4, 405-417 (1970).

Milnor, W.R. and Bertram, C.D. The relation between arterial viscoelasticity and wave propagation in the canine femoral artery in vivo. Circ. Res. 43, 870-879 (1978).

Moodie, T.B. and Barclay, D.W. Propagation and reflection of waves in finite length liquid-filled distensible shells. Acta Mech. 56, 151-163 (1985).

Moodie, T.B. and Barclay, D.W. Wave propagation and reflection in liquid filled distensible tube systems exhibiting dissipation and dispersion. Acta Mech. 59, 139-155 (1986).

Moodie, T.B., Barclay, D.W. and Greenwald, S.E. Impulse propagation in liquid filled distensible tubes: theory and experiment for intermediate to long wavelengths. Acta Mech. 59, 47-58 (1986).

Moodie, T.B., Barclay, D.W., Greenwald, S.E. and Newman, D.L. Waves in fluid filled tubes: theory and experiment. Acta Mech. 54, 107-119 (1984).

Moodie, T.B., Barclay, D.W. and Tait, R.J. A boundary value problem for fluid-filled viscoelastic tubes. Math. Modelling 4, 195-207 (1983).

Moodie, T.B. and Haddow, J.B. Dispersive effects in wave propagation in thin-walled elastic tubes. J. Acoust. Soc. Am. 64, 522-528 (1978).

Moodie, T.B. and Haddow, J.B. Asymptotic analysis for dispersive fluid filled tubes. J. Acoust. Soc. Am. 67, 446-452 (1980).

Moodie, T.B., Mainardi, F. and Tait, R.J. Pressure pulses in fluid filled distensible tubes. Meccanica 20, 33-37 (1985).

Moodie, T.B., Tait, R.J. and Haddow, J.B. Waves in compliant tubes. In Wave Propagation in Viscoelastic Media, ed. F. Mainardi, Research Notes in Mathematics, No. 152. London: Pitman, 1982, pp. 124-168.

Morgan, G.W. and Kiely, J.P. Wave propagation in a viscous liquid contained in a flexible tube. J. Acoust. Soc. Am. 26, 323-328 (1954).

Newman, D.L., Greenwald, S.E. and Denyer, H.T. Impulse propagation in normal and stenosed vessels. Cardiovasc. Res. 15, 190-195 (1981).

Newman, D.L., Greenwald, S.E. and Moodie, T.B. Reflection from elastic discontinuities. Med. & Biol. Eng. & Comput. 21, 697-701 (1983).

Olsen, J.H. and Shapiro, A.H. Large-amplitude unsteady flow in liquid-filled elastic tubes. J. Fluid Mech. 29, 513-538 (1967).

Patel, D.J. and Vaishnav, R.N. Basic Hemodynamics and its Role in Disease Processes. Baltimore: University Park Press, 1980.

Pedley, T.J. The Fluid Mechanics of Large Blood Vessels. Cambridge: Cambridge University Press, 1980.

Pedley, T.J. Wave phenomena in physiological flows. IMA J. Appl. Math. 32, 267-287 (1984).

Pipkin, A.C. Lectures on Viscoelasticity Theory. New York: Springer-Verlag, 1972.

Rubinow, S.I. and Keller, J.B. Wave propagation in a fluid-filled tube. J. Acoust. Soc. Am. 50, 198-223 (1971).

Rubinow, S.I. and Keller, J.B. Wave propagation in a viscoelastic tube containing a viscous fluid. J. Fluid Mech. 88, 181-203 (1978).

Sawatzky, R.P. and Moodie, T.B. Frequency-dependent reflection from mechanical discontinuities. Med. & Biol. Eng. & Comput., in press.

Skalak, R. Wave propagation in blood flow. In Biomechanics, ed. Y.C. Fung, Symposium Proceedings. New York: ASME, 1966, pp. 20-46.

Skalak, R., Keller, S.R. and Secomb, T.W. Mechanics of blood flow. J. Biomech. Engng. 103, 102-115 (1981).

Skalak, R. and Stathis, T. A porous tapered elastic tube model of a vascular bed. In Biomechanics, ed. Y.C. Fung, Symposium Proceedings. New York: ASME, 1966, pp. 68-81.

Stehbens, W.E. Anatomy and structure of blood vessels. In Hemodynamics and the Blood Vessel Wall, ed. W.E. Stehbens. Springfield, Illinois: Charles C. Thomas, 1979, pp. 3-74.

Stettler, J.C., Niederer, P. and Anliker, M. Theoretical analysis of arterial hemodynamics including the influence of bifurcations. Part I: Mathematical model and prediction of normal pulse patterns. Annals of Biomed. Engng. 9, 145-164 (1981).

Streeter, V.L., Keitzer, W.F. and Bohr, F.F. Pulsatile pressure and flow through distensible vessels. Circ. Res. **13**, 3-20 (1963).

Tait, R.J., Moodie, T.B. and Haddow, J.B. Wave propagation in a fluid-filled elastic tube. Acta Mech. **38**, 71-83 (1981).

Westerhof, N. and Noordergraaf, A. Arterial viscoelasticity: a generalized model. J. Biomechanics **3**, 357-379 (1970).

Whitham, G.B. Linear and Nonlinear Waves. New York: Wiley, 1974.

Womersley, J.R. Oscillatory motion of a viscous liquid in a thin-walled tube - I: The linear approximation for long waves. Phil. Mag. **46**, 199-221 (1955).

Womersley, J.R. Oscillatory flow in arteries: the constrained elastic tube as a model of arterial flow and pulse transmission. Phys. Med. Biol. **2**, 178-187 (1957a).

Womersley, J.R. Oscillatory flow in arteries. II: The reflection of the pulse wave at junctions and rigid inserts in the arterial system. Phys. Med. Biol. **2**, 313-323 (1957b).

Young, T. Hydraulic investigations subservient to an intended Croonian lecture on the motion of the blood. Phil. Trans. Roy. Soc. **98**, 164-186 (1808).

Young. T. On the functions of the heart and arteries. Phil. Trans. Roy. Soc. **99**, 1-31 (1809).

APPENDIX

The Function F(z) and Related Functions

In our travelling wave solutions of the variables important in the dynamics of a fluid-filled distensible tube, as contained in eqns. 4.20 - 4.23, there appears a function $F(z)$ involving the ratio of the modified Bessel functions. Here we examine the behaviour of this function of a single complex variable. According to eqn. 4.29, F is defined as

$$F(z) = \frac{zI_0(z)}{2I_1(z)} , \quad z \in \mathbf{C} , \qquad (A.1)$$

where I_0 and I_1 are the modified Bessel functions of the first kind of orders zero and one respectively. A detailed description of the modified Bessel functions is available in the work by Abramowitz and Stegun (1972). We rely on this reference for those properties of these Bessel functions required in what follows.

Since $I_0(z)$ and $I_1(z)$ are entire functions, $F(z)$ is an analytic function of z for all $z \in \mathbf{C}$ except possibly the zeros of $I_1(z)$. The zeros of $F(z)$ can occur at $z = 0$ and at the zeros of $I_0(z)$. The zeros of $I_0(z)$ and $I_1(z)$ are simple and occur along the imaginary axis in +/- pairs. There are an infinite number of them. Along the nonnegative imaginary axis the zeros of $I_0(z)$ and $I_1(z)$ are interlaced, beginning with the zero of $I_1(z)$ at $z = 0$. Consequently, $F(z)$ has an infinite number of simple poles on the imaginary axis at the zeros of $I_1(z)$. There is, however, no pole at

$z = 0$ because the zeros of $I_1(z)$ are simple. Similarly, the zeros of $F(z)$ lie on the imaginary axis, coincident with those of $I_0(z)$, and they too are all simple.

$F(z)$ possesses some symmetry that is noteworthy. First of all,

$$F(-z) = F(z) . \tag{A.2}$$

This follows from the facts that $I_0(-z) = I_0(z)$ and $I_1(-z) = -I_1(z)$. Secondly,

$$F(\bar{z}) = \overline{F(z)} , \tag{A.3}$$

where the bar denotes the complex conjugate. This is a consequence of the facts that $I_0(\bar{z}) = \overline{I_0(z)}$ and $I_1(\bar{z}) = \overline{I_1(z)}$.

In order to evaluate $F(z)$ at a given value of z, it is necessary to evaluate the two modified Bessel functions. This can be done by using either their power series or their asymptotic expansions. We develop both techniques here, as the former method is best when $|z|$ is small and the latter method is valid only when $|z|$ is large. Consider the power series approach first. Since they are entire functions, both $I_0(z)$ and $I_1(z)$ possess power series which converge for all $z \in \mathbf{C}$. These series are

$$\left.\begin{aligned} I_0(z) &= \sum_{k=0}^{\infty} (\tfrac{1}{4} z^2)^k/[k!]^2 , \\ I_1(z) &= \tfrac{1}{2} z \sum_{k=0}^{\infty} (\tfrac{1}{4} z^2)^k/[k!(k+1)!] . \end{aligned}\right\} \qquad (A.4)$$

Therefore, the following representation of $F(z)$, obtained by substituting eqn. A.4 into eqn. A.1, is valid for all $z \in C$ except the poles of $F(z)$:

$$F(z) = \{ \sum_{k=0}^{\infty} (\tfrac{1}{4} z^2)^k/[k!]^2 \}/\{ \sum_{k=0}^{\infty} (\tfrac{1}{4} z^2)^k/[k!(k+1)!] \} . \qquad (A.5)$$

We define $F(0) = 1$, as it follows from eqn. A.5 that $\lim_{z \to 0} F(z) = 1$.

The formula in eqn. A.5 is of the form

$$F(z) = \sum_{k=0}^{\infty} \alpha_k z^{2k} / \sum_{k=0}^{\infty} \beta_k z^{2k} , \qquad (A.6)$$

where the coefficients α_k and β_k are independent of z. Although α_k and β_k can be expressed explicitly for $k = 0,1,2,\ldots$ by picking off the coefficients of z^{2k} in both the numerator and denominator of eqn. A.5, it is more efficient to compute them using their recurrence relations. These relations are

$$\left.\begin{aligned} \alpha_{k+1} &= \alpha_k/4(k+1)^2 , \quad \alpha_0 = 1 , \\ \beta_{k+1} &= \beta_k/4(k+1)(k+2) , \quad \beta_0 = 1 , \end{aligned}\right\} \tag{A.7}$$

for $k = 0,1,2,\ldots$.

When $|z|$ is very small, $F(z)$ can be expanded in a power series about $z = 0$. This series is obtained from eqn. A.5 through formal division of the numerator by the denominator. The first few terms in the series are

$$F(z) = 1 + \frac{1}{8} z^2 - \frac{1}{192} z^4 + \ldots . \tag{A.8}$$

The RHS of eqn. A.8 converges to $F(z)$ for $|z| < j_{1,1}$, as $z = ij_{1,1}$ is the pole of $F(z)$ nearest the origin. The value of $j_{1,1}$ is approximately 3.83. In the same way, the reciprocal of $F(z)$ can be expanded in a power series about $z = 0$ as

$$1/F(z) = 1 - \frac{1}{8} z^2 + \frac{1}{48} z^4 + \ldots . \tag{A.9}$$

The RHS of eqn. A.9 converges to $1/F(z)$ for $|z| < j_{0,1}$, as $z = ij_{0,1}$ is the zero of $F(z)$ nearest the origin. The value of $j_{0,1}$ is approximately 2.40.

Although $F(z)$ can be evaluated at each point in its domain via eqns. A.6 and A.7, these formulae are not practical to use when $|z|$ becomes large. In this case, $F(z)$ can be computed readily by using the

asymptotic expansions of the modified Bessel functions. The asymptotic behaviour of $I_0(z)$ and $I_1(z)$, in turn, is obtained from that of the Bessel functions $J_0(z)$ and $J_1(z)$ in view of the relations

$$I_0(z) = J_1(iz) \ , \quad I_1(z) = -iJ_1(iz) \qquad (A.10)$$

Here J_0 and J_1 are the Bessel functions of the first kind of orders zero and one respectively. As $|z| \to \infty$, for $|\arg z| < \pi$,

$$J_n(z) \sim \left(\frac{2}{\pi z}\right)^{1/2}\left\{P_n(z)\cos\left[z - \left(\frac{n}{2} + \frac{1}{4}\right)\pi\right] - Q_n(z)\sin\left[z - \left(\frac{n}{2} + \frac{1}{n}\right)\pi\right]\right\} \ , \quad n = 0,1 \ , \qquad (A.11)$$

where

$$\left.\begin{aligned} P_n(z) &= 1 - \frac{(4n^2-1)(4n^2-9)}{2!(8z)^2} + \frac{(4n^2-1)(4n^2-9)(4n^2-15)(4n^2-49)}{4!(8z)^4} \\ &\quad + \ldots \ , \\ Q_n(z) &= \frac{(4n^2-1)}{8z} - \frac{(4n^2-1)(4n^2-9)(4n^2-25)}{3!(8z)^3} + \ldots \ . \end{aligned}\right\} \qquad (A.12)$$

Consequently, it follows from eqns. A.10 - A.12 that as $|z| \to \infty$, for $|\arg iz| < \pi$,

$$I_0(z) \sim (2\pi z)^{-1/2}\{e^z[P_0(iz) - iQ_0(iz)] - e^{-z}[iP_0(iz) - Q_0(iz)]\} , \tag{A.13}$$

and

$$I_1(z) \sim (2\pi z)^{-1/2}\{e^z[P_1(iz) - iQ_1(iz)] + e^{-z}[iP_1(iz) - Q_1(iz)]\} . \tag{A.14}$$

According to eqn. A.12, for $n = 0,1$,

$$\left.\begin{aligned} P_n(iz)-iQ_n(iz) &= 1- \frac{(4n^2-1)}{8z} + \frac{(4n^2-1)(4n^2-9)}{2!(8z)^2} \\ &\quad - \frac{(4n^2-1)(4n^2-9)(4n^2-25)}{3!(8z)^3} + \cdots , \\ iP_n(iz)-Q_n(iz) &= i\left[1+ \frac{(4n^2-1)}{8z} + \frac{(4n^2-1)(4n^2-9)}{2!(8z)^2}\right. \\ &\quad \left. + \frac{(4n^2-1)(4n^2-9)(4n^2-25)}{3!(8z)^3} + \cdots\right] . \end{aligned}\right\} \tag{A.15}$$

When eqns. A.13 - A.15 are substituted into eqn. A.11, the following representation for $F(z)$ is obtained, valid as $|z| \to \infty$ for $|\arg iz| < \pi$:

$$F(z) \sim \frac{1}{2} z\{[1 - \frac{(-1)}{8z} + \frac{(-1)(-9)}{2!(8z)^2} - \frac{(-1)(-9)(-25)}{3!(8z)^3} + \ldots]$$

$$- ie^{-2z}[1 + \frac{(-1)}{8z} + \frac{(-1)(-9)}{2!(8z)^2} + \frac{(-1)(-9)(-25)}{3!(8z)^3} + \ldots]\}$$

$$/ \{[1 - \frac{(4-1)}{8z} + \frac{(4-1)(4-9)}{2!(8z)^2} - \frac{(4-1)(4-9)(4-25)}{3!(8z)^3} + \ldots]$$

$$+ ie^{-2z}[1 + \frac{(4-1)}{8z} + \frac{(4-1)(4-9)}{2!(8z)^2} + \frac{(4-1)(4-9)(4-25)}{3!(8z)^3} + \ldots]\} . \quad (A.16)$$

Equation A.16 must hold for $-\frac{\pi}{2} \leq \arg z < \frac{\pi}{2}$, as this sector is contained in $|\arg iz| < \pi$. The asymptotic behaviour of $F(z)$ in the other half of the complex plane can be obtained immediately from eqn. A.16 by making use of the symmetry of $F(z)$ as expressed in eqn. A.2.

The formula in eqn. A.16 is of the form

$$F(z) \sim \frac{1}{2}\{\sum_{k=0}^{\infty} (a_k - ic_k e^{-2z}) z^{-k}\} / \{\sum_{k=0}^{\infty} (b_k + id_k e^{-2z}) z^{-k}\} , \quad (A.17)$$

where the coefficients a_k, b_k, c_k and d_k are independent of z. These quantities can be expressed explicitly for $k = 0,1,2,\ldots$ by picking off the coefficients of z^{-k} in both the numerator and denominator of eqn. A.17. As is the case in the power series approach to representing $F(z)$, however, it is more efficient to compute these coefficients by using their recurrence relations. Thus,

$$\left.\begin{aligned} a_{k+1} &= \frac{(2k+1)^2}{8(k+1)}\, a_k \,, \quad a_0 = 1 \,, \\ b_{k+1} &= \frac{[(2k+1)^2-4]}{8(k+1)}\, b_k \,, \quad b_0 = 1 \,, \\ c_{k+1} &= -\frac{(2k+1)^2}{8(k+1)}\, c_k \,, \quad c_0 = 1 \,, \\ d_{k+1} &= -\frac{[(2k+1)^2-4]}{8(k+1)}\, d_k \,, \quad d_0 = 1 \,. \end{aligned}\right\} \tag{A.18}$$

When $\mathrm{Re}\, z \to \infty$, the asymptotic formula for $F(z)$ can be simplified because e^{-2z} is negligible. Then, for example, eqn. A.17 becomes

$$F(z) \sim \frac{1}{2}\, z \sum_{k=0}^{\infty} a_k z^{-k} \Big/ \sum_{k=0}^{\infty} b_k z^{-k} \,, \tag{A.19}$$

where the coefficients a_k and b_k are those given in eqn. A.18. Equation A.16 changes in a similar fashion. An asymptotic expansion in inverse powers of z can be obtained from eqn. A.19 by dividing the denominator into the numerator. This yields

$$F(z) \sim \frac{1}{2}\, z\left(1 + \frac{1}{2z} + \frac{3}{8z^2} + \ldots\right) \,, \tag{A.20}$$

as $\mathrm{Re}\, z \to \infty$. Similarly, the asymptotic expansion of the reciprocal of $F(z)$ is

$$1/F(z) \sim \frac{2}{z}\left(1 - \frac{1}{2z} - \frac{1}{8z^2} + \ldots\right) . \qquad (A.21)$$

This completes our description of the function F defined in eqn. A.1. We conclude this appendix with a brief examination of some other functions related to F that arise during the analysis of the dispersion equation for waves in a fluid-filled distensible tube, eqn. 4.27. The functions to be considered here are those defined in eqns. 4.46, 4.50, 4.51, and 4.48. Recall that these definitions were

$$F_1(z) = \frac{1}{4} + F(z)[1 - F(z)]/z^2 , \qquad (A.22)$$

$$F_2(z) = 1 - 1/F(z) , \qquad (A.23)$$

$$F_3(z) = [F_1(z) + \tfrac{1}{8}]/F(z) - F_2(z)/z^2 , \qquad (A.24)$$

$$A_1(z) = [F_1(z) - \tfrac{1}{8}]/F(z) . \qquad (A.25)$$

As in eqn. A.1, z is a complex variable in the equations above.

The functions F_1, F_2, F_3 and A_1 are analytic wherever F is analytic, with the following exceptions. It is possible that F_1 is not analytic at $z = 0$. The function F_2 is not analytic at the

zeros of F, but is analytic at the poles. It is possible that F_3 is not analytic at $z = 0$ or at the zeros of F, while it may be analytic at the poles of F. Similarly, it is possible that A_1 is not analytic at the zeros of F and it may be analytic at the poles. It will be shown subsequently that all of the above functions are analytic at $z = 0$.

We are particularly interested in the behaviour of F_1, F_2, F_3 and A_1 in the two extreme cases, firstly when $z \to 0$ and secondly when $\mathrm{Re}\, z \to \infty$. When $|z|$ is small, these functions can be expanded in a power series about $z = 0$. The first few terms in these series can be obtained by substituting eqns. A.8 and A.9 into eqns. A.22 - A.25. The result is

$$F_1(z) = \frac{1}{8}\left(1 - \frac{1}{12} z^2\right) + \ldots , \qquad (A.26)$$

$$F_2(z) = \frac{1}{8} z^2\left(1 - \frac{1}{6} z^2\right) + \ldots , \qquad (A.27)$$

$$F_3(z) = \frac{1}{8}\left(1 - \frac{1}{6} z^2\right) + \ldots , \qquad (A.28)$$

$$A_1(z) = -\frac{1}{96} z^2 + \ldots . \qquad (A.29)$$

Equations A.26 - A.29 demonstrate that F_1, F_2, F_3 and A_1 are indeed analytic at $z = 0$. The series for $F_1(z)$ converges on the same interval as the series for $F(z)$, namely $|z| < j_{1,1}$, while the series for $F_2(z)$, $F_3(z)$ and $A_1(z)$ converge on the same interval as the

series for $1/F(z)$, that is, $|z| < j_{0,1}$. When Re z is very large, the functions F_1, F_2, F_3 and A_1 can be expanded asymptotically in inverse powers of z. These expansions can be generated by inserting eqns. A.20 and A.21 into eqns. A.22 - A.25. This yields

$$F_1(z) \sim \frac{1}{4z} + \ldots , \tag{A.30}$$

$$F_2(z) \sim 1 - \frac{2}{z} + \frac{1}{z^2} + \ldots , \tag{A.31}$$

$$F_3(z) \sim \frac{1}{4z} + \ldots , \tag{A.32}$$

$$A_1(z) \sim -\frac{1}{4z} + \ldots . \tag{A.32'}$$

This ends our brief examination of the functions F_1, F_2, F_3 and A_1.

As a postscript to this appendix, we remark that it is mainly on the ray $\arg z = -\frac{\pi}{4}$ that the functions named above, and F itself, are to be evaluated. In Figs. A.1 - A.5 the real and imaginary parts of these functions are depicted on the segment of the ray $0 \leq |z| \leq 15$. It is evident from these graphs that there is just a short transition zone between the region in which the functions F, F_1 and F_2 are described well by a few terms in their power series and the region in which they are described well by their asymptotic expansions. However, this transition zone is somewhat larger for the functions F_3 and A_1.

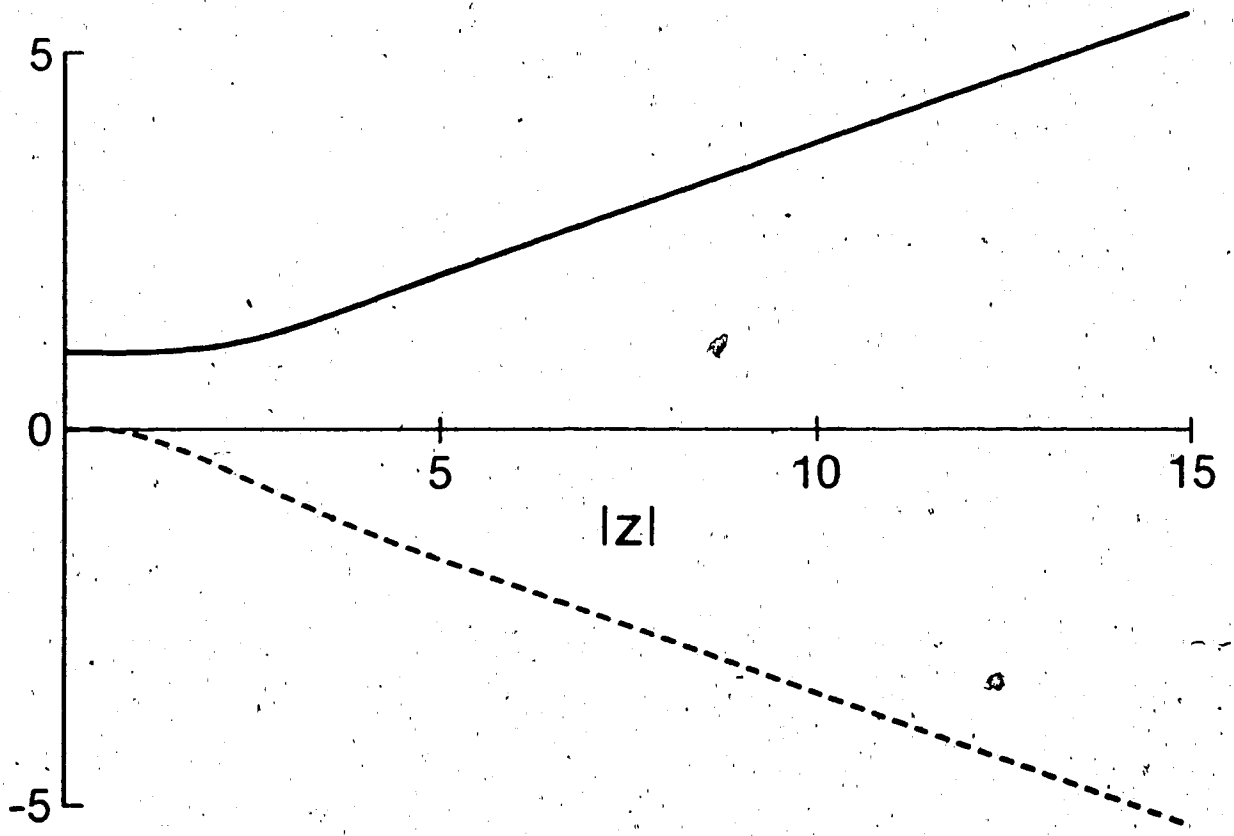

Fig. A.1. Re F (-) and Im F (--) versus $|z|$ along the ray $\arg z = -\pi/4$.

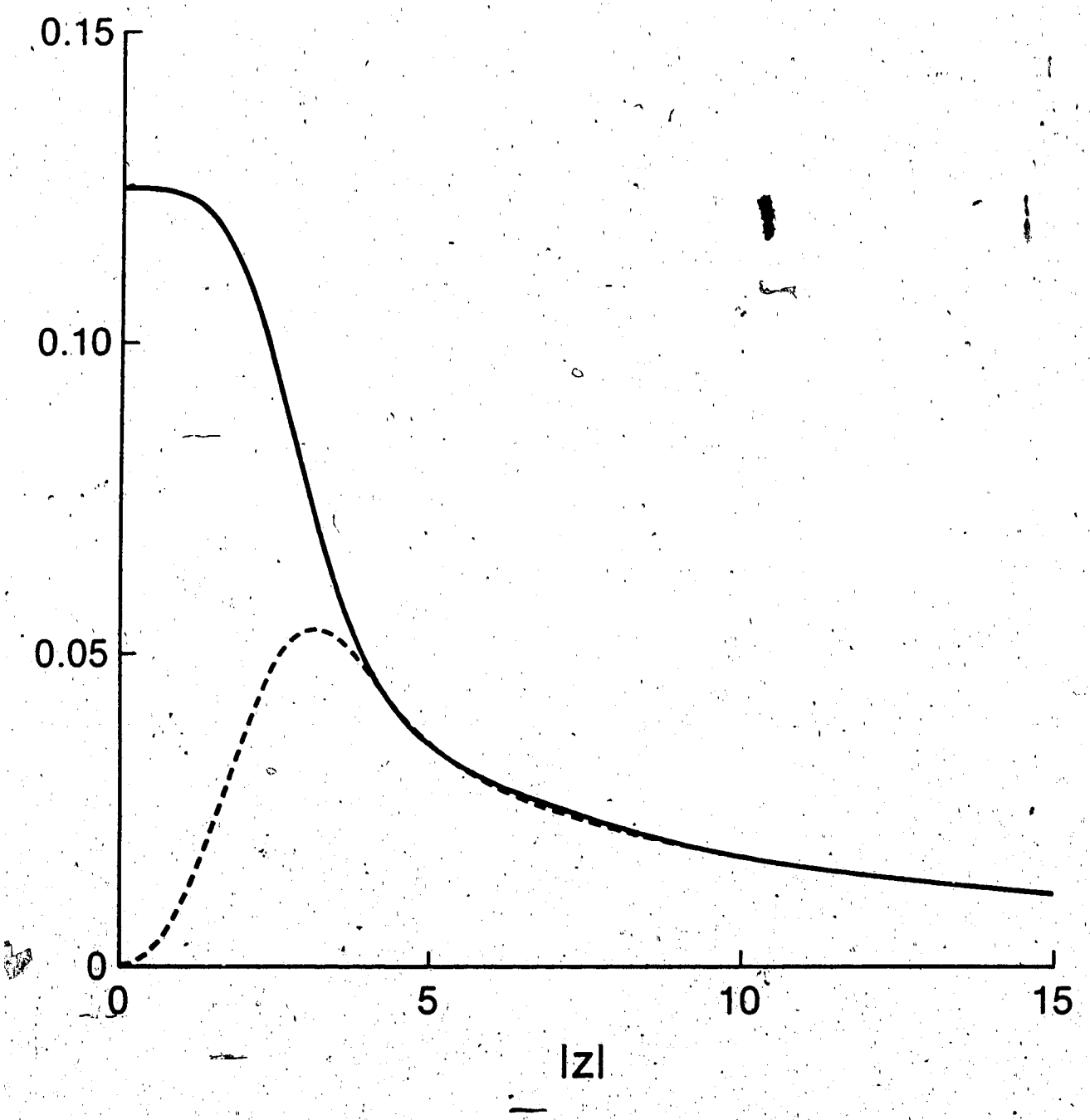

Fig. A.2. Re F_1 (-) and Im F_1 (--) versus $|z|$ along the ray arg $z = -\pi/4$.

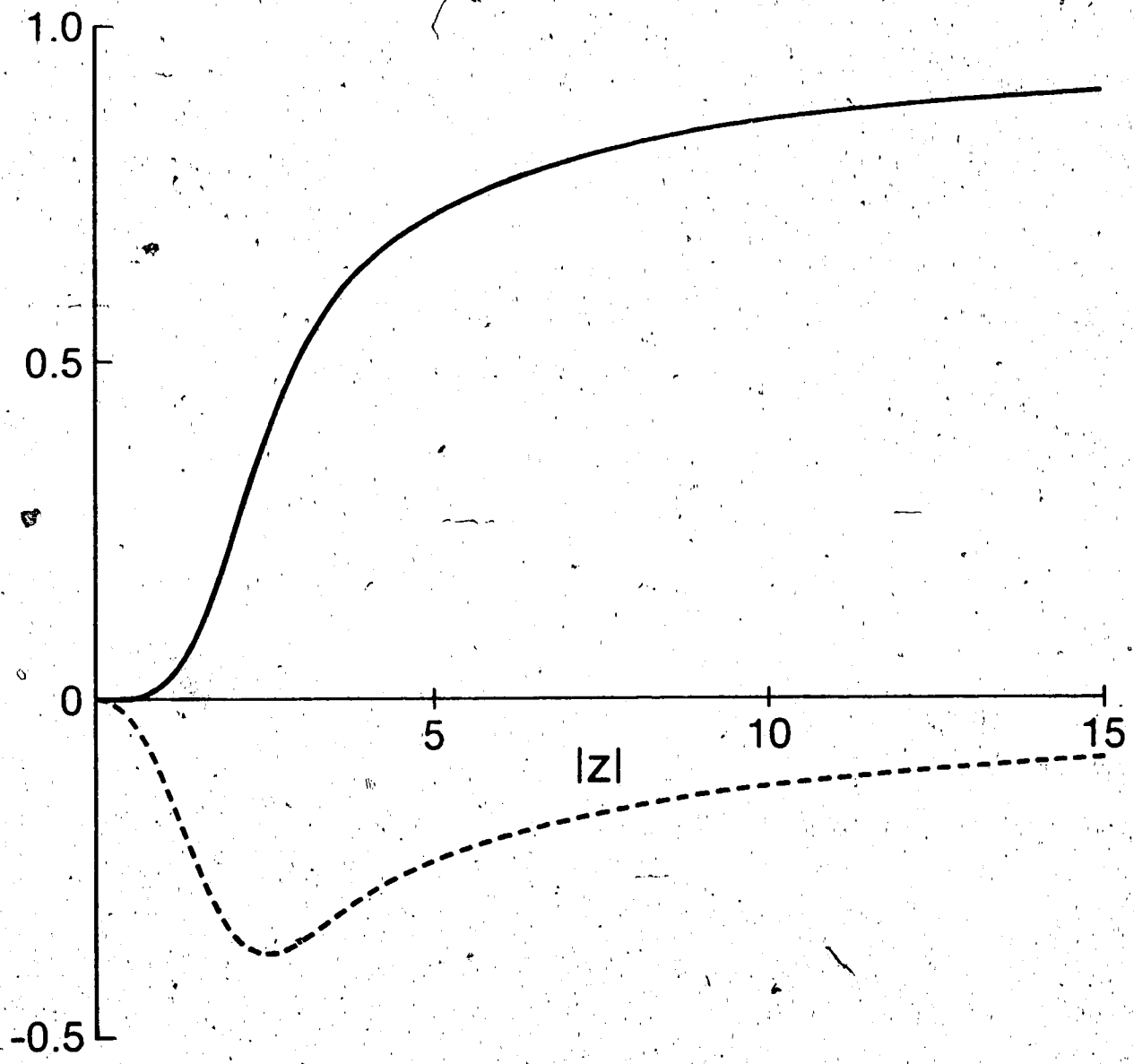

Fig. A.3. Re F_2 (-) and Im F_2 (--) versus $|z|$ along the ray $\arg z = -\pi/4$.

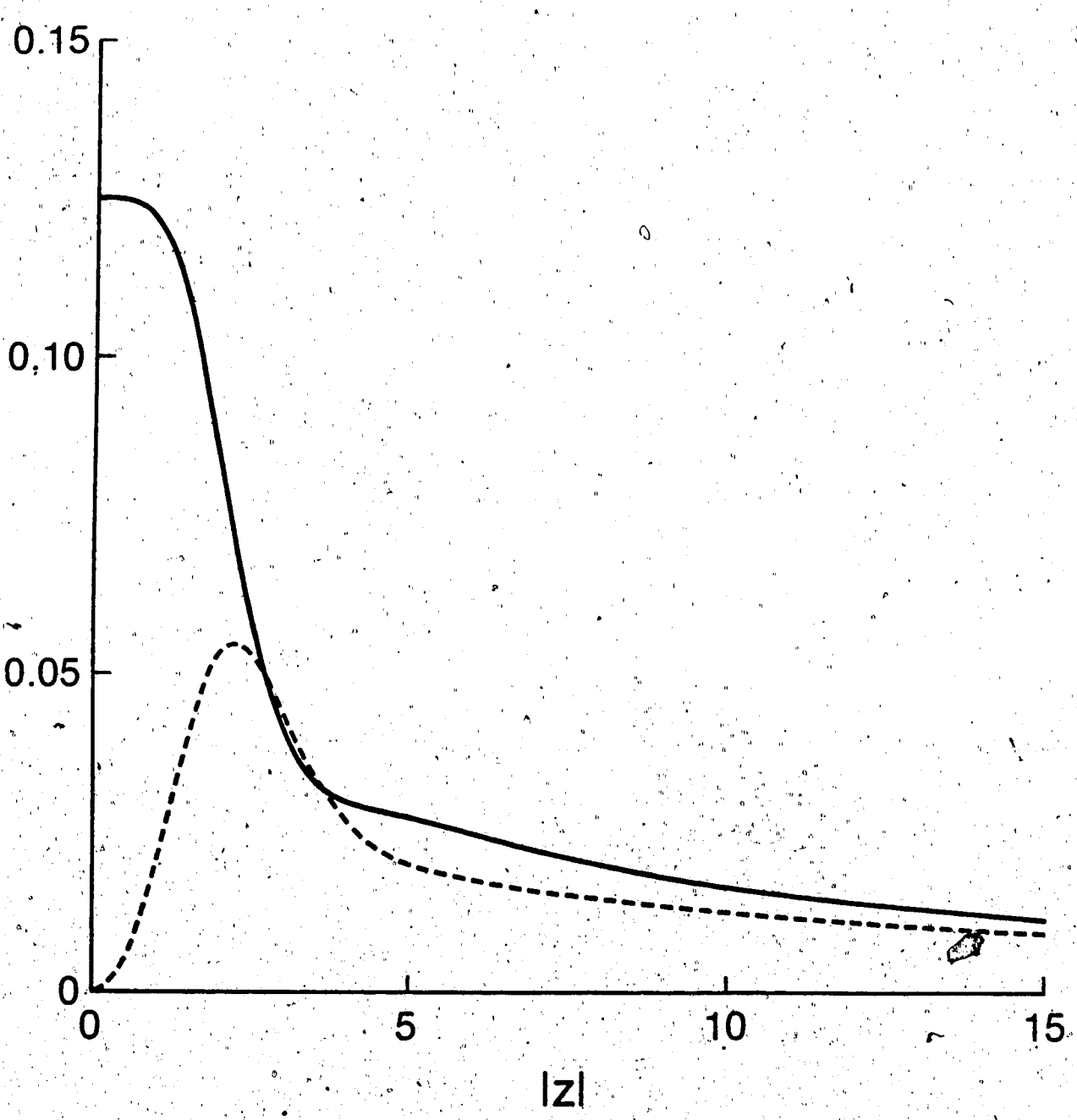

Fig. A.4. Re F_3 (-) and Im F_3 (--) versus $|z|$ along the ray $\arg z = -\pi/4$.

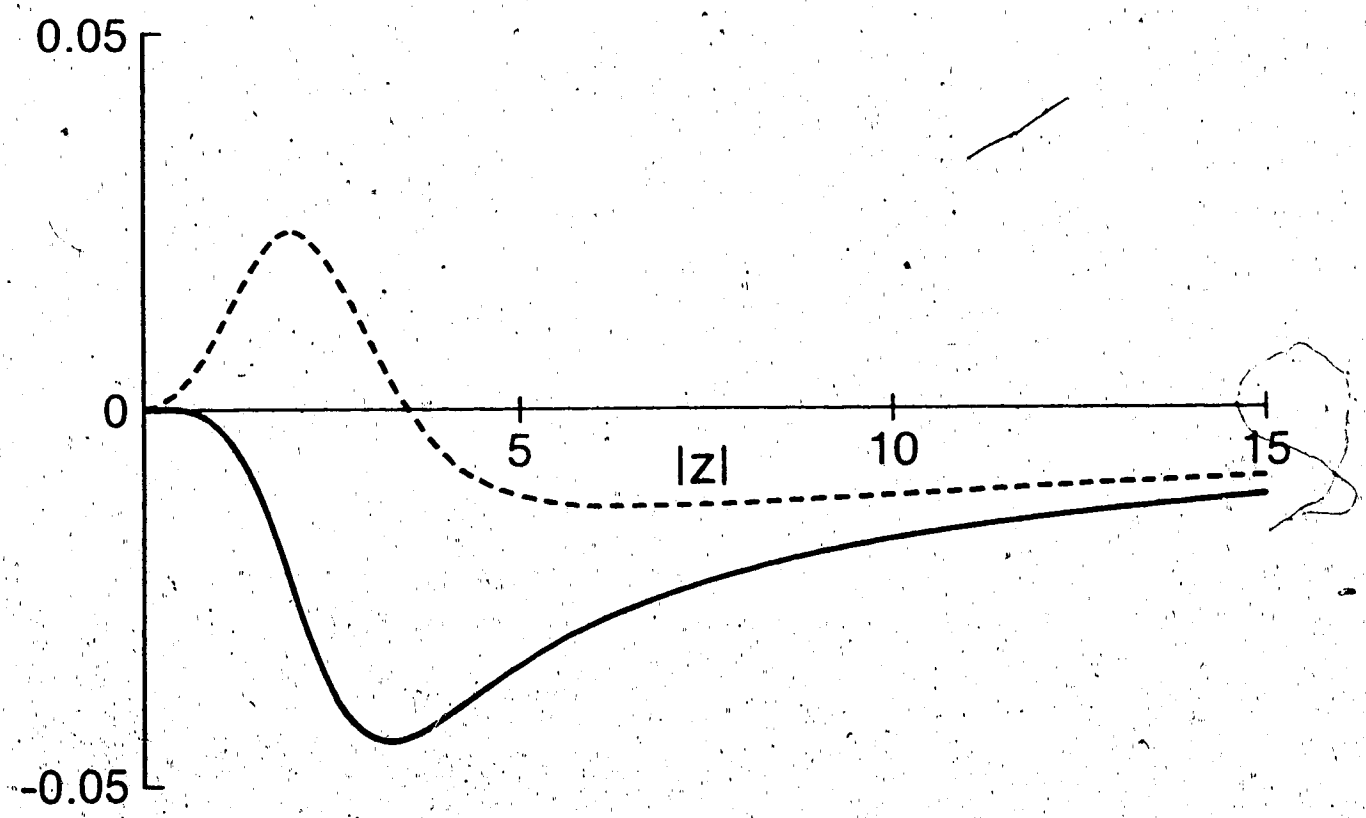

Fig. A.5. Re A_1 (-) and Im A_1 (--) versus $|z|$ along the ray arg $z = -\pi/4$.